AD-A045 672 TEXAS INSTRUMENTS INC DALLAS CENTRAL RESEARCH LABS F/G 20/5
MONOLITHIC LASER.(U)
SEP 77 K L LAWLEY N00014-73-C-0288
UNCLASSIFIED TI-08-77-19 NL

1 OF 2
ADA
045672

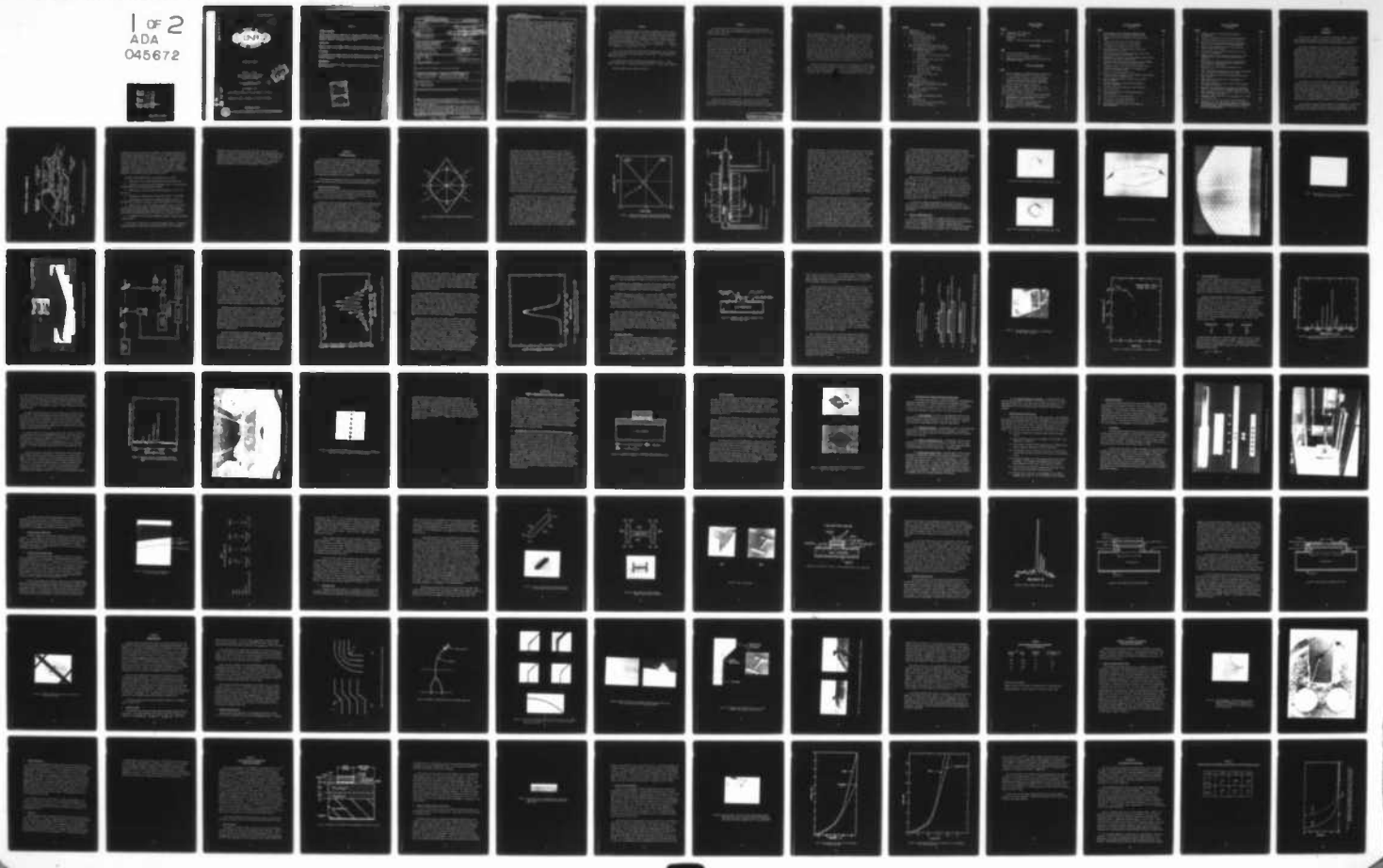

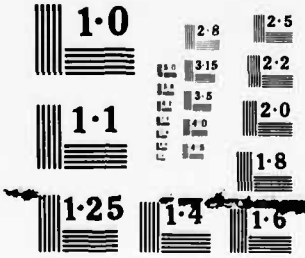

REPORT ONR-288-016-1F

MONOLITHIC LASER

Kenneth L. Lawley

Texas Instruments Incorporated
Central Research Laboratories
Dallas, Texas 75222

Contract N00014-73-C-0288
ONR Task 215-220

30 September 1977

Final Technical Report for Period 1 May 73 - 31 Jan 77

Approved for public release; distribution unlimited.

PREPARED FOR THE

OFFICE OF NAVAL RESEARCH ● 800 N. QUINCY ST. ● ARLINGTON ● VA ● 22217

NOTICES

Change of Address

Organizations receiving reports on the initial distribution list should confirm correct address. This list is located at the end of the report. Any change of address or distribution should be conveyed to the Office of Naval Research, Code 221, Arlington, Virginia 22217.

Disposition

When this report is no longer needed, it may be transmitted to other authorized organizations. Do not return it to the originator or the monitoring office.

Disclaimer

The findings in this report are not to be construed as an official Department of Defense or Military Department position unless so designated by other official documents.

Reproduction

Reproduction in whole or in part is permitted for any purpose of the United States Government.

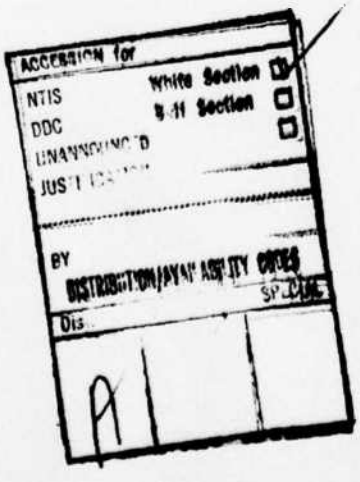

UNCLASSIFIED

SECURITY CLASSIFICATION OF THIS PAGE (When Data Entered)

REPORT DOCUMENTATION PAGE		READ INSTRUCTIONS BEFORE COMPLETING FORM
1. REPORT NUMBER ONR-288-016-1F	2. GOVT ACCESSION NO.	3. RECIPIENT'S CATALOG NUMBER
4. TITLE (and Subtitle) (6) MONOLITHIC LASER		5. TYPE OF REPORT & PERIOD COVERED (9) Final Technical Report 1 May 1973 - 31 Jan 1977
(10)	(14) TI-08-77-19	6. PERFORMING ORG. REPORT NUMBER TI-288-016-1F-ONR
7. AUTHOR(s) Kenneth L. Lawley		8. CONTRACT OR GRANT NUMBER(s) (15) N00014-73-C-0288
9. PERFORMING ORGANIZATION NAME AND ADDRESS Texas Instruments Incorporated Central Research Laboratories 13500 North Central Expressway Dallas, Texas 75222		10. PROGRAM ELEMENT, PROJECT, TASK AREA & WORK UNIT NUMBERS PE 61153N-14, RF 41-423-001, NR 215-220
11. CONTROLLING OFFICE NAME AND ADDRESS Office of Naval Research Arlington, Virginia 22217		(11) 12. REPORT DATE Sep 1977 13. NUMBER OF PAGES 100
14. MONITORING AGENCY NAME & ADDRESS(if different from Controlling Office) (12) 112p.		15. SECURITY CLASS. (of this report) Unclassified 15a. DECLASSIFICATION DOWNGRADING SCHEDULE

16. DISTRIBUTION STATEMENT (of this Report)

Approved for Public Release - Distribution Unlimited

17. DISTRIBUTION STATEMENT (of the abstract entered in Block 20, if different from Report)

(16) F41423 (17) RF41423001

18. SUPPLEMENTARY NOTES

ONR Scientific Officer
Tel: (202) 692-4715

19. KEY WORDS (Continue on reverse side if necessary and identify by block number)

20. ABSTRACT (Continue on reverse side if necessary and identify by block number)

This report describes the accomplishment of a three-phased exploratory research program under Contract No. N00014-73-C-0288 to develop the first integrated optical transmitter.

The initial efforts involved the development of a unique (Ga,In)As surface laser and high index infrared glass waveguides. The surface laser is a vapor-grown mesa structure with vertical grown crystalline facets furnishing the optical feedback. The structure can be placed and grown at will on a GaAs substrate using conventional photolithographic techniques. This unique laser structure →

DD FORM 1 JAN 73 1473 EDITION OF 1 NOV 65 IS OBSOLETE

403 833

UNCLASSIFIED

SECURITY CLASSIFICATION OF THIS PAGE (When Data Entered)

20. ABSTRACT (Continued)

represents a radical departure from conventional semiconductor laser technology. Ternary alloy $Ga_{1-x}In_xAs$ mesas with $0 < x < 0.2$ were grown and the details of their morphology determined. Optically pumped laser emission from mesas with $0 < x < 0.1$ has been observed. Threshold pump powers, efficiencies, and emission characteristics have been determined. Also, a GaAs and $Ga_{1-x}In_xAs (x \leq 0.8)$ mesa diode laser was successfully fabricated. The p-n junction was formed by Zn diffusion and implantation into the top of the mesas. The $Ga_{1-x}In_xAs$ homojunction lasers are the first wavelength-tunable, monolithic electrical injection lasers and have been operated between liquid nitrogen and room temperatures. Monolithic arrays of up to six mesa lasers have been operated with all the lasers oscillating simultaneously. Because these devices are homojunctions, their threshold current densities at room temperature are very high ($\sim$ 170 kA/cm^2), and their efficiencies are low. These diode mesa lasers are the first monolithic nondiscrete injection lasers ever made. They are the first diode lasers ever completely fabricated (including optical cavity formation) monolithically using conventional photolithographic fabrication technology. This development is a significant first in semiconductor laser technology with importance in both integrated optical source development and discrete laser technology.

A monolithic laser structure called an I-bar mesa laser was developed. This double heterojunction GaAs/GaAlAs laser was grown by selective liquid phase epitaxy. The best devices operated at 525 mA drive current with a pulsed, 300 K threshold current density of 7.5 kA/cm^2. Methods of fabricating these devices are discussed. Also, various types of grown waveguides including bends and Y's were demonstrated. For bends, a 3 dB signal attenuation is observed at a radius of curvature of $\sim$ 1.3 mm (50 mils). This radius appears to be a practical lower limit for integrated optical circuit waveguides. The I-bar mesas were combined on a chip with a grown three-layer waveguide. Measured intensity of light transmitted by end-firing from the laser through the curved waveguide was 35% of the laser emission with a narrowband output. Also, etched double heterojunction mesa laser structures were fabricated on underlying waveguides. The emission from these lasers was evanescently coupled to this guide. A coupling of 25% of the laser emission to the guide was observed.

Finally, high quality chalcogenide glass optical waveguides have been developed. Losses as low as 0.4 dB/cm were measured in sputtered As_2S_3 films. Channel optical stripline waveguides were fabricated by overlaying photoresist strips on the glass films. Low-loss channel waveguiding was observed in these structures.

Foreword

This report was prepared by Texas Instruments Incorporated, Dallas, Texas, under Contract No. N00014-73-C-0288. At Texas Instruments the work was performed in the Advanced Technology, Advanced Components, and Physical Sciences Research Laboratories of the company's Central Research Laboratories. Program Managers on this three-phased program were Drs. W. C. Holton, F. A. Blum, and K. L. Lawley. Contributing to the performance of work were Drs. D. W. Bellavance, J. C. Campbell, F. H. Doerbeck, W. C. Scott, and R. K. Watts.

This is the Final Report on the contract and summarizes the results obtained during the period from 1 May 1973 through 31 January 1977. It was submitted for approval in May 1977.

The Program Monitors for the Office of Naval Research were Dr. D. Lewis, CDRs W. Albers and W. F. Hodkins, and LCDRs W. Miller, G. L. Smith, and R. Hudson.

Texas Instruments report number is 08-77-19.

Abstract

This report describes the accomplishment of a three-phased exploratory research program under Contract No. N00014-73-C-0288 to develop the first integrated optical transmitter.

The initial efforts involved the development of a unique (Ga,In)As surface laser and high index infrared glass waveguides. The surface laser is a vapor-grown mesa structure with vertical grown crystalline facets furnishing the optical feedback. The structure can be placed and grown at will on a GaAs substrate using conventional photolithographic techniques. This unique laser structure represents a radical departure from conventional semiconductor laser technology. Ternary alloy $Ga_{1-x}In_xAs$ mesas with $0 < x < 0.2$ were grown and the details of their morphology determined. Optically pumped laser emission from mesas with $0 < x < 0.1$ has been observed. Threshold pump powers, efficiencies, and emission characteristics have been determined. Also, a GaAs and $Ga_{1-x}In_xAs (x < 0.8)$ mesa diode laser was successfully fabricated. The p-n junction was formed by Zn diffusion and implantation into the top of the mesas. The $Ga_{1-x}In_xAs$ homojunction lasers are the first wavelength-tunable, monolithic electrical injection lasers and have been operated between liquid nitrogen and room temperatures. Monolithic arrays of up to six mesa lasers have been operated with all the lasers oscillating simultaneously. Because these devices are homojunctions, their threshold current densities at room temperature are very high (~ 170 kA/cm^2), and their efficiencies are low. These diode mesa lasers are the first monolithic, nondiscrete injection lasers ever made. They are the first diode lasers ever completely fabricated (including optical cavity formation) monolithically using conventional photolithographic fabrication technology. This development is a significant first in semiconductor laser technology with importance in both integrated optical source development and discrete laser technology.

A monolithic laser structure called an I-bar mesa laser was developed. This double heterojunction GaAs/GaAlAs laser was grown by selective liquid phase epitaxy. The best devices operated at 525 mA drive current with a pulsed,

Abstract
(Continued)

300 K threshold current density of 7.5 kA/cm^2. Methods of fabricating these devices are discussed. Also, various types of grown waveguides including bends and Y's were demonstrated. For bends, a 3 dB signal attenuation is observed at a radius of curvature of ~ 1.3 mm (50 mils). This radius appears to be a practical lower limit for integrated optical circuit waveguides. The I-bar mesas were combined on a chip with a grown three-layer waveguide. Measured intensity of light transmitted by end-firing from the laser through the curved waveguide was 35% of the laser emission with a narrowband output. Also, etched double heterojunction mesa laser structures were fabricated on underlying waveguides. The emission from these lasers was evanescently coupled to this guide. A coupling of 25% of the laser emission to the guide was observed.

Finally, high quality chalcogenide glass optical waveguides have been developed. Losses as low as 0.4 dB/cm were measured in sputtered As_2S_3 films. Channel optical stripline waveguides were fabricated by overlaying photoresist strips on the glass films. Low-loss channel waveguiding was observed in these structures.

TABLE OF CONTENTS

TABLE OF CONTENTS
(Continued)

LIST OF TABLES

LIST OF ILLUSTRATIONS

LIST OF ILLUSTRATIONS

(Continued)

LIST OF ILLUSTRATIONS

(Continued)

SECTION I

INTRODUCTION

This is the final report for Contract No. N00014-73-C-0288. It summarizes the accomplishments, previously presented in Annual Reports,[1,2,3] of a three-phase program to develop the first prototype integrated optical transmitter.

The general development of individual circuit elements for fabrication of integrated optical circuits (IOCs) for high data rate optical communications is now receiving much attention. Surface lasers, waveguides, couplers, switches, modulators, and photodetectors are being developed in a number of laboratories both in the United States and abroad. However, the progress toward actual integration of monolithic circuits has been rather slow. One of the most promising emerging technologies for monolithic IOCs is the formation of optical microcircuitry in GaAs and its ternary alloys with Aℓ and In. The Central Research Laboratories of Texas Instruments Incorporated has a program whose aim is to fabricate a monolithic IOC transmitter in epitaxial GaAs and its alloys. The first-generation IOC transmitter will consist of a localized surface laser, which occupies a small portion of a large chip, and channel optical waveguides into which the output of the laser is coupled (see Figure 1).

The properties of (Ga,Aℓ)As and (Ga, In)As permit performance, in principle, of each of the basic functions included in the device of Figure 1: coherent optical emission, passive optical coupling, optical waveguiding and electro-optic modulation/switching. Also, the emission wavelength of the surface laser can be tailored to match regions of low fiber loss by changing the alloy composition. The TI research program will ultimately yield a device that emits coherent radiation into an optical waveguide circuit and operates at room temperature. This device is a prototype optical transmitter in its simplest form.

This exploratory research program emphasized the development of a monolithic laser source of III-V materials grown in place on a semiconductor substrate. Such a source is the heart of an active integrated optical transmitter. Two

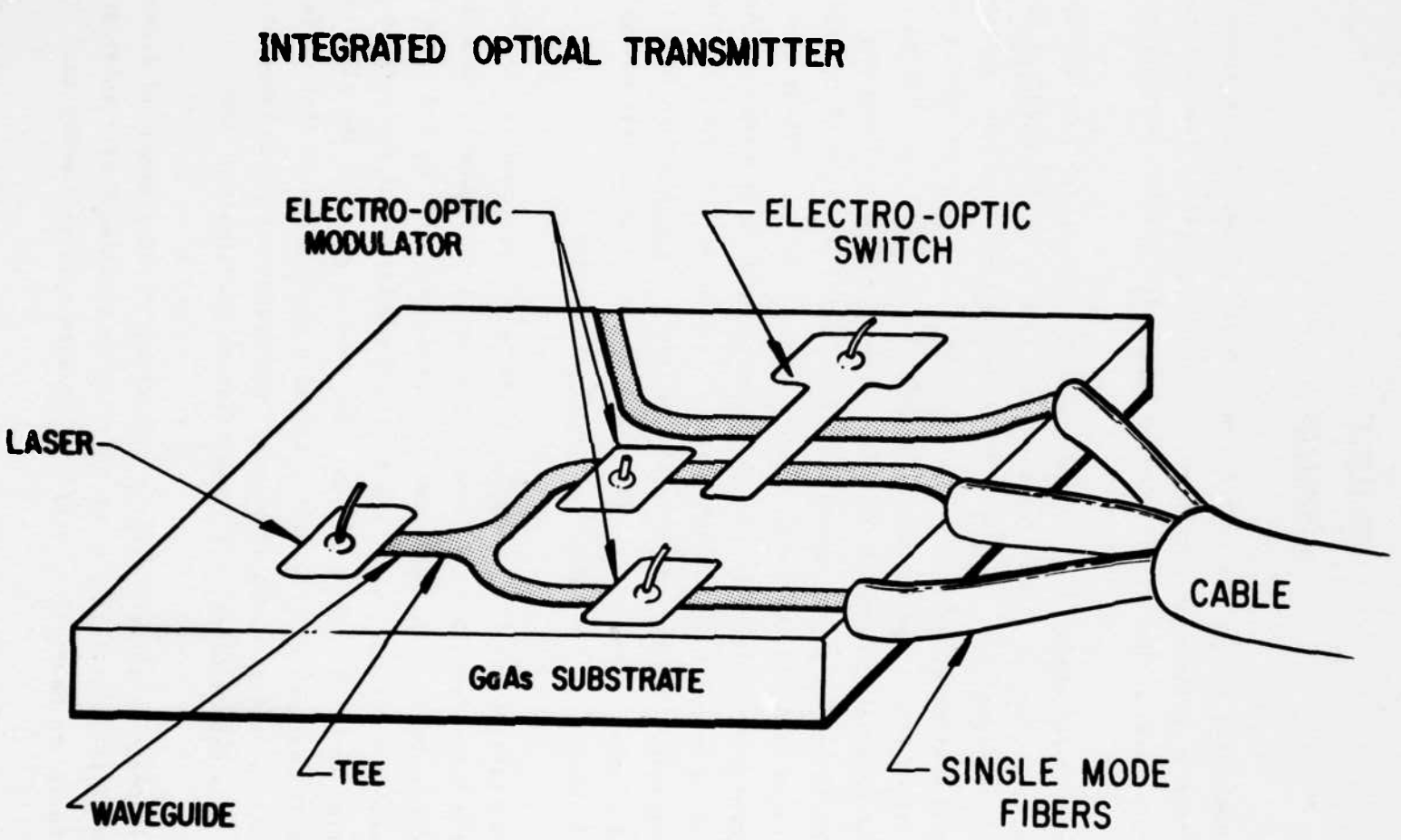

Figure 1 Artist's Schematic of a Monolithic GaAs IOC Transmitter with Its Outputs Coupled to a Fiber Optic Cable

different grown laser sources were investigated: the diamond mesa homojunction laser grown by vapor phase epitaxy (VPE), and, later, the I-bar double heterojunction (DHJ) laser grown by liquid phase epitaxy (LPE). The monolithic laser structures are the first ever to be grown directly without mechanical formation (cleaving, grinding, or polishing of facets or reflecting surfaces to provide an optical resonant cavity). In addition to the laser development, passive waveguides were also grown and integrated with a DHJ I-bar mesa. Complementary experiments with etched mesa DHJ lasers coupled to waveguides and with non-III-V waveguides of chalcogenide glasses were also carried out.

The major accomplishments made on this program are as follows:

- Demonstration of a diffused homojunction GaAs diamond mesa laser.
- Extension of the laser emission wavelength to near 1 μm with (Ga,In)As diffused homojunction diamond mesa laser structures.
- Demonstration of room temperature pulsed operation of a DHJ I-bar mesa laser.
- Development of techniques for the mass fabrication of laser diodes.
- Demonstration of various passive waveguide structures such as rib and dielectric striplines in straight, curved, and divided ("Y's") sections.
- Demonstration of the first prototype integrated optical circuit with an I-bar mesa laser whose output is end-fired coupled to a grown waveguide. These elements combined with optical modulators and switches being developed under Contract No. N00014-75-C-0501 are required for a transmitter circuit.
- Development of very low-loss chalogenide glasses for passive waveguides in the infrared.

The remainder of this report is divided into eight sections. In Section II, diamond mesa lasers of GaAs and (Ga,In)As are discussed. This is followed in

Section III with a discussion of the DHJ I-bar mesa laser and of possible structural variations for performance optimization. Grown waveguide results are presented in Section IV. Coupling experiments with I-bar and etched mesa laser sources and grown waveguides are discussed in Sections V and VI. The final technical section (VII) reviews progress on chalcogenide glass waveguides. A summary with emphasis on unresolved issues appears in Section VIII.

SECTION II

DIAMOND MESA LASERS

The first nondiscrete laser structure demonstrated on this program was the diamond mesa laser. The name is derived from the unique shape of the structure and its relationship to growth morphology in III-V compounds. Structures of GaAs and (Ga,In)As alloys were made. These lasers were the first of any type to use as-grown crystalline facets for optical feedback. Furthermore, they are the first nondiscrete diode lasers, and, as such, represent a radical departure from conventional semiconductor laser technology.

The following three subsections describe the growth and morphology, optical pumping, and injection laser operation of these unique semiconductor lasers.

A. Mesa Growth and Morphology

Methods were developed for the growth of mesa structures of GaAs and (Ga,In)As alloys that have the requisite geometry of an optical Fabry-Perot cavity. In this section the aspects of material synthesis that relate to the formation of these unique structures are presented.

The method of selective vapor phase epitaxy developed for this program takes advantage of the unique crystallographic variation of the growth rates of the major planes in GaAs and (Ga,In)As materials. To illustrate this point, Figure 2 shows a stereographic projection of the {111} and {100} planes and their angular relationship to the {110} planes. This projection shows that four {111} planes are perpendicular to the (011) plane. Specifically, the A-set, $(\bar{1}\bar{1}1)$ and $(\bar{1}1\bar{1})$, and the B-set, $(1\bar{1}1)$ and $(11\bar{1})$, are perpendicular to the (011) plane. The A and B-sets refer to the gallium and arsenic planes, respectively. A diamond pattern with its points defined by the angular relationship between {111} planes then represents a suitable geometry for growth on the {110} planes because the resulting opposite {111} planes would be parallel to each other and perpendicular to the {110} plane. The difficulty in using this specific geometry is

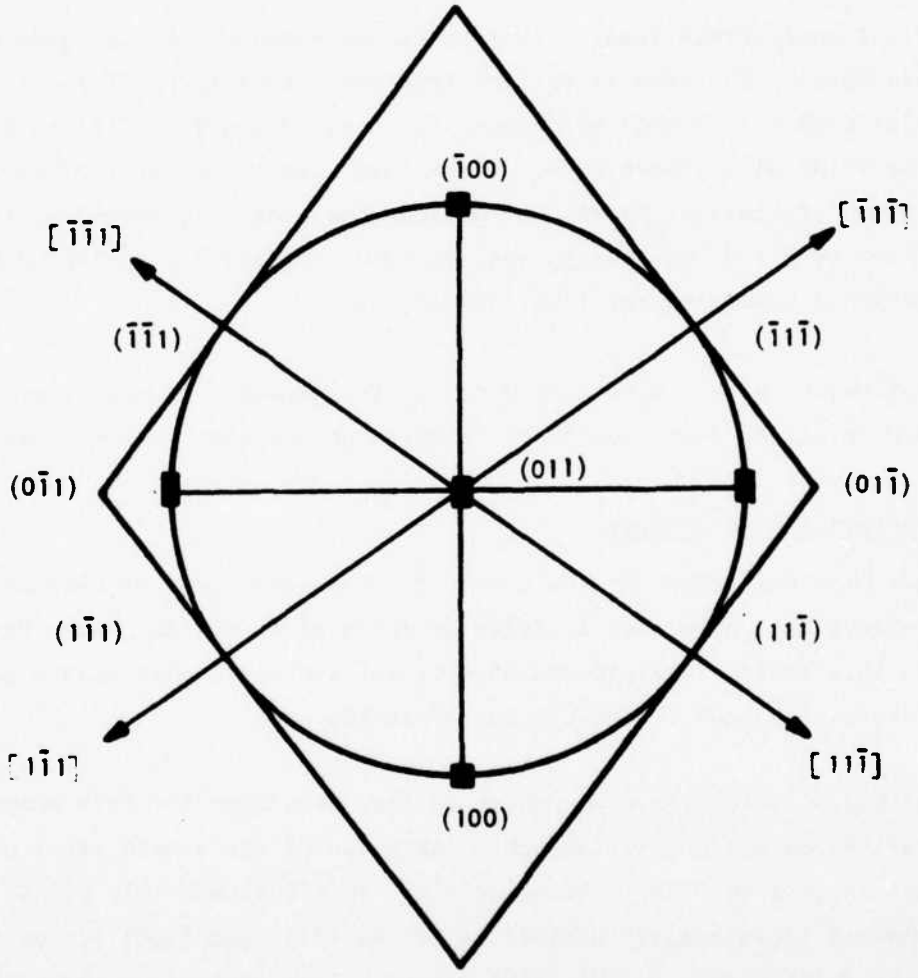

Figure 2 {110} Stereographic Projection Diamond Mesa Geometry

that under normal growth conditions of excess arsenic in the gas phase, the growth rate of the A-faces is greater than that of the B-faces. Symmetric growth would not be realized. Earlier investigations by Shaw[4,5] of the growth of GaAs by vapor phase methods showed that the relative growth rates of the A and B-faces could be varied drastically by changing the ratio of gallium species to arsenic species in the gas phase from which epitaxial layers were deposited. This variation is shown in Figure 3 where the growth rate in μm/hr is plotted against the Ga/As ratio. The growth rate on the A-faces decreases with increasing Ga/As; whereas, the rate on the B-faces increases with increasing ratios. The A and B-face rates are equal at about a ratio of one. Not only are the rates equal, but they are reasonably low, i.e., about 10 μm/hr. Shaw's observations formed the basis for satisfying a necessary condition for growth of a diamond structure. The other necessary condition is that the {111} planes must be faceted to form the walls of a cavity. This condition exists if the growth rate of the {111} represents a local minimum in the rate of adjacent planes. This situation also exists. The remaining problem was the verification of this concept by determining the operating parameters of a suitable vapor growth system.

A vapor phase system using AsH_3, $HC\ell$, H_2, and gallium (and later a separate source of indium) was utilized. Figure 4 is a schematic drawing of the system. The diameter of the tube in the deposition zone was 52 mm; in the gallium and indium source zone, 18 mm. The exposed gallium and indium surfaces are about 40 cm^2. Utilization of the reacting $HC\ell$ for both gallium and indium reactions was measured to be between 90 and 95% for the flow rates and source temperatures generally used. An additional $HC\ell$ source was added to prevent the formation of GaAs or (Ga,In)As in the vicinity of the AsH_3 input downstream from the group III sources. The $HC\ell$ and AsH_3 were supplied as mixtures diluted to either 5 or 10% in hydrogen. Bottled gases were purchased from Precision Gas Co., the gallium from Alusuisse Metals, and the indium from Atomergic Chemmetals. Additional hydrogen from a Pd-Ag diffuser was used. The system was loaded and

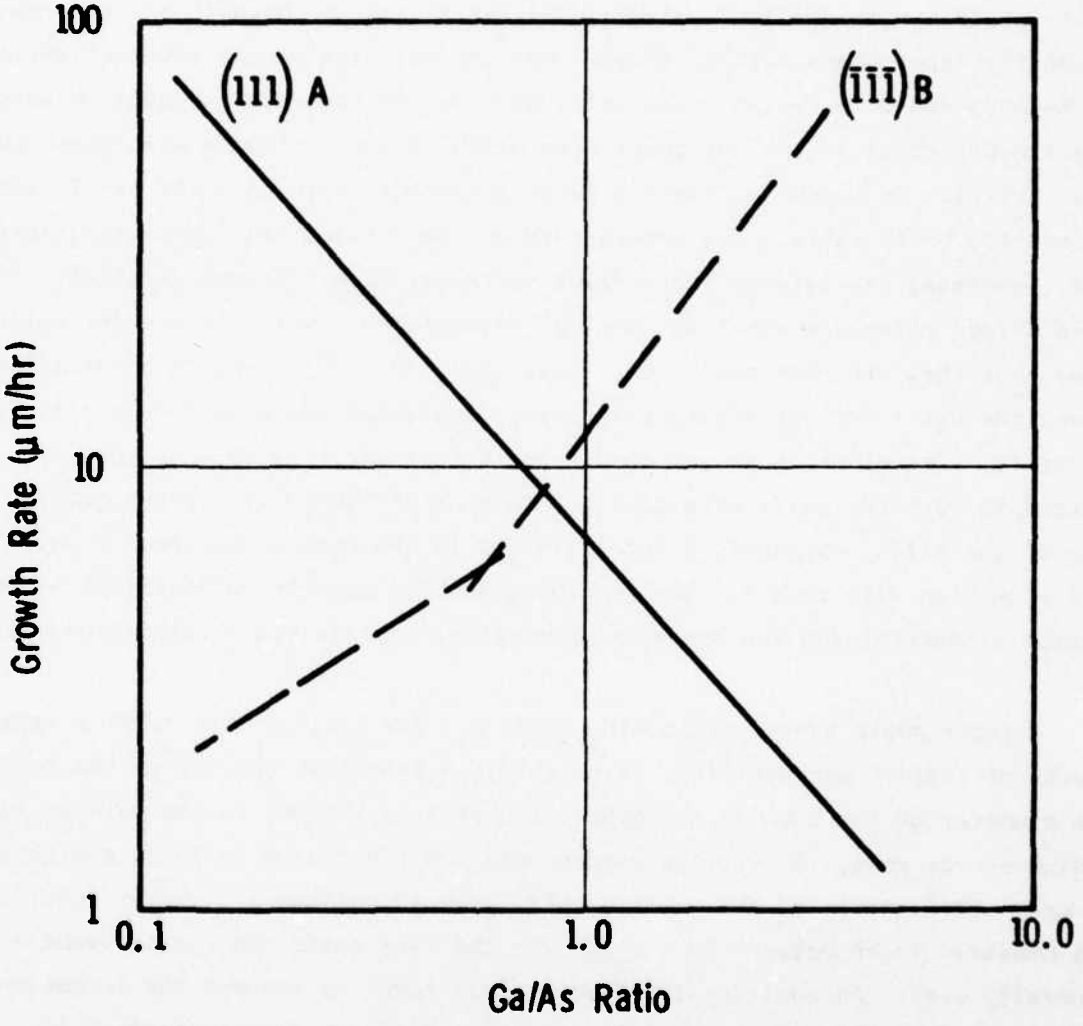

Figure 3 Variation of the Growth Rates of the A and B-Face of GaAs as a Function of the Ga/As Gas Composition

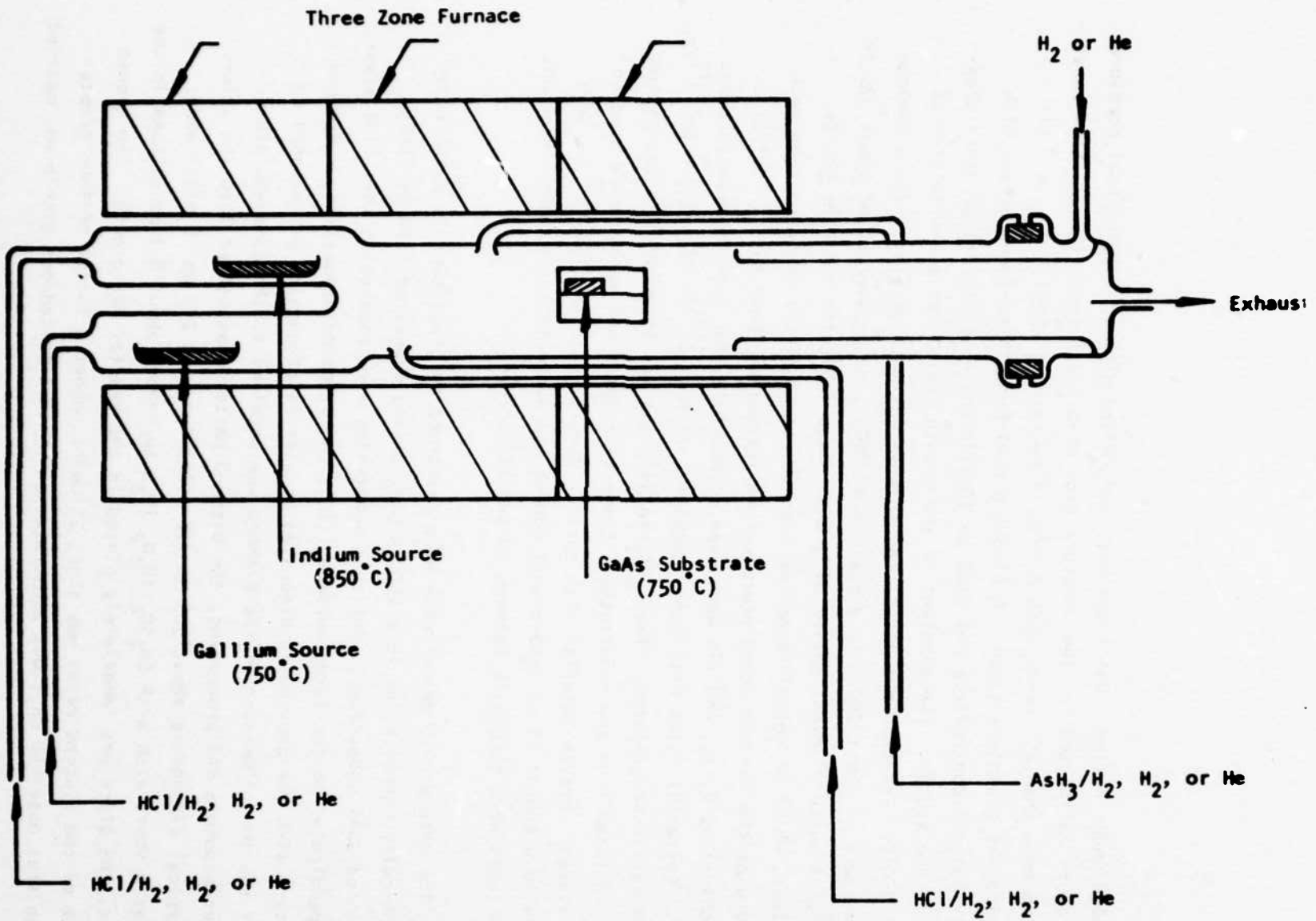

Figure 4 (Ga,In)As Vapor Phase Reactor Schematic

unloaded under helium. Gas flows were controlled with stainless steel pressure regulators calibrated for the pressure drop across a Pyrex orifice: flow rates were no more than 250 cc/s, with a total flow rate of about 450 cc/s. All plumbing was stainless steel. A Lindberg Hevi-Duty three-zone furnace with Barber-Coleman controllers was used to provide the necessary temperature gradient in the system. The gradient in the growth region was about 10°C/cm at about 750°C. The gradient across the sources was much greater, with a minimum temperature of about 700°C to a maximum of 850°C, or an average of about 775 to 800°C. A cursory investigation of growth rates indicated that the source gradient, which is certainly not necessary, had no effect on deposition rate so long as the maximum temperature was maintained at about 850°C. Sulfur monochloride, $S_2C\ell_2$, and tin were used successfully for growing heavily doped GaAs. Epitaxial films with donor densities in the 10^{18}/cc range to high 10^{17}/cc could easily be prepared. The $S_2C\ell_2$ in hydrogen was introduced to the system just upstream from the substrates. Commercial gases and metals were used in the system. N-type material with carrier densities in the low 10^{16}/cc were normally prepared if no intentional dopant was added to the system. Reactant flow rates were generally between 50 and 150 cc/min.

The mesa growth experiments were performed by depositing in photolithographically formed holes in a 1500 Å SiO_2 plasma deposited film on {110} oriented GaAs substrates. Polished substrates were cleaved on the {110} planes perpendicular to the large surface {110}. After oxide deposition, a diamond pattern with the previously discussed angular relationships was aligned so that the long dimension of the diamond was parallel to the cleavage plane. After exposure and processing, the diamond pattern was etched into the oxide. A typical diamond is about 305 μm (12 mils) long and 203 μm (8 mils) wide. After a short etch with $5H_2SO_4:1H_2O_2:1H_2O$ to remove about 0.1 μm of GaAs in the hole, the slice was immediately placed in the reactor for growth. The growth rate of the diamond mesas was about 25 μm/hr, about a factor of four greater than that observed on {100} substrates on which simultaneous growth was carried out.

The mesas prepared by the technique described above have well-developed {111}, {110}, and {100} facets, provided the Ga/As ratio is properly chosen. To illustrate the effect of ratio variation, a ratio of 1.94 results in well-formed symmetric diamonds, but a ratio of 1.00 does not, as illustrated in Figure 5. Figure 6(a), an SEM photograph of a grown GaAs mesa, shows the well-defined facets which define the sides of the optical cavity. A photograph of an array of GaAs mesas is shown in Figure 6(b). The top surface of the best mesas is flat to within about 0.05 μm, as illustrated in Figure 7. Approximately 80 to 90% of the mesas on a good slice several square centimeters in area are suitable for optical experiments.

Mesas of (Ga,In)As alloys were also prepared. To do this, a ratio of In to Ga of about two in the gas phase results in mesa compositions of about $Ga_{0.95}In_{0.05}As$. This ratio is achieved by varying the HCℓ inputs over the Ga and In charges and assuming complete conversion of the HCℓ to the monochlorides of In and Ga. The InAs content of the alloys was determined by room-temperature photoluminescence measurements. No grading of InAs content during growth was attempted. Mesas with as much as 20% InAs have been grown, but the perfection of these mesas is not as good as that of GaAs ones. An SEM micrograph of a $Ga_{0.92}In_{0.08}As$ mesa is shown in Figure 8.

In conclusion, a method was developed for the growth of GaAs and (Ga,In)As mesas. This method depends upon the proper choice of major plane relationships and associated growth rate control for the formation of symmetric faceted mesas.

B. Optically Pumped Mesa Lasers

In order to test the suitability of mesas as lasers prior to fabrication into p-n junction injection lasers, the diamond structures were optically pumped. A schematic of the apparatus used for the optical pumping experiments is shown in Figure 9. The pump laser is a Chromatix, doubled Nd:YAG laser operating at 0.532 μm and Q-switched at a 50 Hz repetition rate. The pump laser pulses

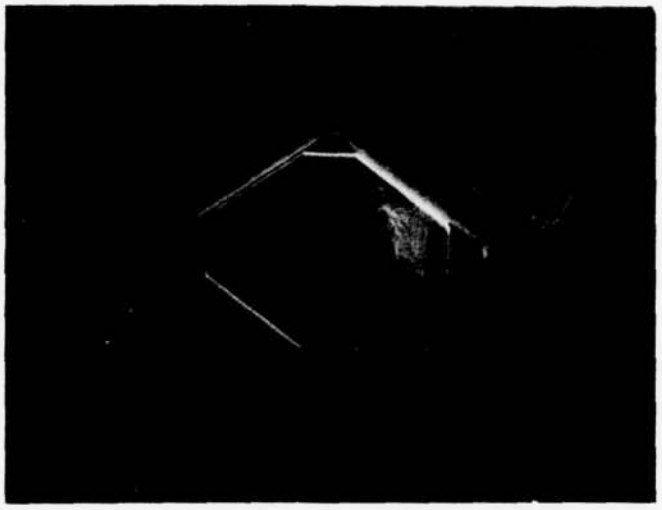

Figure 5(a) Photomicrograph of a Symmetric Mesa, Ga/As = 1.94

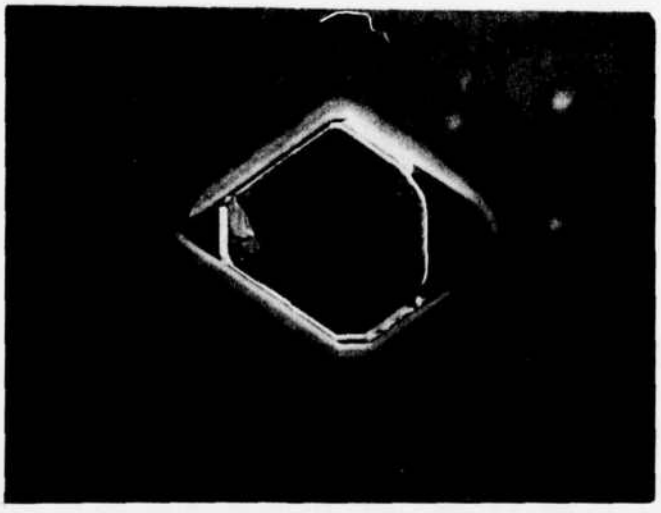

Figure 5(b) Photomicrograph of an Asymmetric Mesa, Ga/As = 1.00

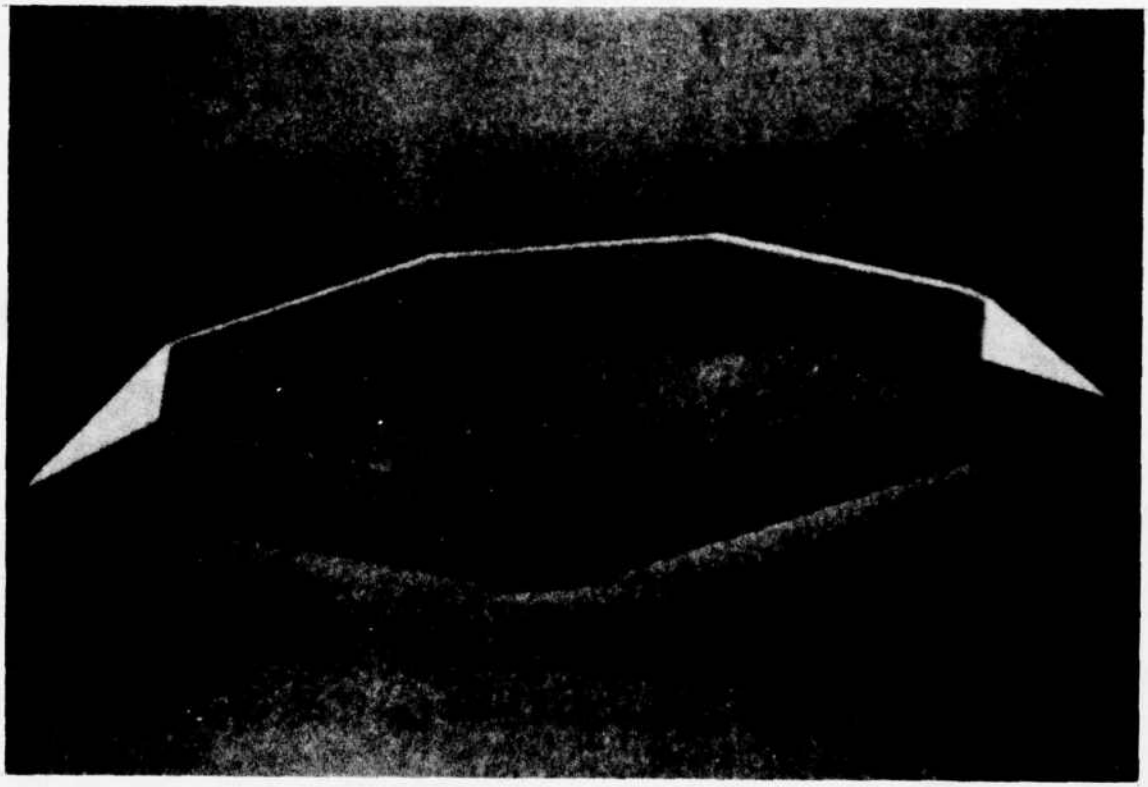

Figure 6(a) SEM Photomicrograph of a GaAs Mesa

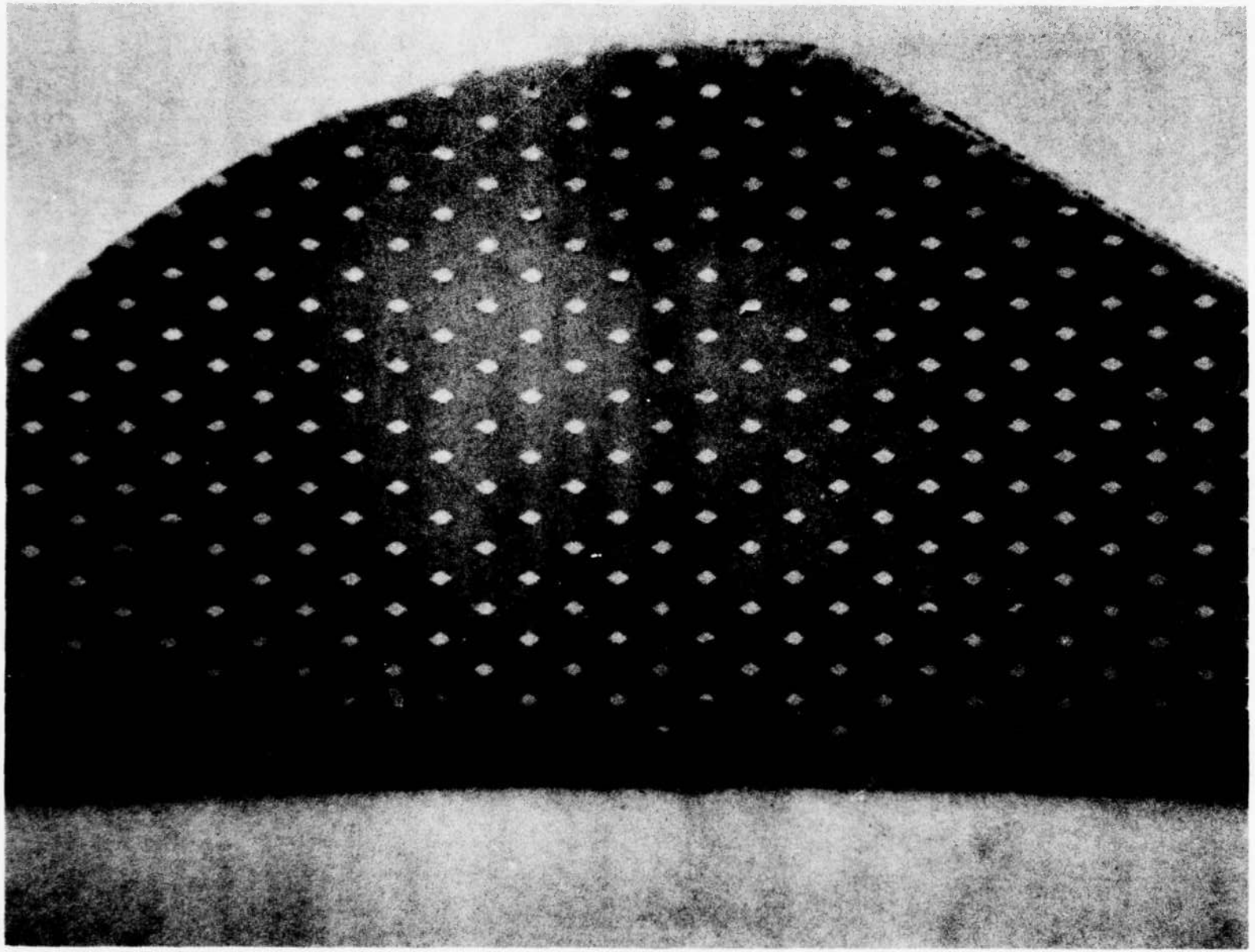

Figure 6(b) Photograph of a Slice Containing Several Hundred Mesas

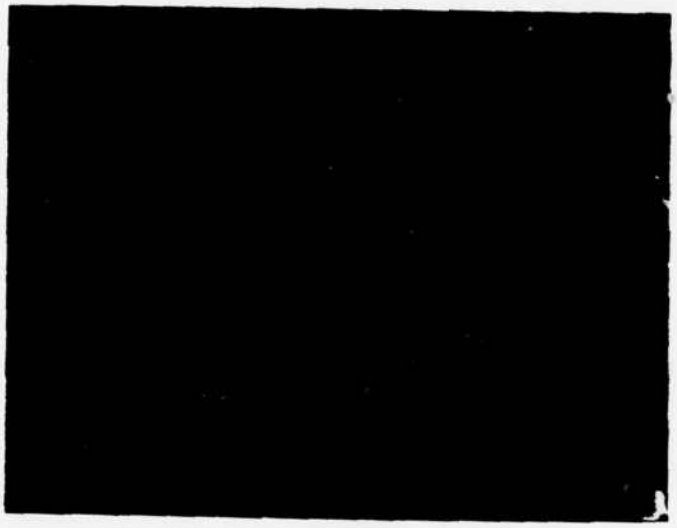

Figure 7 Photomicrograph of an Interference Fringe Pattern Superimposed on a GaAs Mesa Surface

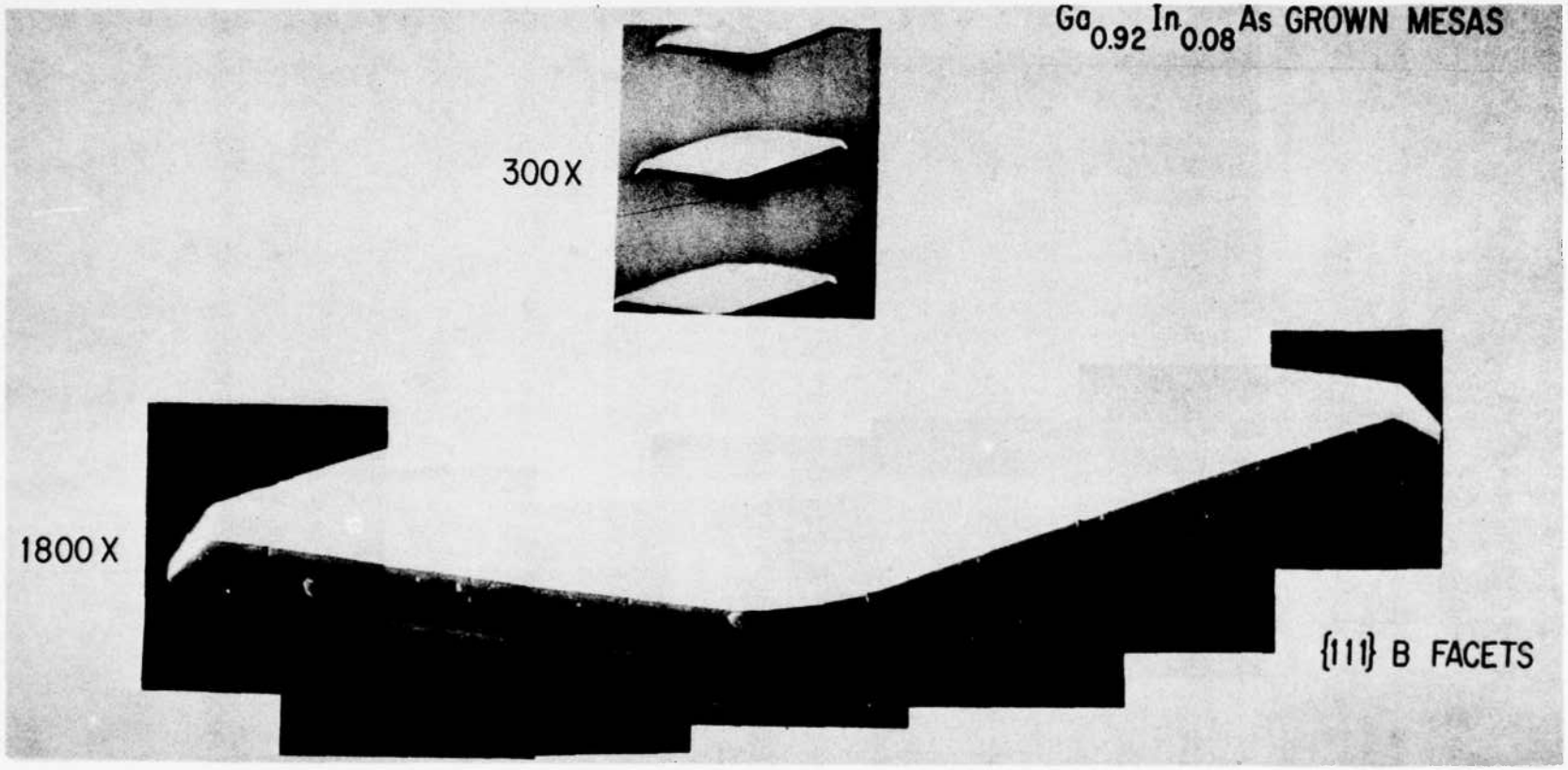

Figure 8 SEM Photomicrograph of a $Ga_{0.92}In_{0.08}As$ Mesa

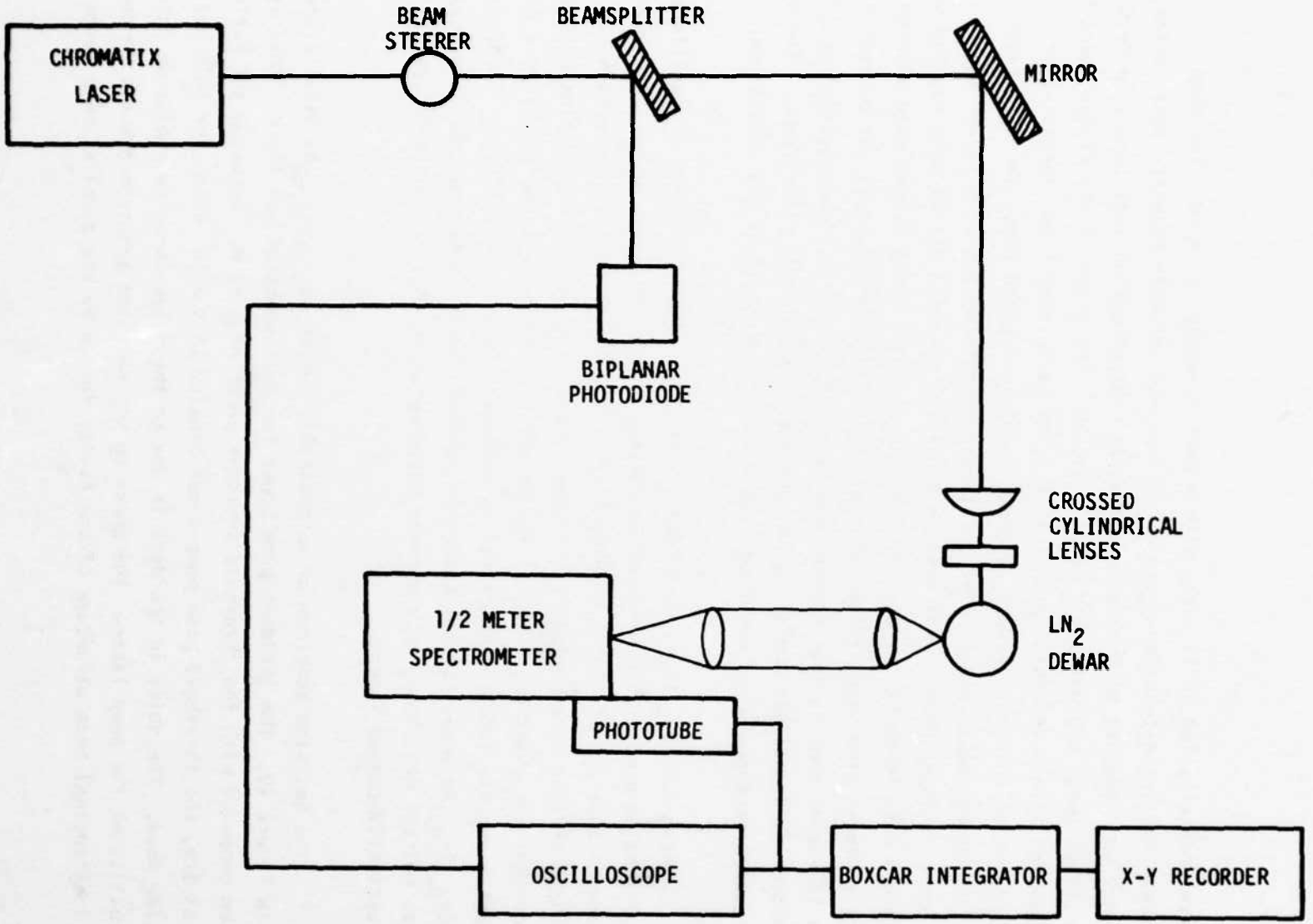

Figure 9 Diagram of the Optical Pumping Apparatus

were nominally 100 ns in width with a peak intensity of 3 kW. The pump laser beam was attenuated using a continuously variable Inconel coated attenuator and focussed on the mesas using two crossed cylindrical lenses to form a stripe image approximately 50 μm x 250 μm. The width of the stripe focus was measured with a variable optical slit. The strip pump focus forces laser oscillation to occur between opposite parallel diamond faces and eliminates circulatory bounce modes. The mesas were mounted on the cold finger of a liquid nitrogen dewar. For ease in handling, the mesa slices were usually cut into 4 x 4, 16-member arrays for optical pumping. These arrays were mounted to a copper stud using vacuum grease. Emission from the mesas was passed through a 1/2-meter grating spectrometer and detected with an S-1 photomultiplier. The phototube signal was amplified and averaged with a boxcar integrator. The mesa laser output power was measured with a calibrated biplanar S-1 photodiode.

As-grown $Ga_{1-x}In_xAs$ mesa lasers with $0 < x < 0.1$ were made to oscillate by optical pumping. This range of In content (0 to 10%) gives an emission wavelength coverage of 8300 Å to 9400 Å at 77 K. The threshold pump powers for these devices were nominally the same, i.e., no significant variation with In content was observed. Typical lasers efficiencies were a few tenths of a percent, again roughly independent of the In content of the ternary alloys. While the $Ga_{0.9}In_{0.1}As$ mesas did not generally exhibit the perfection of the GaAs mesas, as pointed out above, this was not detrimental to their characteristics as optically pumped lasers.

The emission spectrum of an optically pumped $Ga_{0.92}In_{0.08}As$ mesa is shown in Figure 10. The incident pump power for this spectrum was 110 W. This is to be compared with the threshold incident power of ~ 60 W. Assuming 30% reflectivity, the threshold peak pump power density is 3×10^5 W/cm^2 for this particular mesa. The noise in the data is due to the pulse-to-pulse amplitude instability of the pump laser. The peaks in the emission spectrum are due to the longitudinal mode structure of the cavity formed by the parallel mesa faces

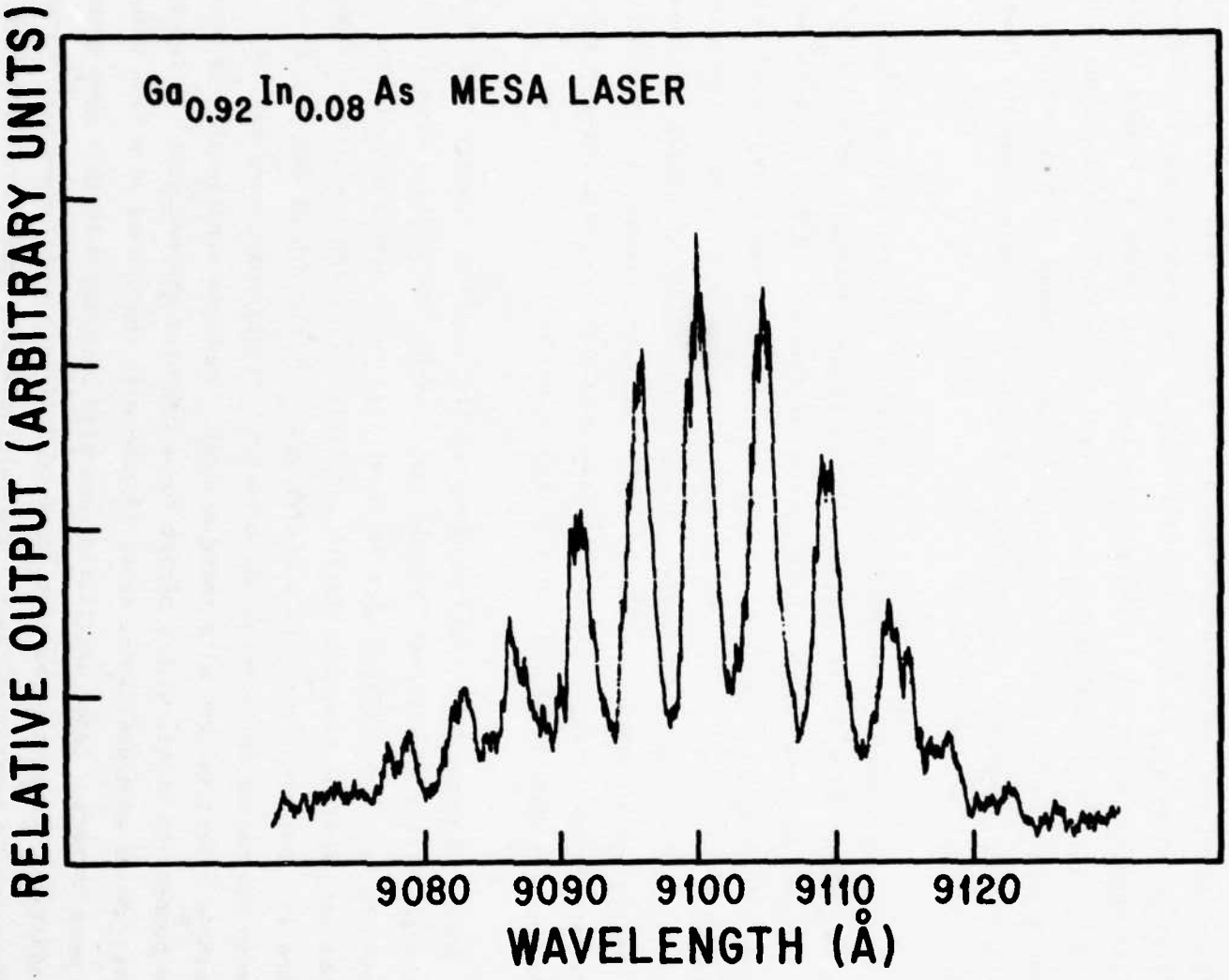

Figure 10 Emission Spectrum of an Optically Pumped $Ga_{0.92}In_{0.08}As$ Mesa Laser

($\simeq$ 175 μm apart) and are uniformly separated by 4.5 Å. This mode spacing yields an effective index $n_{eff} = [n - \lambda(dn/d\lambda)] \simeq 5.3$. The spectrometer resolution for this spectrum was $\simeq$ 0.5 Å; whereas the individual peaks of Figure 10 are about 2 Å wide. This width probably results from unresolved transverse mode structure typical of lasers of this type. When the mesas were pumped into saturation, the transverse mode structure became more apparent and the longitudinal mode structure was obscured.

The lowest threshold incident powers observed for both GaAs and (Ga,In)As mesas were about 25 W, which yields a threshold pump intensity of $\sim 1 \times 10^5$ W/cm^2. This is to be compared to the threshold intensities of $\sim 0.5 \times 10^5$ W/cm^2 which we observed using the same laser to pump cleaved, discrete platelets of epitaxial GaAs with $n \sim 1 \times 10^{16}$ cm^{-3}. The threshold pump intensities vary from mesa to mesa. Typically, the ratio of the highest to the lowest threshold was about 3, and the average threshold was about double the lowest threshold. Generally, every mesa (> 95%) that appeared well developed under examination with a microscope could be made to oscillate by optical pumping.

Some GaAs mesas were found to have peculiar emission spectra thought to be characteristic of internal "bounce" modes within the mesas. However, the thresholds for these devices were no lower than those previously observed for normal longitudinal mode oscillation. A typical emission spectrum is shown in Figure 11. Note that there is a single peak with a width of about 20 Å, which is much too narrow for spontaneous emission. Furthermore, very definite threshold effect is seen with these devices. In these experiments the mesas were pumped, as usual, with a stripe focus oriented perpendicular to two parallel faces. Mesas were positioned so as to pump with the stripe on a line between the mesa corners. Laser oscillation was also observed with this pump geometry. In addition, the same mesas were found to oscillate when pumped with a round spot formed by a spherical lens. The threshold pump power densities were nominally the same for all three cases. The reason for the preferential

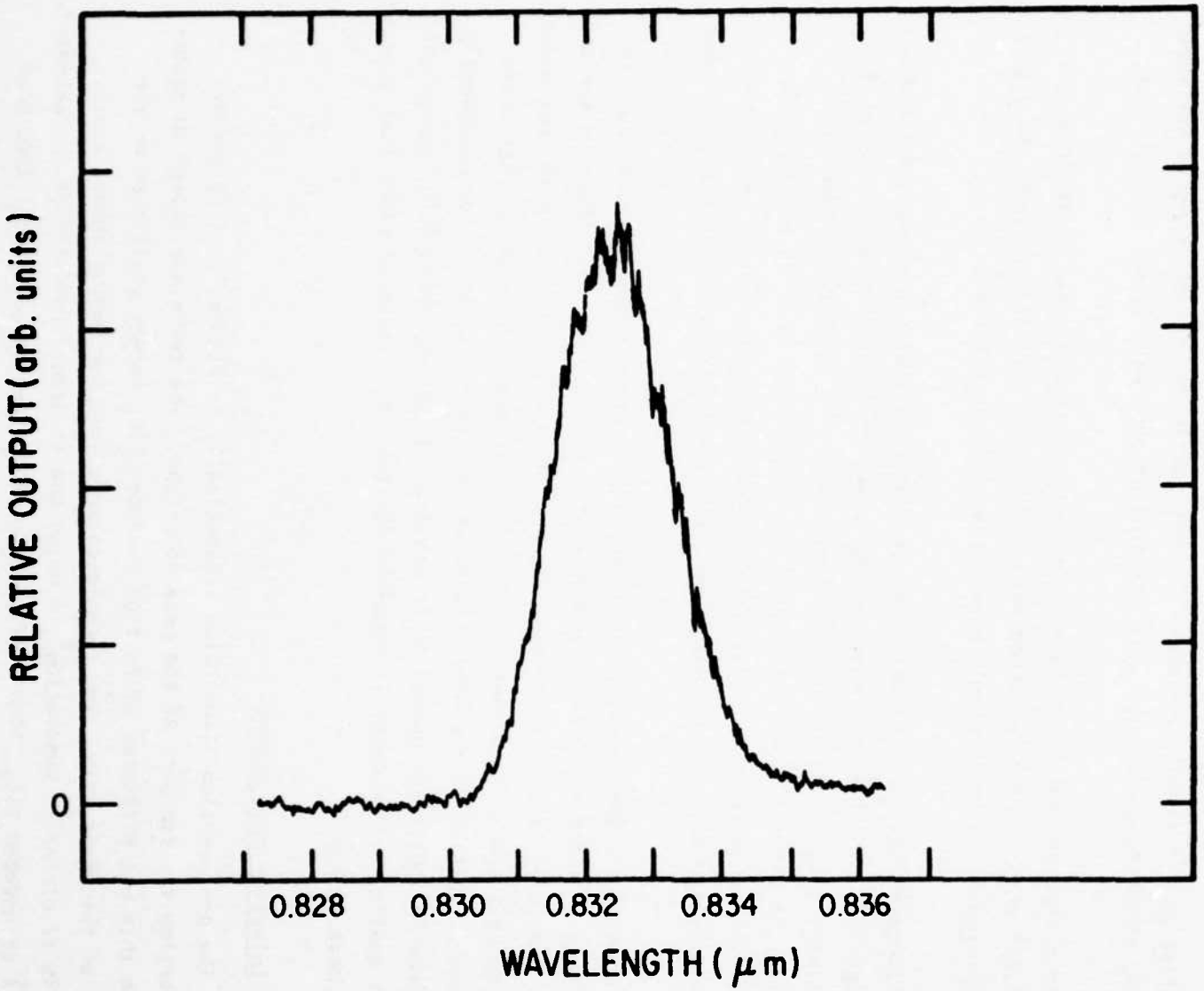

Figure 11 Emission Spectrum of an Optically Pumped GaAs Mesa Laser Showing a Lack of Longitudinal Mode Structure. This suggests the laser is operating in circulatory bounce modes (see text).

excitation of the circulatory modes in this particular set of mesas is not known. However, it may be associated with material of particularly low optical loss.

In a separate set of measurements, several runs of mesas [both GaAs and (Ga,In)As] were chemically etched before they were optically pumped. No significant reduction in threshold power densities was observed.

Elongated $Ga_{0.9}In_{0.1}As$ bar mesas were also optically pumped. Longitudinal mode spacings of 7.8 Å were observed for a 102 μm (4 mil) wide bar. From this we estimate $n_{eff} \approx 5.7$, in close agreement with the value determined for $Ga_{0.9}In_{0.1}As$ diamond mesas with facet separations of 178 μm (7 mils). This result further supports our previous conclusion that the diamond mesas showing strong longitudinal mode structure were not running in circulatory bounce modes.

Some of the GaAs mesa slices of poorer geometrical quality were found to oscillate in spite of surface roughness of 0.5 to 1.0 μm. The observed threshold power densities were in the range 1 to 4×10^5 W/cm^2, identical with that observed for the best smooth (roughness $\lesssim$ 0.05 μm) GaAs mesas. This shows that while extreme perfection of the mesa structures is attainable, it is not necessarily required for optically pumped laser action. Of course, reasonably high geometrical quality of the mesas is required for the fabrication of electrical injection mesa lasers.

C. Injection Mesa Lasers

The p-n junction illustrated schematically in Figure 12 is formed by converting the top part of the mesa to p-type. The technique chosen to accomplish this was diffusion of Zn from Zn-doped SiO_2 layers positioned on the tops of the mesas only. Two techniques were used for making these layers. One is rf discharge deposition[6] in which the structure consists of approximately 100 Å of undoped SiO_2, 1000 Å of Zn-doped SiO_2, and an additional 2000 Å of undoped SiO_2 deposited over the whole slice. The 100 Å SiO_2 layer prevents

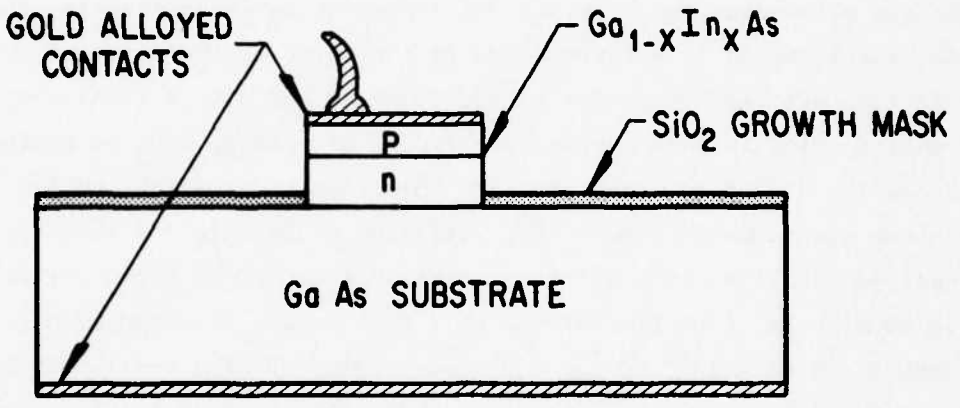

Figure 12 Schematic Cross Section Diagram of the Injection Mesa Laser

direct reaction of the GaAs with Zn. The top 2000 Å layer seals the Zn-doped layer, thereby reducing the loss of Zn from the source layer. With conventional photolithographic masking, the oxide sandwich was removed from all portions of the slice except the tops of the mesas.

A second technique is to implant Zn into a 500 Å thick layer of SiO_2. This technique eliminates the necessity of photomasking and patterning the doped oxide, since the Zn is not implanted in the oxide on the sides of the mesas. The Zn ions are implanted with an energy of 20 keV with a total dose of 10^{16} cm^{-2}. The entire slice is then coated with 2000 Å of undoped SiO_2 to protect the mesa walls during diffusion. The junction formation steps using the ion implantation technique are shown in Figure 13. Diffusion of Zn into the slice is accomplished by heating the slice in a nitrogen atmosphere at 800 to 850°C for periods from 10 to 40 minutes. Junction depths of 1 to 6 μm are obtained with a surface Zn concentration of $\sim 10^{20}$ cm^{-3}. A stained angle-lap of a p-n junction in a heavily doped mesa ($n \sim 10^{18}$ cm^{-3}) is shown in Figure 14. The junction is 4.0 μm deep and flat across the full width of the mesa. A plot of Zn concentration vs depth for a GaAs device is shown in Figure 15. These data are taken using a calibrated spreading resistance probe on an angle-lapped device. Some of the devices have been diffused without patterning the Zn-doped oxide so that Zn enters both the sides and the tops of the devices. While this does produce a narrow lossy region at the edges of the optical cavity, low threshold lasers have been successfully fabricated in this manner.

After removal of the SiO_2 layers, electrical contacts are formed by (1) selectively electroplating gold to the mesa tops and the back of the slice, (2) alloying the gold at $\sim$ 450°C in a forming gas atmosphere, and (3) again electroplating gold on the mesa tops and back of the slice. Photomasking is used to prevent plating on other parts of the slice. Both full surface and 64 μm (2.5 mil) stripe contacts are used. Diced chips, each containing two to six mesa devices, are then soldered to a gold-plated header (mesa up). The individual mesas are contacted with 25 μm (1 mil) gold wire using a thermo-compression ball bonder or solder.

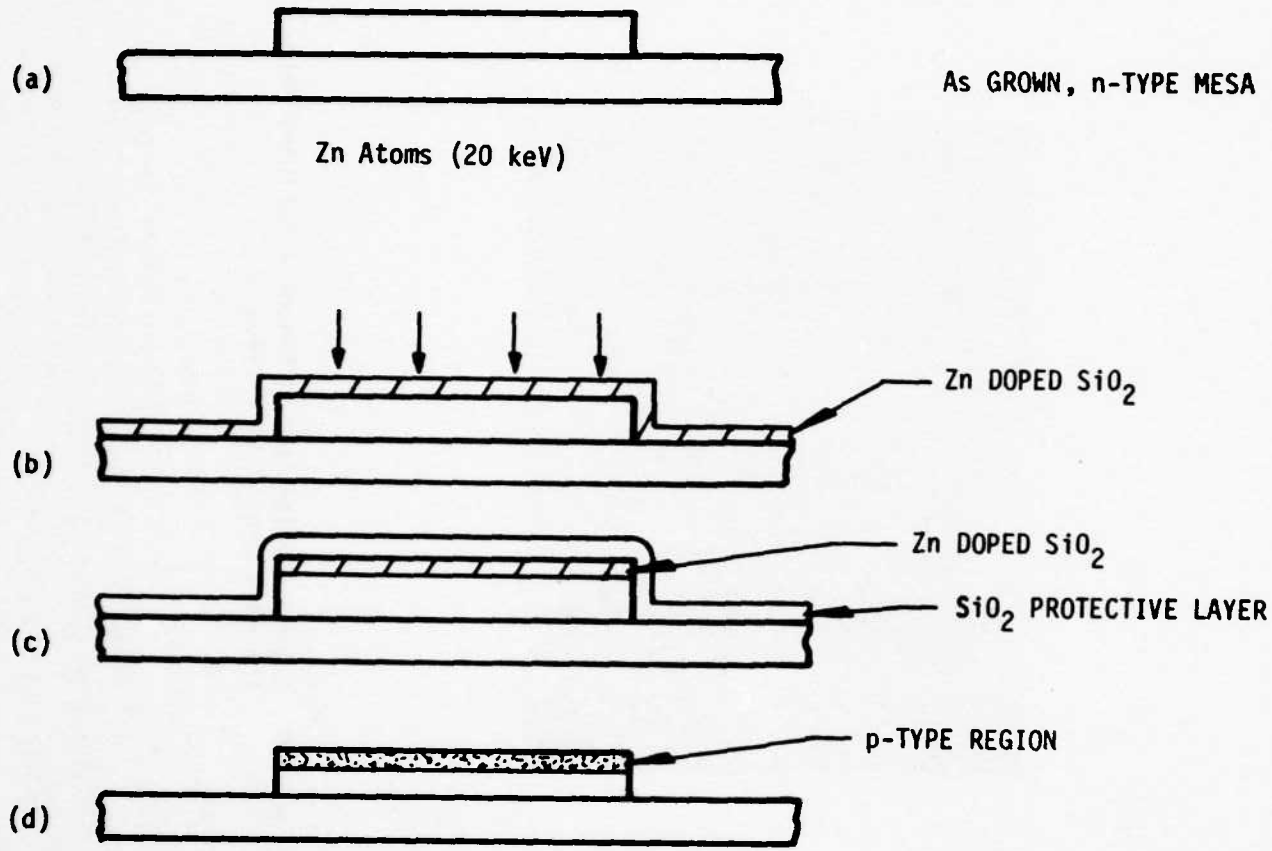

Figure 13 Injection Mesa Laser Junction Formation Steps: (a) As-Grown, n-Type Mesa; (b) Slice Zn Implanted; (c) Slice after Photolithography; (d) Slice after Diffusion and Oxide Removal

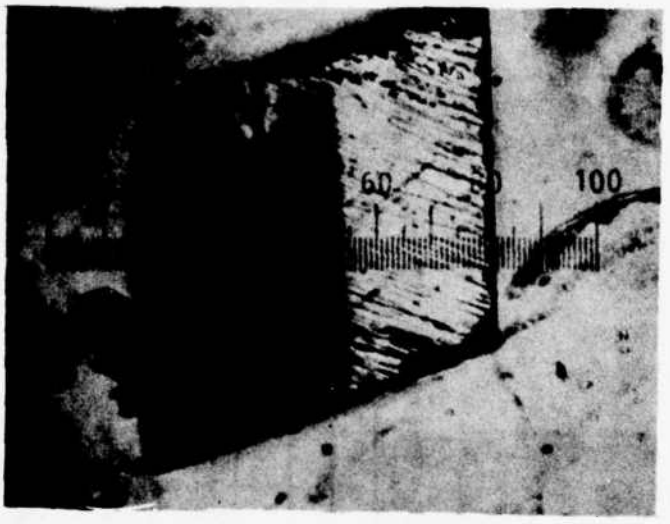

Figure 14 Stained Angle-Lap Section of a Diffused Mesa. The dark region is p-type.

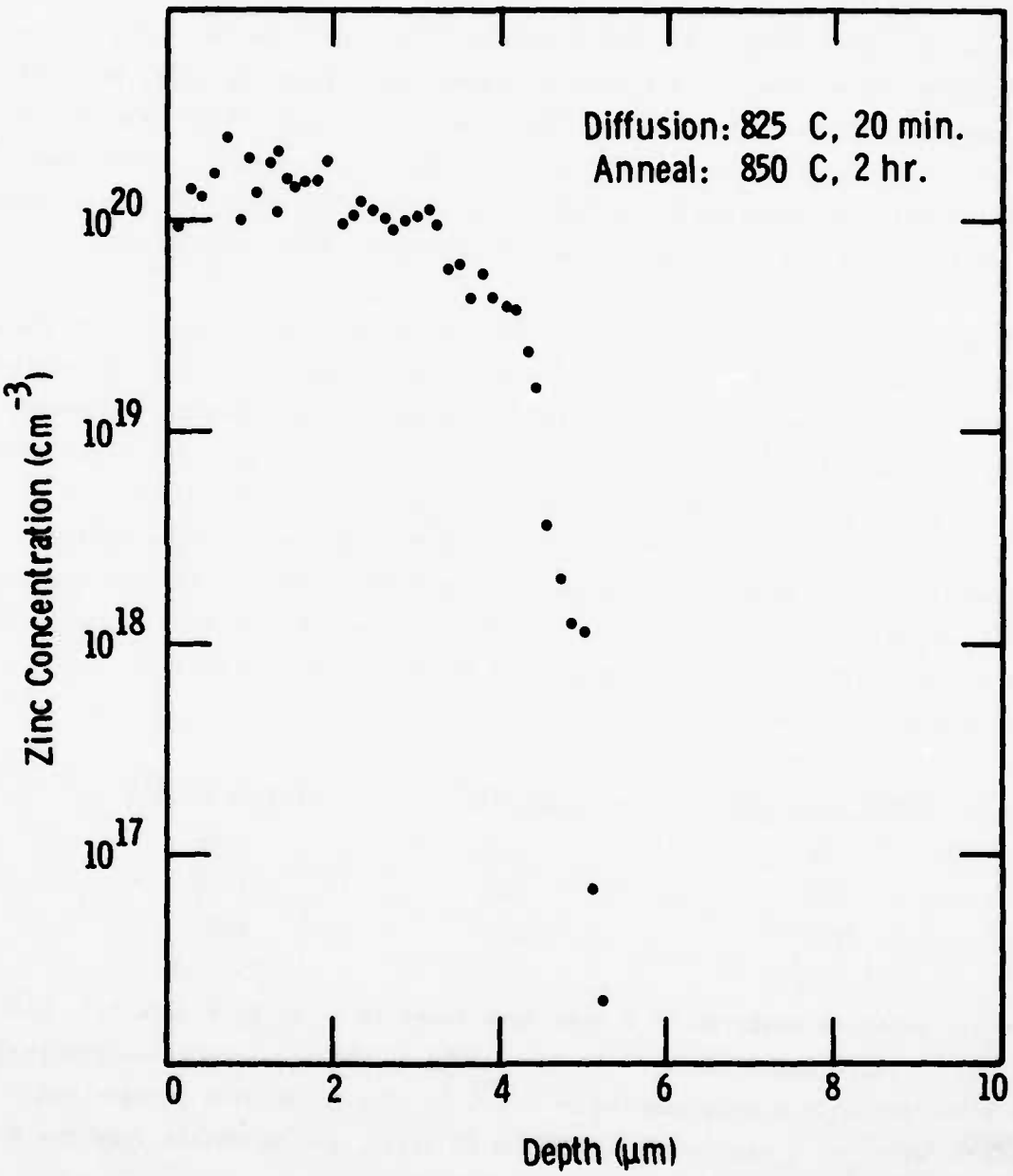

Figure 15 Zn Concentration vs Depth for a Mesa Junction

D. Laser Characteristics

After the mesa diodes were fabricated and mounted on headers, the devices were attached to a copper cold finger in a dewar and cooled (usually to 77 K). The diodes are excited with a 100 to 200 ns pulse at a repetition rate of 100 to 500 Hz. The laser emission spectra are obtained with a 3/4 m monochromator and an ITT FW118 photomultiplier which has an S-1 photocathode. The peak output power of the lasers is measured with an ITT F-4000 biplanar photodiode.

Injection lasers have been fabricated from mesas with n-type carrier concentrations between 10^{16} cm^{-3} and 3×10^{18} cm^{-3}. The threshold current densities (at 77 K) of the GaAs lasers are strongly dependent on the carrier concentration,[7] ranging from ~ 2 kA/cm^2 for the best heavily doped devices to ~ 100 kA/cm^2 for lightly doped ones. The high thresholds for the lightly doped diodes are a result of the difficulty of achieving population inversion in these devices. Selected Zn-implant GaAs devices have been operated at dry ice (200 K) and room (300 K) temperatures with threshold current densities of ~ 30 kA/cm^2 and 100 kA/cm^2, respectively. The emission wavelength and threshold current density of one device are given below.

Temperature (K)	J_{th} (kA/cm^2)	Wavelength (Å)
77	2.0	8470
200	24	8750
297	170	8980

A typical emission spectrum of a GaAs mesa laser is shown in Figure 16. Note that the emission spectrum is centered at 8390 Å, showing strong longitudinal mode structure with a mode spacing of ~ 4.5 Å. The separation between two parallel facets of a mesa diode is 178 μm (7 mils), and we obtain from the 4.5 Å longitudinal mode spacing

$$n_{eff} \equiv n - \lambda \frac{dn}{d\lambda} = 4.5 \quad .$$

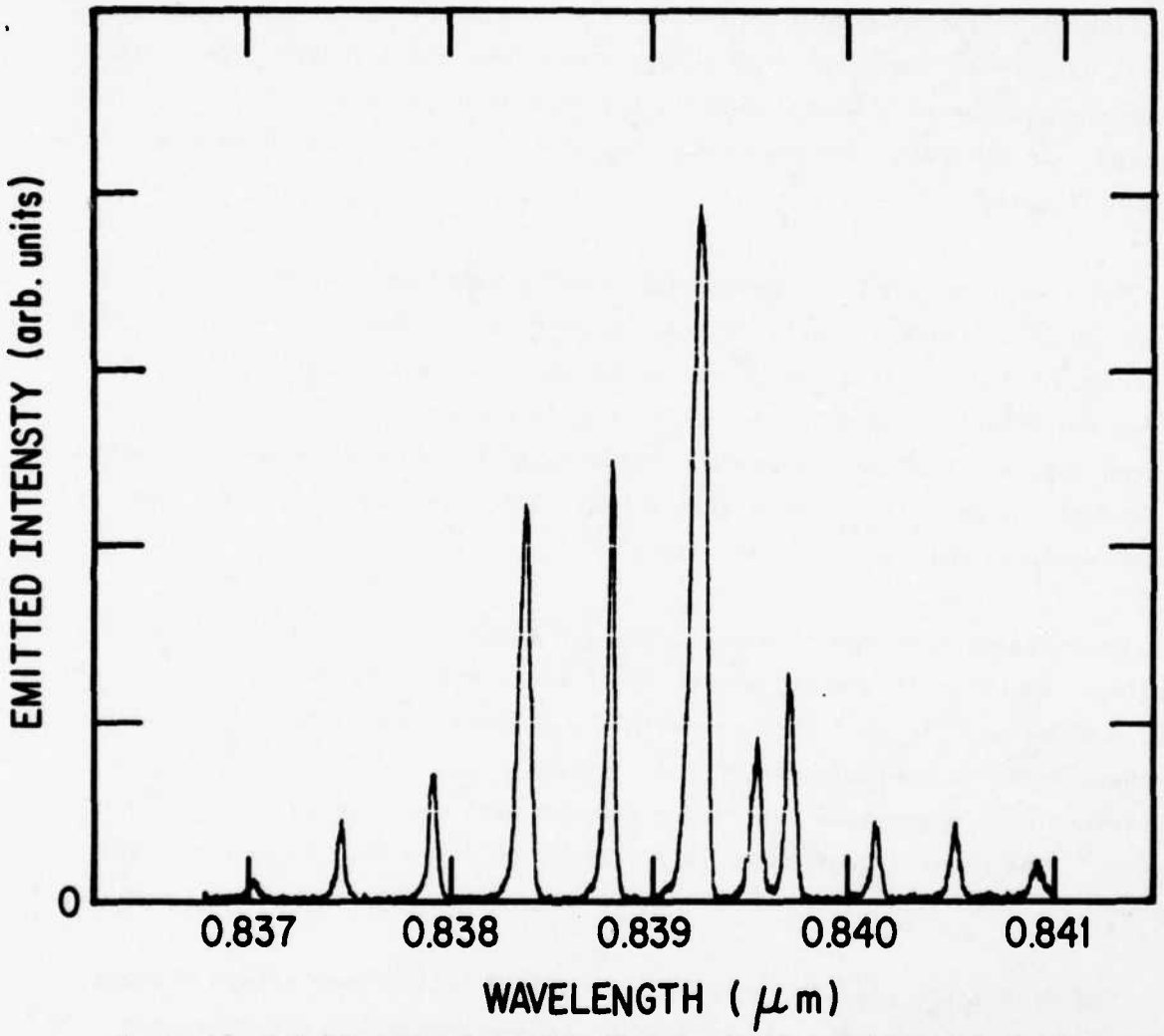

Figure 16 Emission Spectrum of a GaAs Mesa Laser Driven with a Bias Current of 10 A at 77 K

This rather low value for the effective index is consistent with our observation that laser oscillation occurs on the low energy side of the emission spectrum.[8] Typical values for the total peak output power from heavily doped GaAs lasers are several tenths of a watt; however, a peak output in excess of 3 W has been measured. In contrast, the peak power outputs of lightly doped lasers are usually a few milliwatts.

The lowest thresholds observed for heavily doped $Ga_{1-x}In_xAs$ mesa lasers are 20 kA/cm^2. These higher threshold currents are probably a result of higher densities of nonradiative recombination centers that are caused by lattice strain and defects such as dislocations resulting from the lattice mismatch between the mesa and the substrate. Evidence of strain can be seen in the top surface of the $Ga_{1-x}In_xAs$ mesas that appear pitted in comparison with the mirror smooth surfaces observed in GaAs mesas.

An emission spectrum of a $Ga_{0.95}In_{0.05}As$ mesa laser is shown in Figure 17. The laser emission is shifted almost 700 Å with respect to the GaAs mesas, thus making these $Ga_{1-x}In_xAs$ lasers compatible with GaAs waveguides. The spacing of these modes is approximately 6.3 Å, yielding $n_{eff} \simeq 3.7$. This value is consistent with a previous report for conventional discrete $Ga_{1-x}In_xAs$ laser diodes.[9] The highest peak power output observed for a $Ga_{1-x}In_xAs$ laser was 0.8 W.

The mesa laser readily lends itself to fabrication into arrays because several hundred lasers are grown adjacent to one another on a single chip. To make a linear array of mesa lasers, a strip containing the desired number of devices is cut from a batch-processed slice and mounted on a header as shown in Figure 18. This particular array contains six stripe contact GaAs mesa lasers. By connecting the diodes in parallel with an appropriate series resistance for each device, it is possible to obtain the rather uniform laser emission illustrated in Figure 19. In this figure the radiation from the

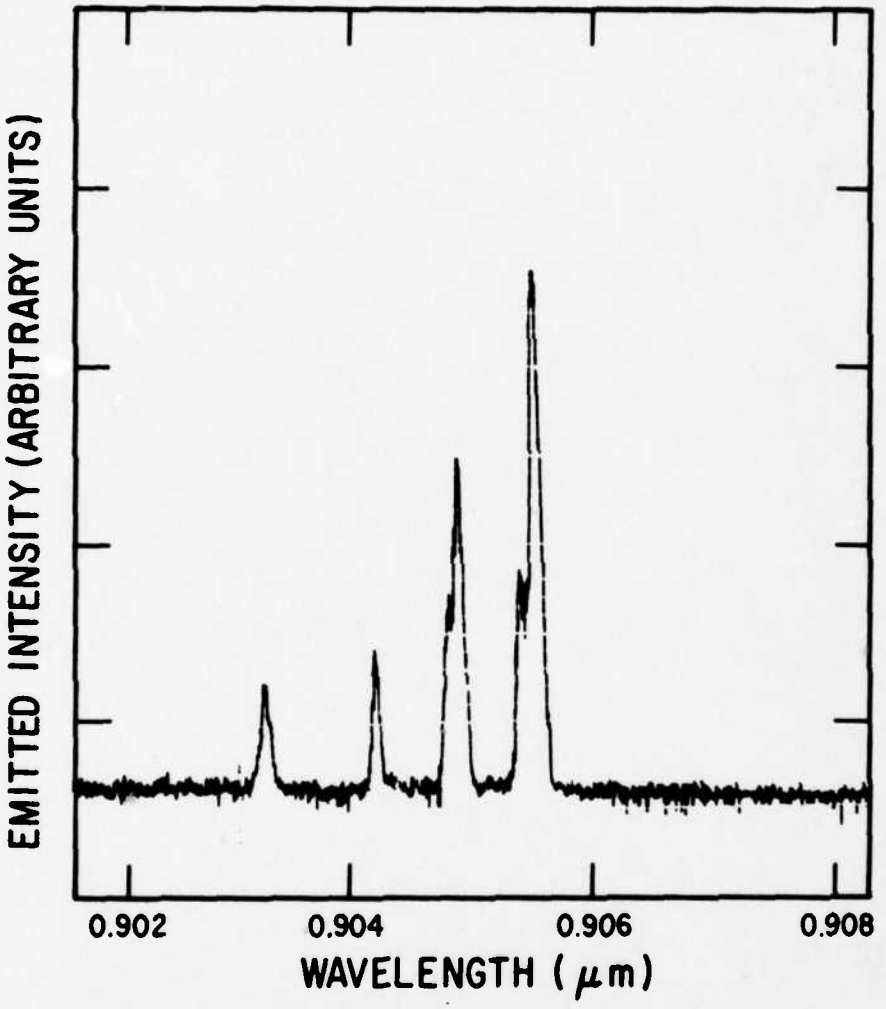

Figure 17 Emission Spectrum of a $Ga_{0.95}In_{0.05}As$ Mesa Laser Driven with a Bias Current of 11 A at 77 K

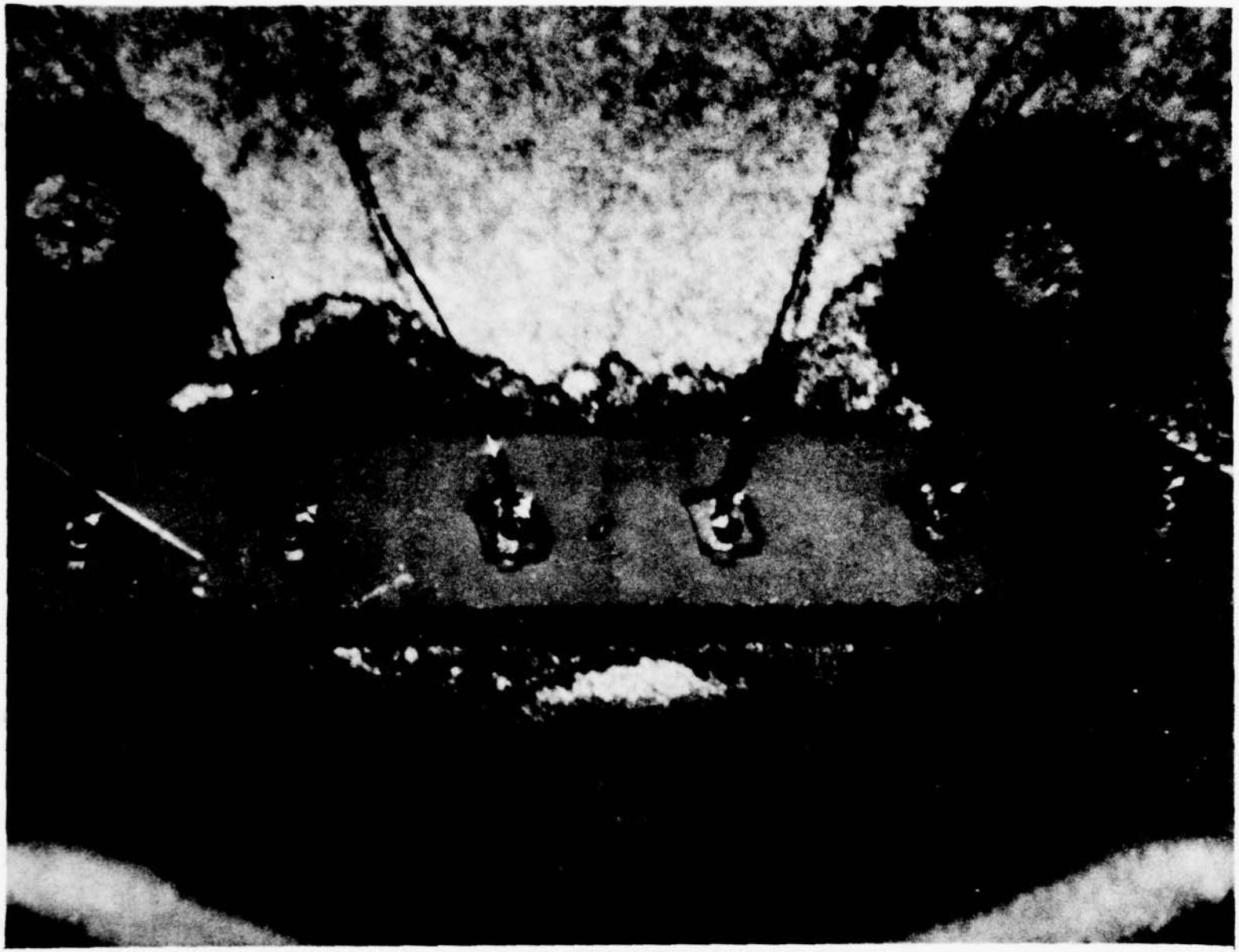

Figure 18 Photograph of an Array of Six Stripe Geometry GaAs Diode Mesa Lasers Cut from a Batch Processed Slice

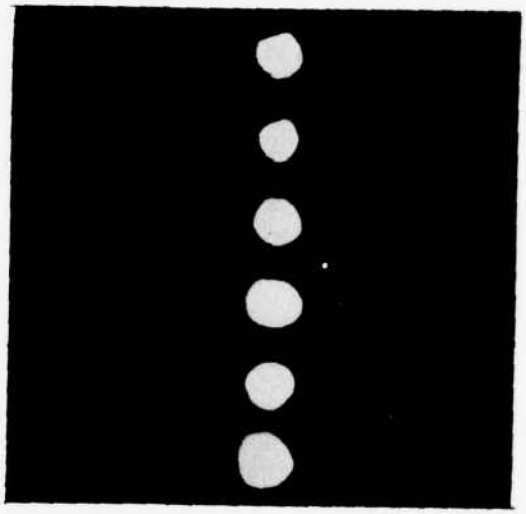

Figure 19 Infrared Vidicon Display of the Emission from a Six-Element Monolithic Array of Zn-Implanted GaAs Mesa Lasers

array has been focused on an infrared vidicon and displayed on a CRT. To obtain this picture, a 1 Ω resistor was placed in series with two of the lasers. This method of mounting lasers also allows us to check variations of the laser thresholds from one device to another along the chip. The laser threshold currents for the individual diodes in the array of Figure 19 ranged from 1.2 to 2.6 A. A peak power output of 3 W was obtained from the six laser array when driven by a total current of 50 A. Laser arrays have been previously fabricated from discrete diodes.[10,11] However, this is the first report of a monolithic array.

SECTION III

DOUBLE HETEROJUNCTION GaAs-GaAℓAs MESA LASERS

The development of single heterojunction (SH) diamond mesa laser represented an intermediate stage in the development of a prototype optical transmitter. This approach combined the latest developments of vapor phase epitaxy (VPE) and liquid phase epitaxy (LPE) in a hybrid device. At Texas Instruments a new mesa structure, however, was developed under a TI-funded program for the selective LPE growth of monolithic mesa lasers. This new mesa structure presented the opportunity to work on advanced device structures capable of room temperature, cw operation. The successful development and operation of double heterojunction (DHJ) mesa lasers at room temperature was a major milestone and accomplishment in this program. The following subsections will discuss the considerations for the choice of the DHJ mesa laser, the materials technology and development of the DH mesa laser, and DHJ devices.

A. Considerations for the Choice of the Double Heterojunction Mesa Laser

The single heterostructure diamond mesa laser is a prototype optical transmitter in its simplest form. As shown conceptually in Figure 20, it consists of a single heterostructure injection mesa laser grown on top of a (Ga,Aℓ)As waveguide. Radiation is coupled downward from the active region into the passive (Ga,Aℓ)As waveguide and continues to propagate across the chip. The device structure requires a unique combination of two separate materials technologies: (1) LPE for the growth of the (Ga.Aℓ)As waveguides, and (2) VPE for the formation of the diamond mesas. Although each technology has been successful in its own applications, the two technologies were marginally successful when combined. For simplicity the materials problems can be broken into three broad, but interdependent, areas: (1) the LPE growth of (Ga,Aℓ)As, which is both an integral part of the laser structure and serves as the optical waveguide; (2) the LPE-VPE interface; and (3) the growth of high-quality VPE mesas for the laser cavity on the LPE (Ga,Aℓ)As.

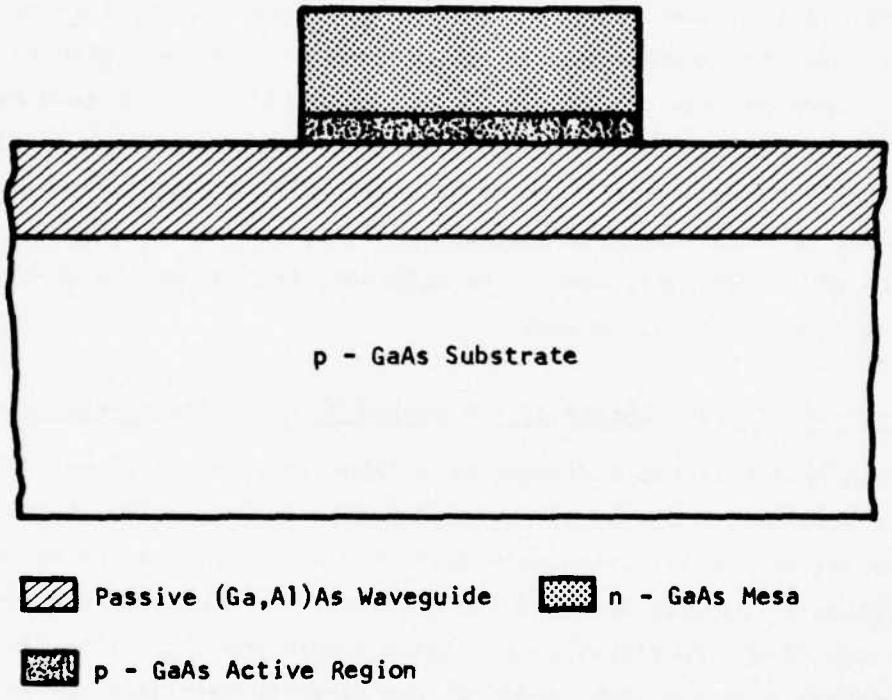

Figure 20 Conceptual Diagram of the Coupled Laser-Waveguide Device

1. LPE-VPE Interface

The LPE-VPE interface is the key problem in this structure because it controls many important processes: (1) electrical contact between the substrate and the mesa laser, (2) diffusion of the Zn from the LPE layer into the mesa, and (3) the quality of the surface on which the mesa is grown. Unwanted interfacial layers could degrade any of these important areas and affect device performance. Many of these problems are enhanced by attempting to use a hybrid LPE-VPE growth process.

The effect of interfacial layers is particularly evident in the electrical properties and the growth of the VPE mesa.[2] The difficulties in the device design were found to be related primarily to limitations in the processing, particularly the cleaning procedures that could be effectively used. Neither chemical nor *in situ* vapor etch techniques alleviated these problems. The presence of Aℓ in the top LPE layer particularly degraded materials and device properties, probably due to the formation of insoluble aluminum oxides. No high quality mesas were grown on $Ga_{1-x}Al_xAs$ layers with $x \geq 0.01$. An example is shown in Figure 21(a).

To overcome the difficulties encountered in the growth of GaAs mesas directly on $Ga_{1-x}Al_xAs$ layers, the structure was modified to include a thin LPE GaAs buffer layer that overlies the $Ga_{1-x}Al_xAs$ waveguide layers. The buffer layer must be kept very thin (≤ 1 μm) to minimize the separation between the heterojunction and the p-n junction in the mesa. High-quality mesas such as shown in Figure 21(b) have been grown on this structure. Devices have been made with this structure where the waveguide layer was $Ga_{0.8}Al_{0.2}As$. The p-n junction was formed by diffusing Zn from the LPE layer into the VPE mesa. These devices lased at 77 K with threshold current densities ≤ 10 kA/cm^2.

(a)

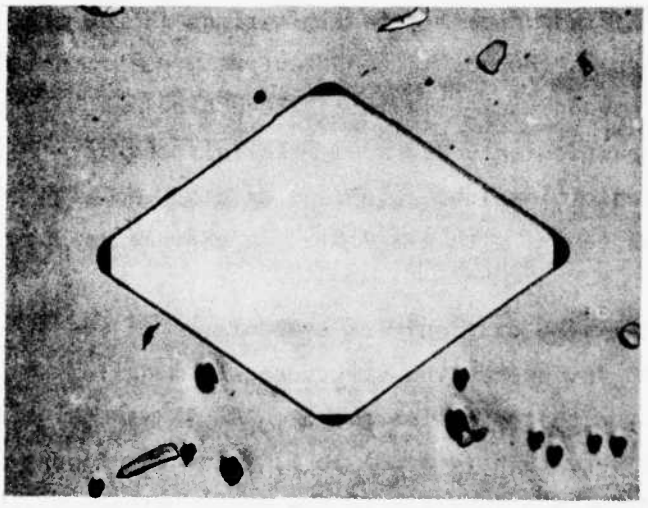

(b)

Figure 21 VPE GaAs Mesas Grown (a) Directly on $Ga_{0.85}Al_{0.15}As$, and (b) on a GaAs Buffer Layer

2. Limitations of the Single Heterostructure Mesa Laser

The SH mesa laser represents a simple prototype of a room temperature, monolithic transmitter and is best considered as an intermediate step to a practical working device. During the course of investigation, the limitations of this structure were clarified. Some of these limitations are related to the materials technology, and some are basic to the structure itself.

(1) High Thresholds. The SH is a room temperature device, but by nature has relatively high threshold current densities compared to DH lasers. For low threshold cw operation at 300 K, DHJ lasers are required. These can only be grown by liquid phase epitaxy or molecular beam epitaxy.

(2) Substrate Orientation. The mesas must be grown on {110} substrates to be properly oriented for vertical faceting of the mesas. The waveguide studies are all on {100} substrates and the electrooptic effects are strongest for the ⟨110⟩ directions.

(3) Doping in the Waveguide Layer. The waveguide layer also serves as the diffusion source to form the p-n junction in the mesa. The very heavy Zn doping will make the waveguides very lossy. All current waveguide research was directed towards low carrier concentration, n-type waveguides.

(4) LPE-VPE Hybird Growth System. VPE mesa growth on LPE (Ga, Al)As waveguides introduces many problems for the materials technology that can be attributed to interfacial layers. The major difficulties are: (1) erratic current-voltage characteristics, (2) erratic diffusion behavior, and (3) the need for a GaAs buffer layer. The latter requirement increases the distance between the p-n junction and the heterojunction in the laser cavity and will effect the laser threshold. In situ vapor etch techniques were not successful in overcoming these problems. Chemical etch techniques often create a hole in the waveguide layer that introduces additional difficulties.

(5) P-n Junction Formation by Diffusion. As mentioned above, the diffusion behavior tends to be erratic. The Zn dopant is difficult to contain and control because of its high vaporization pressure and high mobility. Zn contamination of the top of the mesa during the diffusion causes processing problems.

3. Double Heterojunction Mesa Laser

The SH mesa laser was a major step toward a monolithic, room temperature laser source for integrated optical circuits. Development work on this structure has clarified the technical difficulties with this design as indicated previously. The DHJ mesa laser, described in detail in the following sections, clearly has the potential of being a monolithic, low threshold, room temperature cw laser source. This structure offers many advantages and in particular the following:

(1) The mesa is monolithic, with grown facets forming the optical cavity.

(2) Double heterostructure lasers are capable of low threshold, room temperature, cw operation.

(3) The structure is grown on {100} substrates and is compatible with present waveguide, modulator, and switch technology.

(4) The waveguide layers are not part of the laser structure and are not restricted in their structure, carrier type, or carrier concentration.

(5) All materials growth is by liquid phase epitaxy and not a hybrid technology. The techniques are compatible with the low-cost batch processing currently used in the electronics industry.

(6) Since the lasers can operate cw, modulation can be done in the optical circuit rather than at the laser source.

(7) The laser cavity is grown in a stripe geometry with a totally embedded active region for very low threshold current operation.

B. Materials Technology

Liquid phase epitaxy has been used at Texas Instruments in the integrated optics program for the growth of both DHJ lasers and waveguide structures. The realization of the DHJ mesa laser, however, required the development of selective LPE technology. The guidelines for selective LPE have now been established at TI and applied to growth in various crystallographic orientations. I-bar DHJ mesa lasers grown by selective LPE have been successfully operated at room temperature and represent a major accomplishment in the development of integrated optical circuits. This section will discuss the LPE growth parameters, selective LPE, mesa morphology, and development of the I-bar DHJ mesa laser.

1. LPE Reactors

The liquid phase epitaxial reactors currently in use at TI have been refined to meet the high standards of controlled uniform submicron layers required in the growth of low threshold DHJ laser material. The graphite slider assembly shown in Figure 22 is capable of growing up to six different epitaxial layers on a 2.5 cm^2 GaAs substrate. The graphite assembly is machined from high purity, high density DFP-3-2 graphite (Poco Graphite, Decatur, Texas).

Figure 23 shows the reactor furnace and chamber with the graphite slider assembly in position for an epitaxial growth. The three-zone Lindberg furnaces are equipped with an isothermal liner to minimize the temperature gradients in the slider assembly. Typical gradients of 2 to 3°C over a 16 cm length are achieved with this system. The furnace is mounted on a rolling platform to permit rapid heating and cooling of the reaction chamber. The reaction chamber is continually flushed during growth with H_2 purified in a Pd diffusion furnace. The oxygen content of the input H_2 and exhaust gas is monitored with a Panametrics Model 2000 hygrometer.

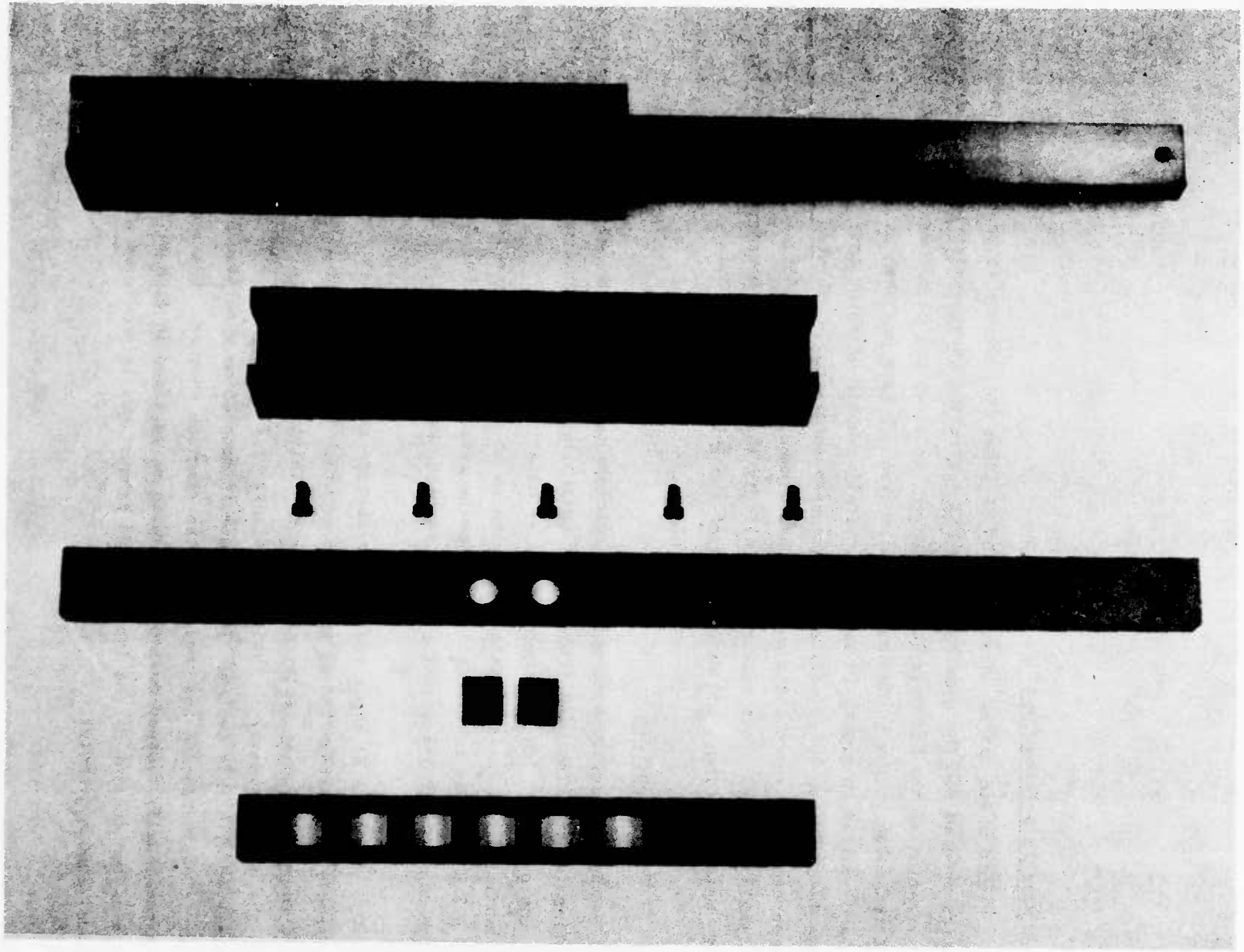

Figure 22 Graphite Sliding Boat Assembly for LPE

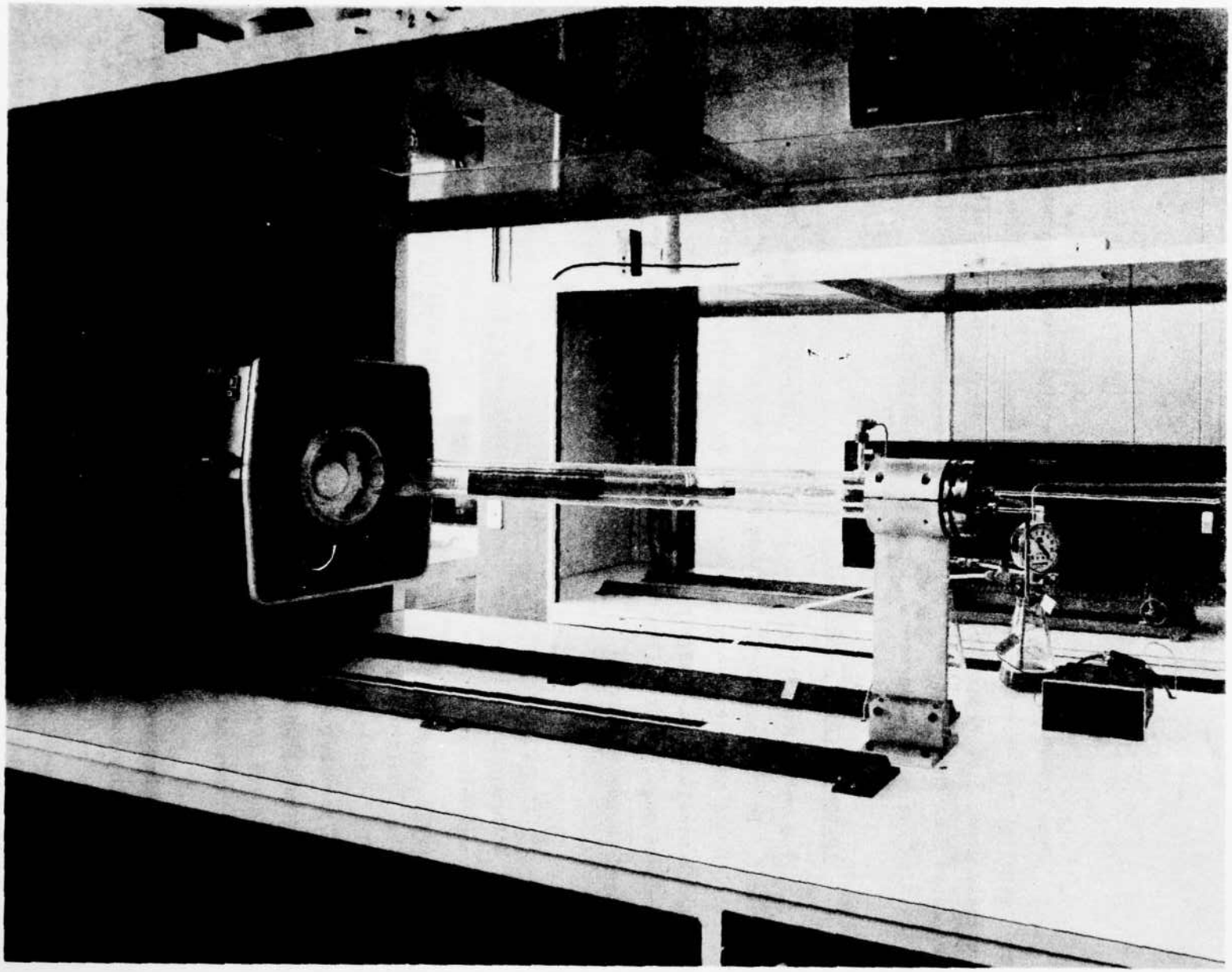

Figure 23 Reactor Furnace and Chamber with the Graphite Slider Assembly in Position for an Epitaxial Growth

This reactor system has been used extensively in the growth of DH laser material for discrete lasers. Epitaxial layers 0.1 to 0.2 μm thick are routinely grown (see Figure 24) for this device structure. Discrete lasers fabricated from this material have measured threshold current densities as low as 585 A/cm^2 at room temperature under 200 ns pulsed conditions.

2. Epitaxial Layer Compositions

The melt compositions used to grow a typical DHJ I-bar mesa are given in Table I. In this system, Sn is used as the n-type dopant and Ge as the p-type dopant. The Aℓ concentrations were verified by growing a series of single layers for standardization and determining the actual grown composition from photoluminescence measurements. The melt compositions for the carrier concentrations were based on published data.[12-17]

3. Selective Liquid Phase Epitaxy

Although there have been several extensive investigations of growth rates and morphologies of III-V materials in selected patterns and directions for vapor phase epitaxy (VPE),[4,5,18-20] there was very limited information available for selective liquid phase epitaxy (LPE).[21,22] During the course of this work, Samid, et al.,[23] published further work on the use of stripes grown by selective LPE for discrete devices. In some instances, such as the dominance of {111} facets along the ⟨110⟩ substrates, selective VPE and LPE behave in a similar manner.[4,23] Quite different growth occurs, however, for LPE diamond mesas[24] on (110) substrates compared with VPE diamond mesas.[2,25,26]

There are two significant limitations inherent in the LPE growth process that must be recognized when comparing selective VPE technology with selective LPE. First, VPE has an additional degree of freedom in the wide range of Ga/As ratios available for growth. This ratio can be varied to affect the growth rate for different directions.[5] This phenomenon is possible because of the polar nature of the GaAs crystal and has been applied to grow new device structures such as

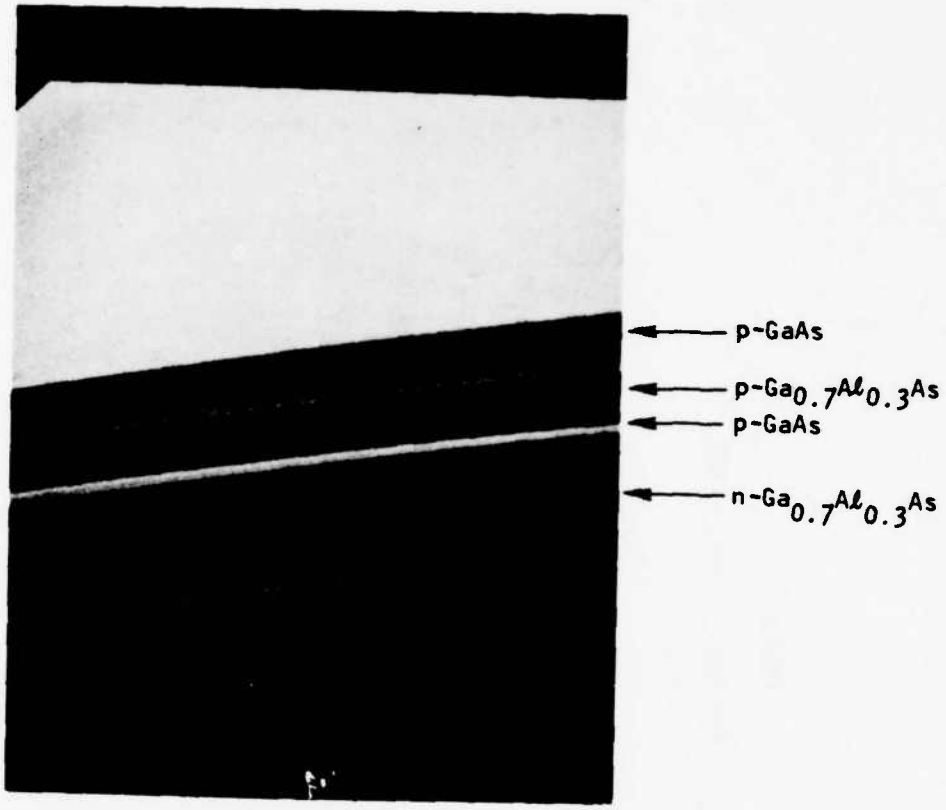

Figure 24 SEM of Cleaved and Stained Cross of DH Laser Material (6640X)

Table I

DHJ I-Bar Melt Compositions

	Layer 1	Layer 2	Layer 3	Layer 4
Ga(g)	2	2	2	2
Al(g)	0.002	--	0.002	--
Sn(g)	0.6	--	--	--
Ge(g)	--	0.01	0.02	0.02
Composition	$Ga_{0.7}Al_{0.3}As$	GaAs	$Ga_{0.7}Al_{0.3}As$	GaAs
Carrier Concentration (cm^{-3})	8×10^{17}	1×10^{18}	1×10^{18}	3 to 5×10^{18}

the VPE mesa laser.[2,25,26] In LPE, a limited range of Ga/As ratios determined by the growth temperature is available only in the Ga-rich regime of the phase diagram. Second, the LPE growth mechanism is a diffusion rate limited process. To obtain uniform thickness in the epitaxial layers and avoid edge effects at the mask/growth area boundary, the growth geometries are limited to small mask widths[21] or narrow stripes (< 50 μm). Selective VPE is capable of 250 μm geometries[4] and larger.

Several types of mask materials were considered. Al_2O_3 has been used by several workers.[21,23] However, this material is difficult to deposit and to etch. Silicon oxide can be readily deposited and etched, but is soluble in the Ga melt. Silicon nitride is readily deposited and patterned by plasma techniques and is not dissolved by the Ga melt. Silicon nitride was used as the mask for all selective LPE investigations. All epitaxial depositions were performed in the reactor system previously described.

Prior to crystal growth, the polished substrate is coated with ~ 2000 Å of plasma-deposited silicon nitride for a mask and then with a layer of photoresist. Standard photolithographic techniques are used to define the pattern openings in the photoresist and plasma etching to open the pattern in the silicon nitride mask. The window area is cleaned with a common oxide etch just prior to resist removal and placement in the LPE growth system. Starting growth temperatures are ~ 735°C and the cooling rate is 0.2°C/min. The growth rate for the masked substrates is greatly enhanced compared to unmasked substrates. Slow cooling rates, short growth times, and low growth temperatures are used to improve control of the growth and to obtain reasonably thin layers (~ 1 μm).

4. I-Bar Mesa Laser

In designing new grown devices, it is necessary to consider both the limitations imposed by the LPE process and the requirements of the device. It is clear from the previous discussion that the LPE process limits the design to

working with (1) narrow stripe geometries and (2) naturally occurring facets (i.e., no manipulation of the Ga/As ratio). An IOC monolithic mesa laser requires (3) facets perpendicular to the substrate to provide optical feedback, (4) uniformly flat and parallel epitaxial layers, and (5) growth on {100} substrates. The last requirement is for compatibility with presently developed active devices.

It was observed early in the investigation and later confirmed by Samid, et al.,[23] that for {100} GaAs substrates, stripes grown parallel to the {110} cleavage planes have facets that are not perpendicular to the substrate. Rectangular structures would have similar features; this orientation, therefore, does not satisfy the perpendicular facets in requirement (3). For a rectangle with all sides along {100} planes, however, the structure shown in Figure 25 results. The resulting mesa has a flat top and facets perpendicular to the substrate along the long dimension. The ends with the short dimension, however, are dominated by nonperpendicular {111} facets, and the structure is not useful as a laser. The I-bar mesa laser, as shown in Figure 26, results from combining three of these rectangles into one structure. In this new structure the central member serves as the laser cavity, and the perpendicular facets at the ends of the laser cavity region provide the optical feedback. The nonperpendicular facets are removed from the central cavity to the ends of the cross members. The length of the cross members has been exaggerated in Figure 26 and must only satisfy the requirement of moving the nonperpendicular facets out of the central laser region. SEM photographs illustrating the high quality of as-grown facets are shown in Figure 27. Contrary to previous observations by Kawakami, et al.,[22] the growth morphology is not dependent on the Al concentration.

Double heterojunction lasers with the I-bar structure have been grown. A cross section illustrating layer structure and compositions is shown in Figure 28. Typical I-bar dimensions for the central laser cavity are 350 to 400 μm long, 25 μm wide; and for the cross members, 150 to 350 μm long, 25 μm wide. The

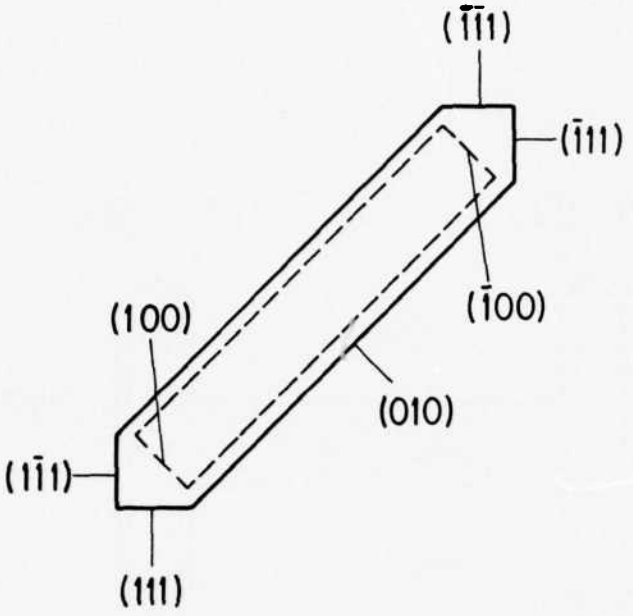

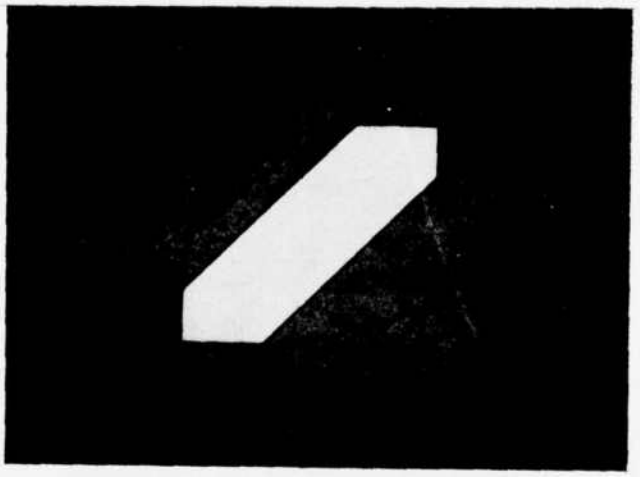

Figure 25 Selective LPE Rectangle Mesa Showing Mask Opening (dashed line) and Facet Formation

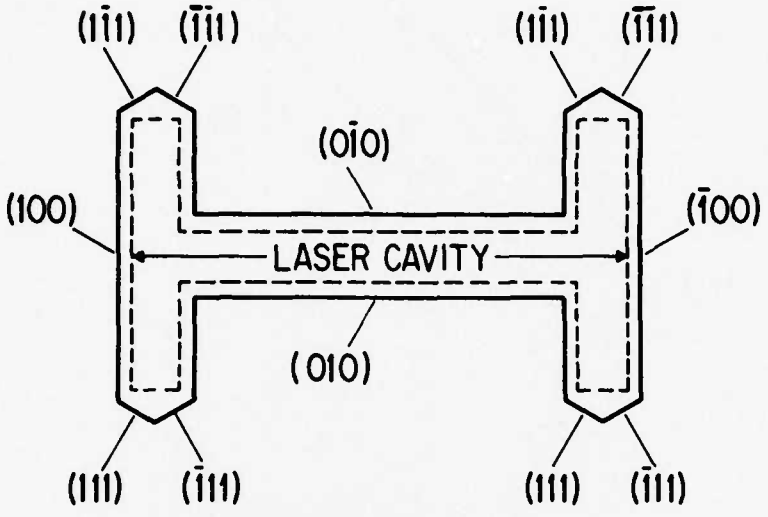

Figure 26 I-Bar Mesa Showing Mask Opening (dashed line) and Facet Formation

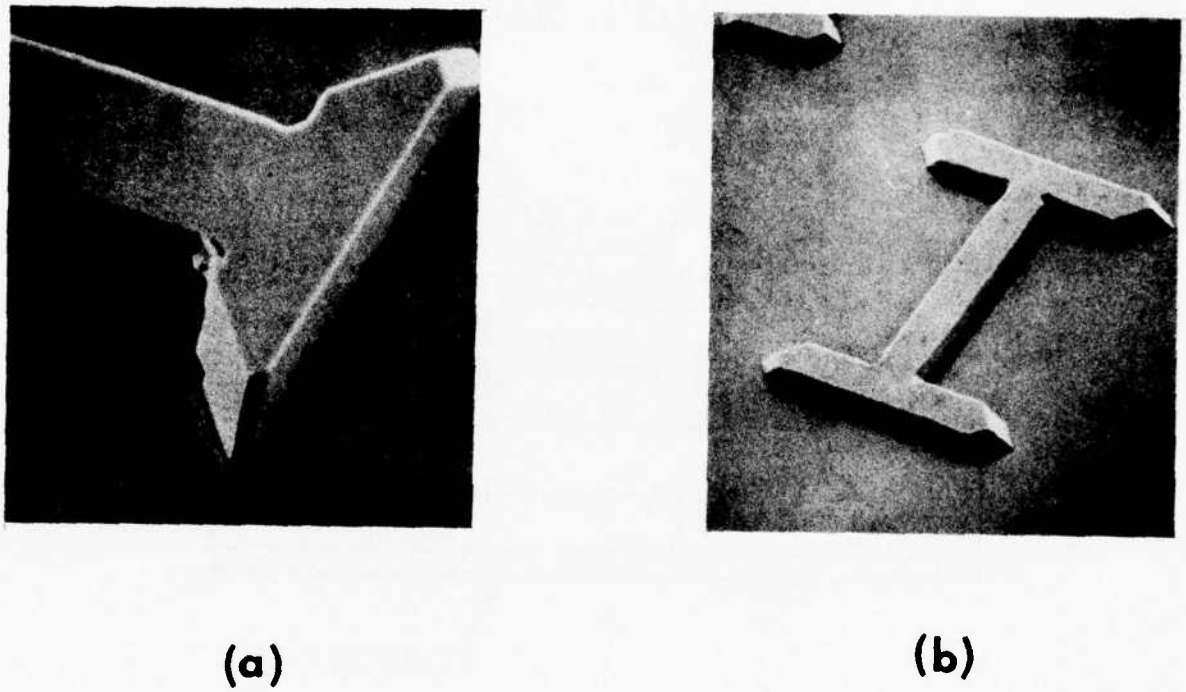

Figure 27 SEM of I-Bar Mesas

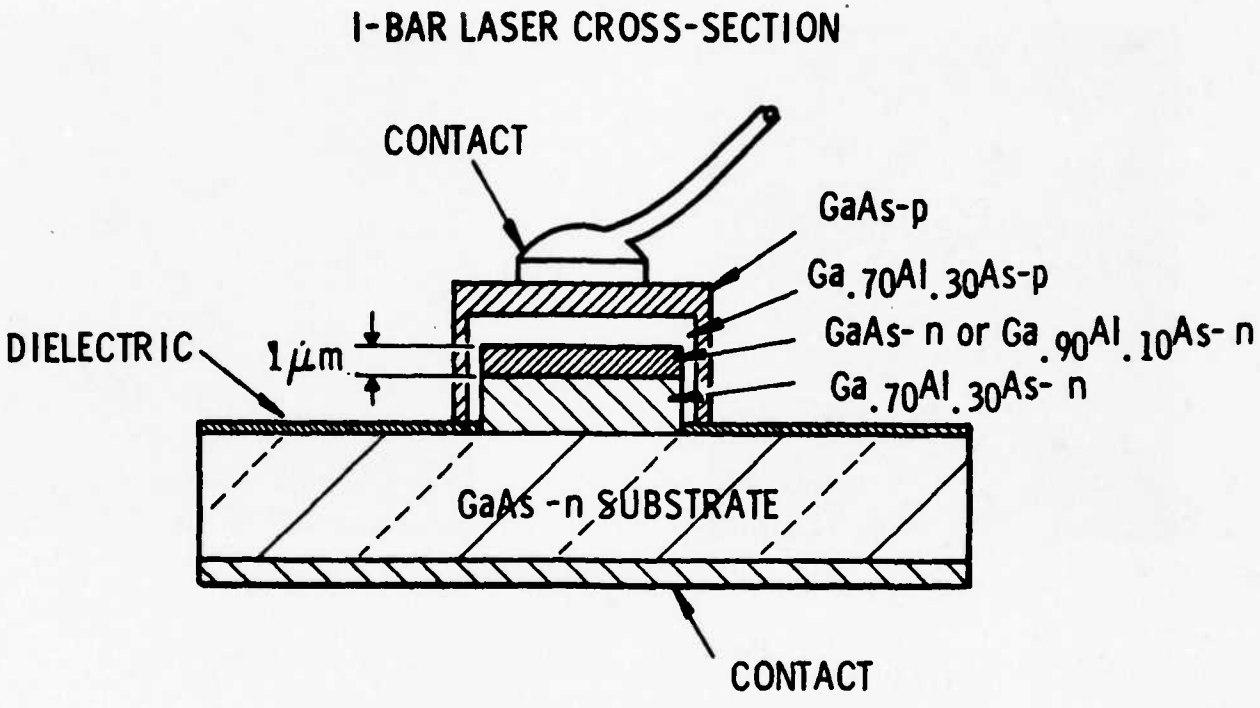

Figure 28 Cross Section of Layers in Double Heterojunction I-Bar Mesa Laser

I-bar lasers are grown in a stripe geometry that simplifies the fabrication process. Only p- and n-type contacts need to be affixed to the as-grown I-bars. The n-type contacts are made by electroplating Au-Sn to the substrate. Evaporated Cr-Au is used for the p-type contacts. Since the top p-GaAs layer surrounds the other layers and extends slightly over the silicon nitride growth mask, large area contacts to facilitate bonding can be used without shorting to the n-type layers.

The I-bar lasers have been tested at a 500 pulses/s repetition rate with a 200 ns pulse width. The light output is detected with an ITT FW 118 photomultiplier attached to a Spex 3/4 m spectrometer. Room temperature threshold current densities are typically 8 to 10 kA/cm^2 for lasers having an active layer thickness of approximately 1 μm. The best device tested has a 7.5 kA/cm^2 threshold current density with a 525 mA drive current. I-bar mesa lasers exhibit the longitudinal mode spectra commonly observed for Fabry-Perot cavity lasers. A typical spectrum is shown in Figure 29. Filaments are often observed in the plane of the junction, indicating that these lasers are not operating in a single transverse mode. I-bar lasers have been driven at a 40% duty cycle with a 1 MHz data rate with no additional provisions for heat sinking. External differential quantum efficiencies have been measured with a calibrated PIN photodiode,[27] and efficiencies as high as 15% have been observed.

5. Improved I-Bar Mesa Laser

The initial design of the I-bar mesa laser produced devices with 7.5 to 10 kA/cm^2 threshold current densities and 525 to 800 mA drive currents. To become acceptable for cw operation, these parameters must be reduced by at least a factor of 5, and a factor of 10 reduction will be necessary for them to become comparable to the better cleaved devices. Improvements in performance should be obtained from changes in the device geometries (dimensions) and fabrication process. A cross section of initial devices is shown in Figure 30. Using the as-grown narrow stripe geometry to obtain a buried heterostructure device

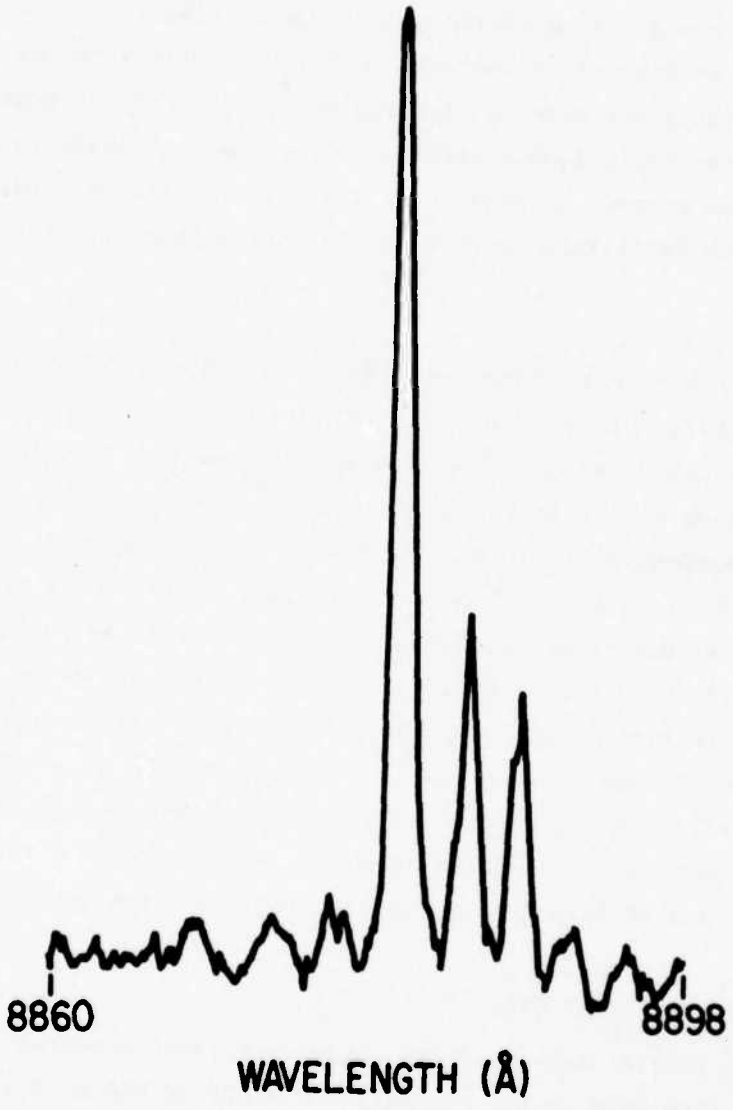

Figure 29 Optical Spectrum of I-Bar Mesa Laser

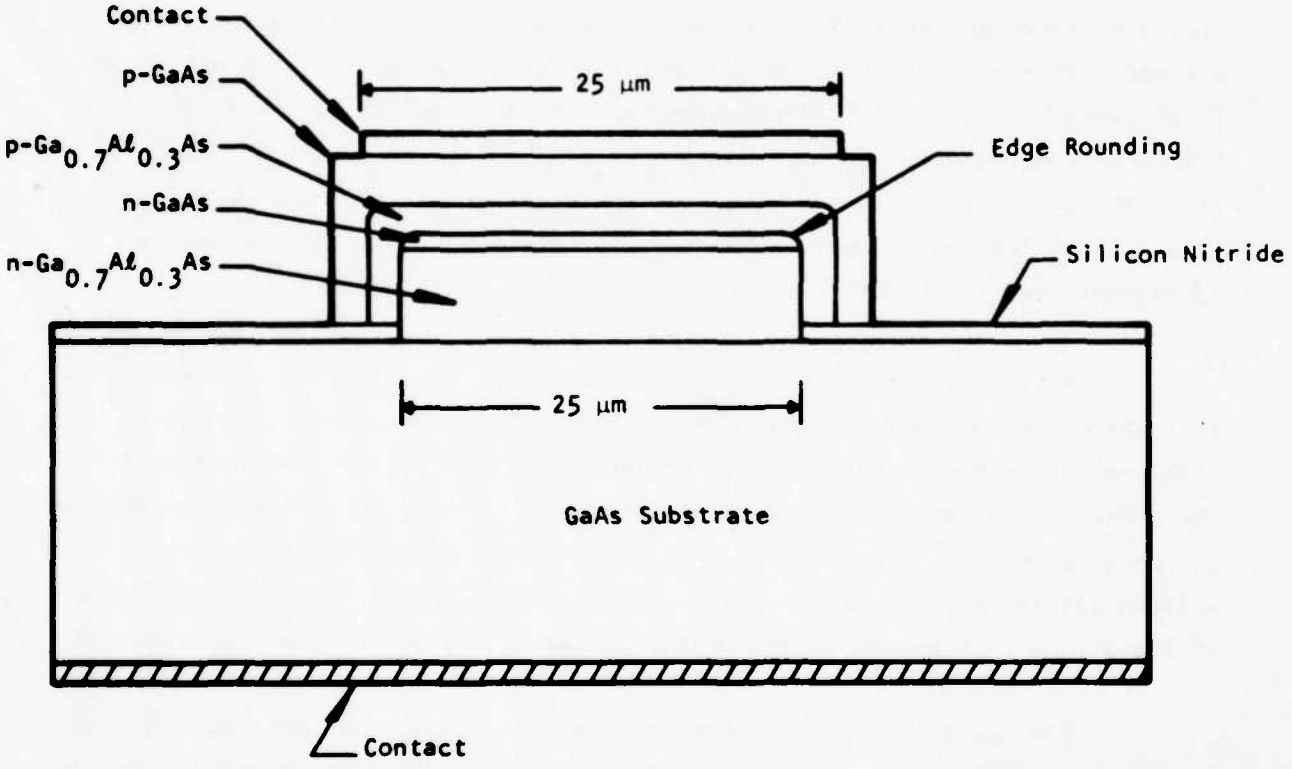

Figure 30 Cross Section of Initial I-Bar Devices

appears to have several practical drawbacks. First, to be truly effective as a buried heterostructure, the device should be very narrow (< 5 μm). We have been able to grow good I-bar devices with 25 μm wide stripes, but have not been able to control layer thicknesses for narrower stripe geometries. Although this may not be an insurmountable problem, it certainly increases the difficulties and decreases the yield. Second, the edges of the active layer usually are not a square facet, but are somewhat rounded or tapered. The nonuniformity in thickness can lead to filament-type behavior and inefficiencies in the laser. A stripe geometry over the more uniform central portion of the I-bar would be preferable. Third, because of the overlapping structure of the layers, there is a natural leakage current in the p-layers around the active layer and a subsequent loss in injection efficiency.

A cross section of a modified I-bar structure is shown in Figure 31. This structure combines the unique monolithic properties of the I-bar laser with present technologies involving stripe laser fabrication. The width of the I-bar is increased to 50 μm to improve layer control and decrease thicknesses. Stripe geometry lasers are fabricated on the I-bar using Zn diffusion and a silicon nitride mask to define the stripe injection region. The central location of the stripe is expected to minimize the edge effect and current leakage problems.

The new I-bar mesa structures have been grown, and the mesa features were found to be comparable to those of full surface discrete structures except for a minor loss in flatness in the top p-type GaAs contact layer. This could be corrected, if necessary, by minor modifications in the mask design. As anticipated, the change in geometry has altered the thicknesses of the epitaxial layers. Device fabrication procedures have been changed to incorporate stripe geometry fabrication technology. A new I-bar mesa laser after device processing is shown in Figure 32. The appropriate materials parameters for good lasers are presently being investigated. However, initial results are most encouraging for this new structure.

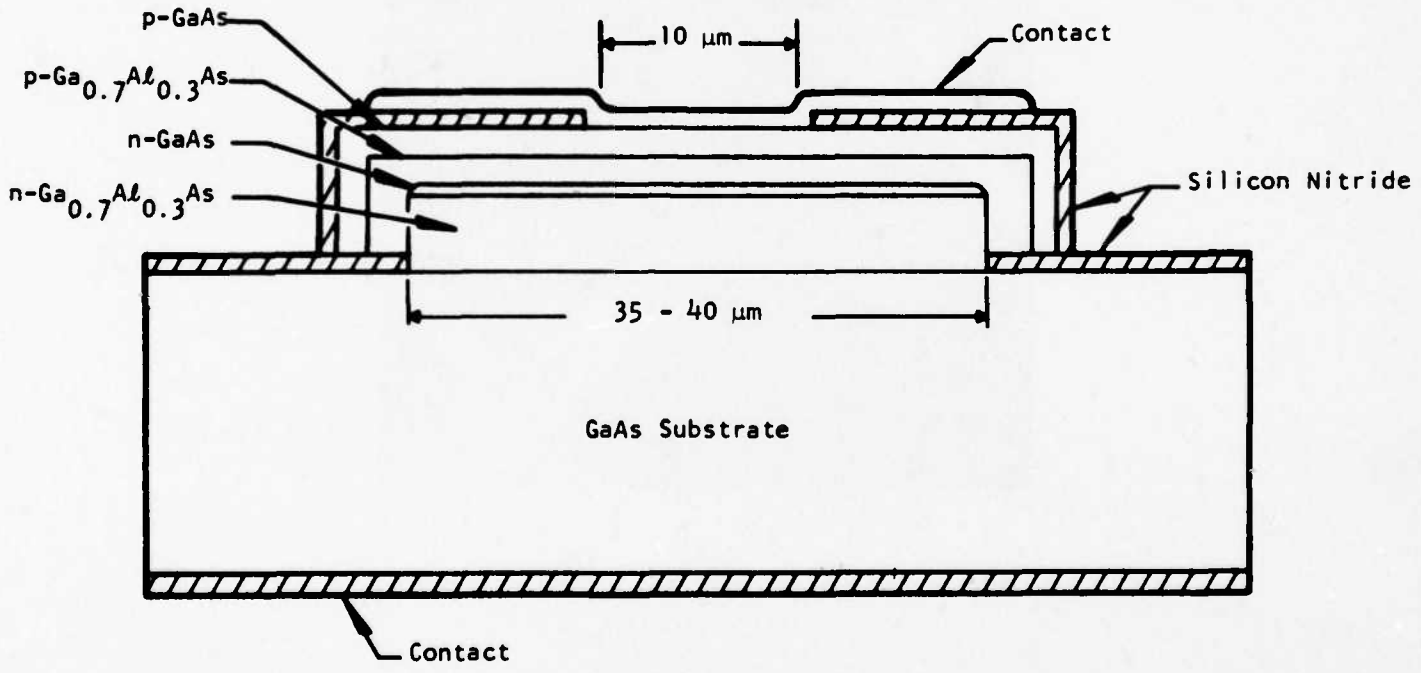

Figure 31 Cross Section of Modified I-Bar Laser

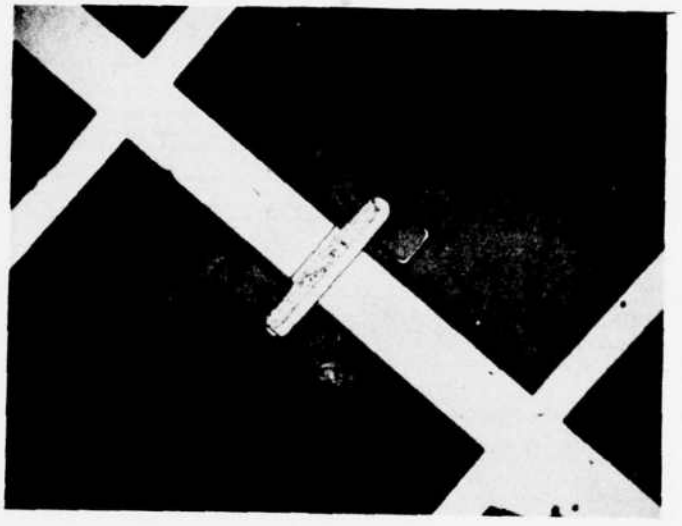

Figure 32 Modified I-Bar Mesa Laser after Zn Diffusion and Metal Contacting

SECTION IV

GROWN WAVEGUIDES

The application of selective LPE to obtain an as-grown waveguide structure was spurred by the difficulties encountered in guiding light around bends. This capability is, of course, an absolute necessity to accomplish any light processing on a chip and thus achieve a truly integrated optical circuit. Early investigations using conventional dielectric striplines and rib waveguides were effective only for waveguides with a very large (> 1 cm) radius of curvature. Later work showed that closer confinement and guiding around bends could be obtained with very thin waveguides.[28-30] Waveguides grown by selective LPE have a larger change in the index of refraction in the lateral directions due to the embedded nature of the structure and thus should have improved confinement over the conventional planar structure. However, the increase in the index of refraction discontinuity will also increase the propagation losses of the guide.

Selective LPE waveguides have very different functional and structural requirements from the mesa laser. In addition to the general LPE limitations of narrow stripe geometries and naturally occurring facets mentioned previously, the waveguide must also (1) guide light in straight-line sections, (2) guide light around curves, (3) guide light from any one point on the chip to any other point, and (4) grow on {100} substrates. Straight-line waveguide sections can be readily grown in both the ⟨100⟩ and ⟨110⟩ directions and satisfies the straight-line sections in requirement (1). The combination of straight lines (1) and curves (2) can be designed to guide light between any two points (3).

The following subsections discuss the growth and properties of waveguides grown by selective LPE.

A. Materials Growth

The waveguides were grown by the same process described previously for the mesa lasers. The as-grown waveguides were usually three-layer structures with compositions of $Ga_{0.85}Al_{0.15}As$ - $Ga_{0.9}Al_{0.1}As$ - $Ga_{0.85}Al_{0.15}As$. Each of the

layers is about 2 μm thick. All of the layers were n-type, nominally undoped, with carrier concentrations in the low- to mid-$10^{16}/cm^3$ range. Several two-layer structures were also grown in which the top $Ga_{0.85}Al_{0.15}As$ layer was omitted.

Three different types of masks shown in Figure 33 and 34 were used for this study. Figure 33 shows two different waveguide patterns used only for waveguide studies. The radius of curvature (r_c) was set at values of 0, 0.254 mm (10 mils), 0.635 mm (25 mils), 1.27 mm (50 mils), 2.54 mm (100 mils), and 6.35 mm (250 mils). Stripe widths of both 10 μm and 25 μm were investigated.

Figure 34 shows a schematic of a more complex pattern used to form an integrated circuit with a laser. For waveguide test purposes, this pattern was cleaved along lines A and B. The two "legs" of the remaining structure had r_c values of 0 (9° angle of incidence) and 1.27 mm (50 mils). Only 25 μm stripe widths were used in this pattern. The unusual structural features of this pattern include the Y divider in the cleaved portion of the structure and the "funnel" at the top of the guide for collecting light from the laser.

The faceting in the bend for waveguides with different radii of curvature is shown in Figure 35. For $r_c \leq 0.254$ mm (10 mils), there is substantial overgrowth and faceting in the bend. For $r_c \geq 0.635$ mm (25 mils), however, smooth nonfaceted outer surfaces can be obtained. Figure 36 contains SEM photographs of sets of four 10 μm wide, three-layer waveguides with r_c = 1.27 mm (50 mils) and 2.54 mm (100 mils) and a cross section of a three-layer waveguide. Complex patterns containing straight lines, curves, and Y dividers, such as shown in Figure 37 can be readily grown. This structure will be discussed further in the section on integrated structures.

B. Waveguide Characteristics

Light guiding has been observed for all waveguide structures including r_c = 0 (9° angle of incidence) with 2 to 3 μm thick waveguide layers. Figure 38

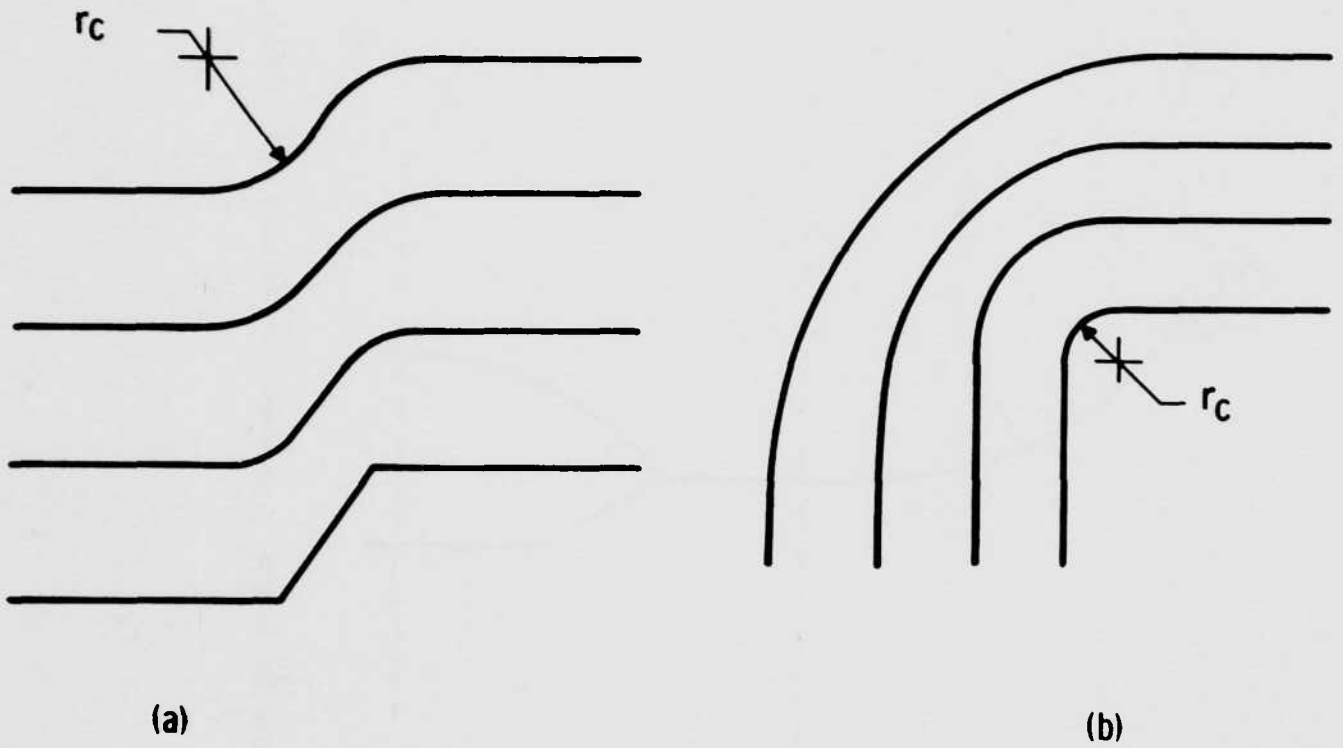

Figure 33 Schematic Drawing of Various Bend Configurations for Waveguides

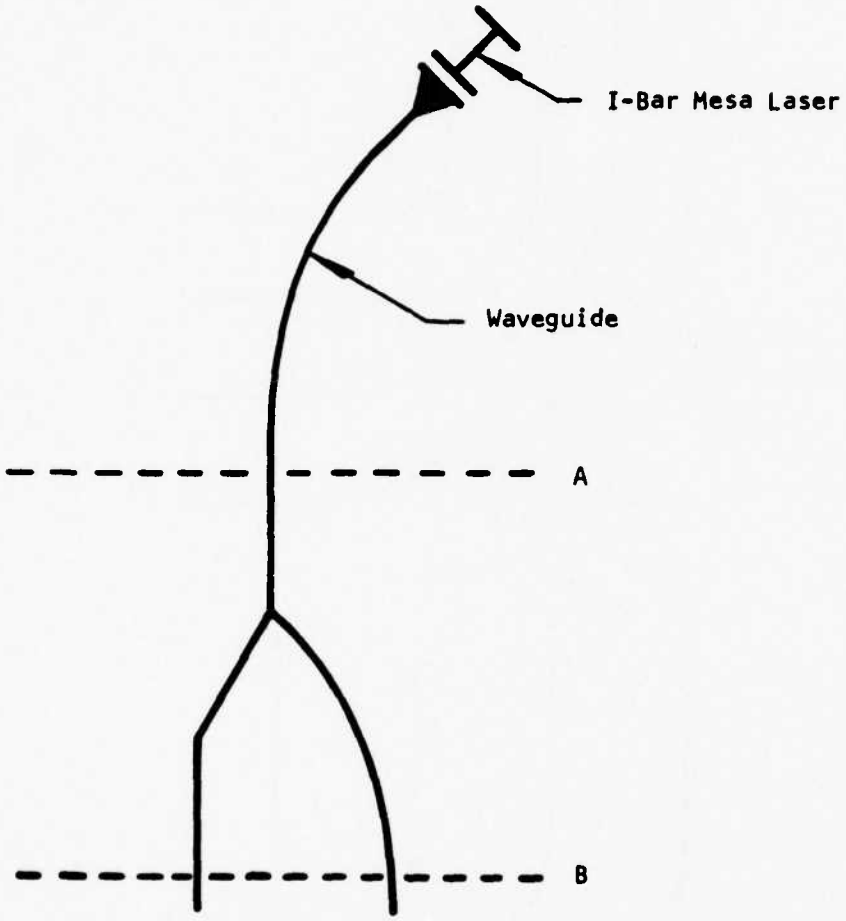

Figure 34 Schematic of Waveguide Pattern with Complex Geometries

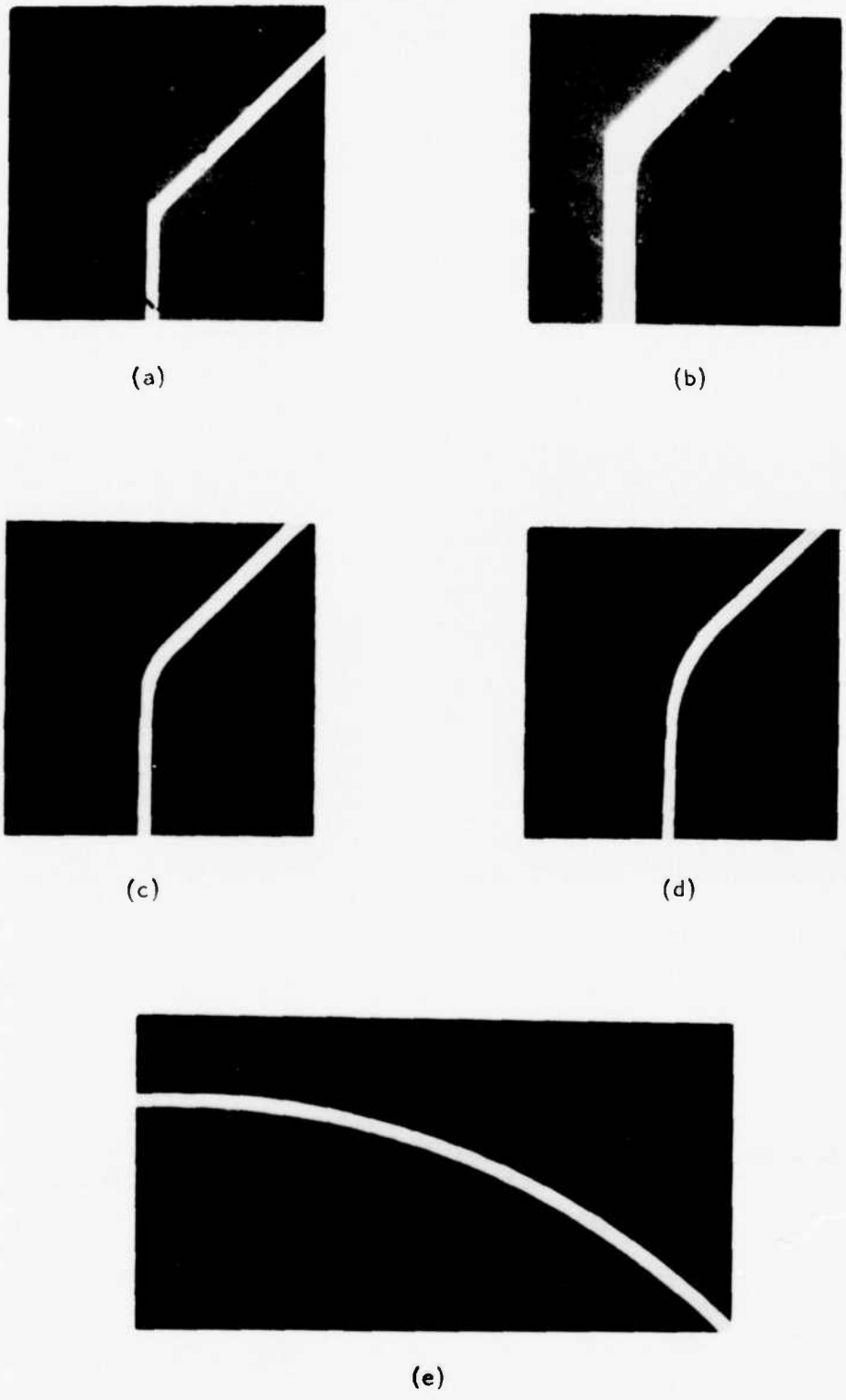

Figure 35 As-Grown Waveguides with Radii of Curvature (a) 0, (b) 0.254 mm (10 mils), (c) 0.635 mm (25 mils), (d) 1.27 mm (50 mils, and (e) 6.35 mm (250 mils)

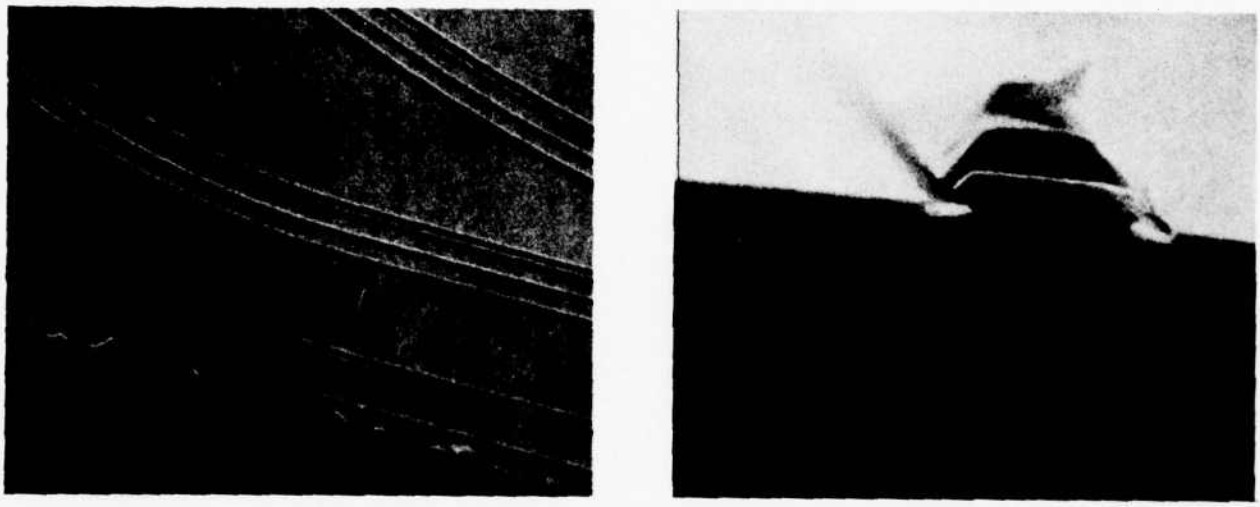

Figure 36 SEM of Selective LPE Waveguides Showing Growth Around a Bend and a Cross Section of a Three-Layer Waveguide

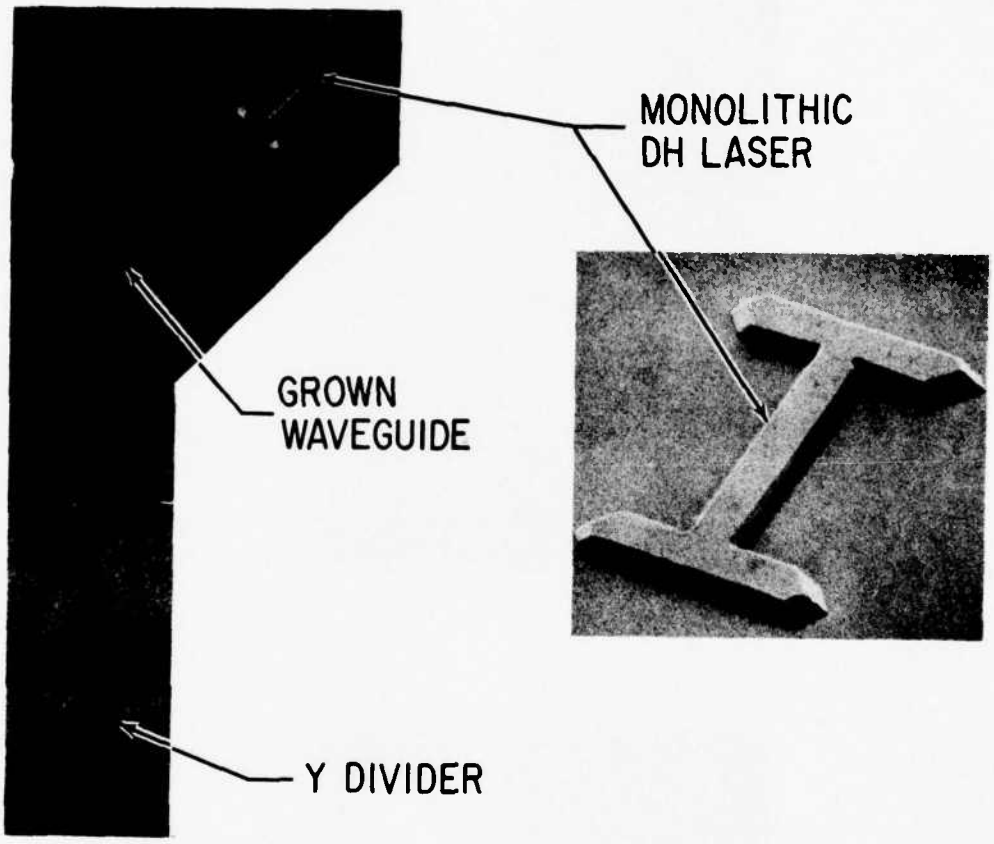

Figure 37 Complex Grown Waveguide Structure Including Straight Lines, Curves, and Y Dividers

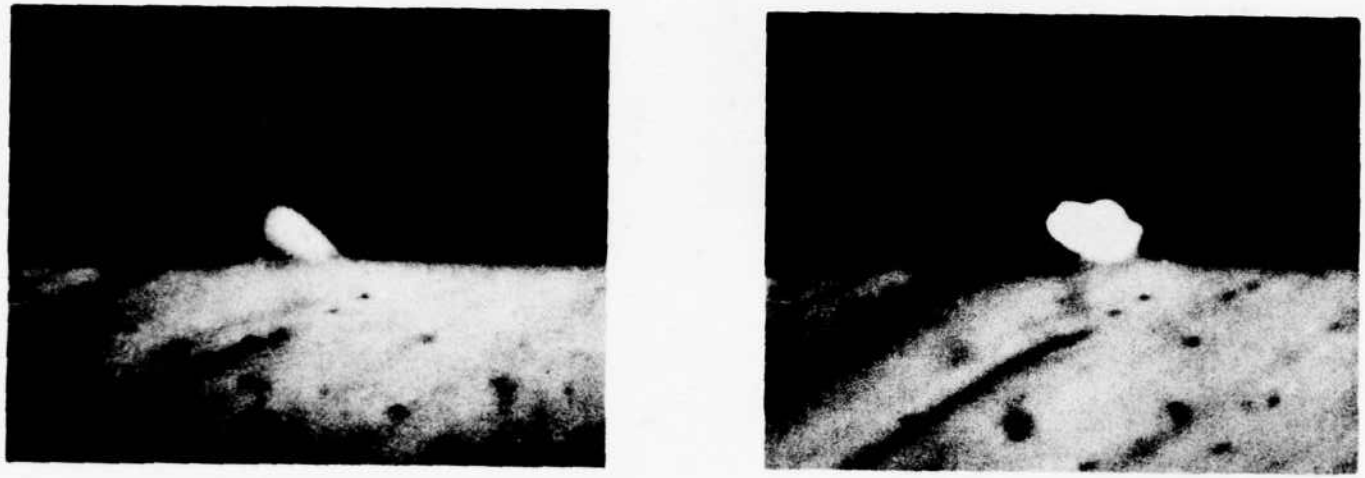

(a) (b)

Figure 38 TV Pictures of (a) an As-Grown Waveguide and (b) Light Guiding in the Waveguide

shows TV pictures taken with a vidicon camera of (a) an as-grown waveguide above the substrate, and (b) light guiding in the waveguide. As anticipated from the larger index of refraction discontinuity, the losses in straight-line sections are higher for the as-grown waveguides (9 to 18 dB/cm) than for the LPE (Ga,Aℓ)As planar rib waveguides (5 to 7 dB/cm). The loss values are also enhanced by materials inhomogeneities and defects in the long guide sections required to make these measurements. Improvements in the materials growth process would be expected to lessen the contribution from this area.

Due to the uncertainty in the loss measurements, it has not been possible to define absolute loss values associated with different radii of curvature. However, some relative values and trends have been obtained. Table II indicates the typical values obtained for a three-layer, as-grown waveguide. In this sample, ∞ is a straight-line guide adjacent to the curved guides and used as standard. As expected, the trend is toward increasing loss with decreasing radius of curvature. Rapid degradation occurs for $r_c < 1.27$ mm (50 mils) and places a lower limit on the range of interest for practical circuit design. Similar behavior was observed for the waveguide section of Figure 15 where the relative outputs of the two "legs" was $r_c(1.27\ \text{mm})/r_c(0) \sim 12$.

The as-grown waveguides have proved to be efficient in guiding light around bends. The straight-line losses, however, are too high at this time to be efficient in all sections of a waveguide circuit. Improvements in materials technology may lower the loss values to a more acceptable level, but with the present technology a hybrid circuit with as-grown guides around bends and low-loss planar rib guides in straight sections and for active devices appears to be the best compromise.

Table II

Signal Output for Three-Layer Waveguides
for 25 μm Wide Stripe

R_c (Mils)	R_c (mm)	Signal Out (mV)[b]	Normalized Signal[c] (mV)[b]
∞[a]	∞	6	1
100	2.540	4.2	0.7
50	1.270	3.8	0.63
25	0.635	0.6	0.1
0	0	0	0

[a]Straight-line waveguide

[b]Output voltage of photodetector is proportional to transmitted power

[c]Normalized signal is not corrected for variation in curve length

SECTION V

COUPLED I-BAR DOUBLE HETEROJUNCTION MESA LASERS AND WAVEGUIDES

Selective LPE mesa lasers and waveguides can be combined in a two-step process to produce an integrated circuit. This has been accomplished as shown in Figure 37 and marks a major milestone in the progress of this program. The following subsections will discuss the materials technology, fabrication, and test results for this device.

A. Materials Growth and Fabrication

The integrated I-bar mesa laser structure is produced in a two-step selective LPE process. The selective LPE procedures are the same as those described in the previous two sections. The overall design of the device as shown in Figure 34 consists of two separate masks, one for the waveguide structure and one for the mesa laser structure. In the first growth step the three-layer waveguide structure is grown in the waveguide pattern only. The mesa laser area in this step is covered by the silicon nitride mask. After the first growth step, the silicon nitride mask is stripped and the entire substrate, including the grown waveguide, is covered with fresh silicon nitride. The laser pattern is then opened in the mask and the DHJ I-bar mesa laser is grown in the second LPE growth step. Figure 39 shows the position of the mesa laser relative to the waveguide after the second growth step. The laser in this circuit is end-fired into the waveguide. Differences in the reflectivity in Figure 39 are due to the dielectric coating over the waveguide in this step. Ohmic contact to the back of the unthinned substrate is made by alloying electroplated Ni-Au at 300°C. The p-type contact on the top of the mesa is made by evaporating Cr-Au. A wide bonding pad at the side of the mesa permits off-mesa bonding. The final test device is cleaved along line A of Figure 34 to give single-channel light output. A finished device mounted on a TO-46 header is shown in Figure 40.

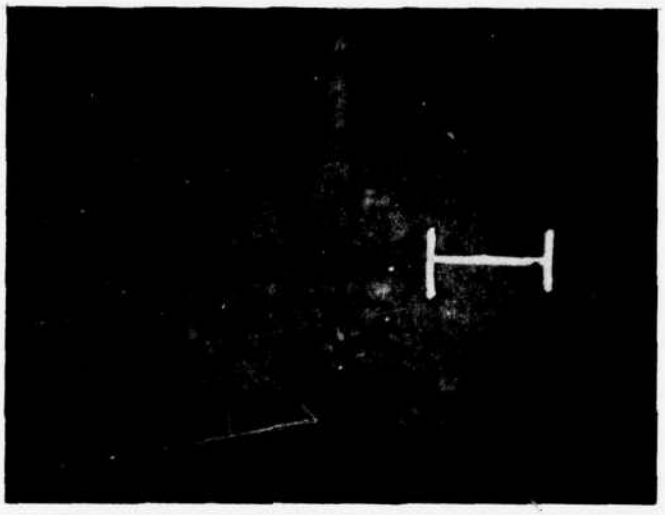

Figure 39 Photomicrograph (~ 20X) Showing the As-Grown Mesa Laser-Waveguide with a 0.254 mm (10 Mils) Radius Prior to Contacting. Differences in reflectivity are due to the dielectric coating over the waveguide.

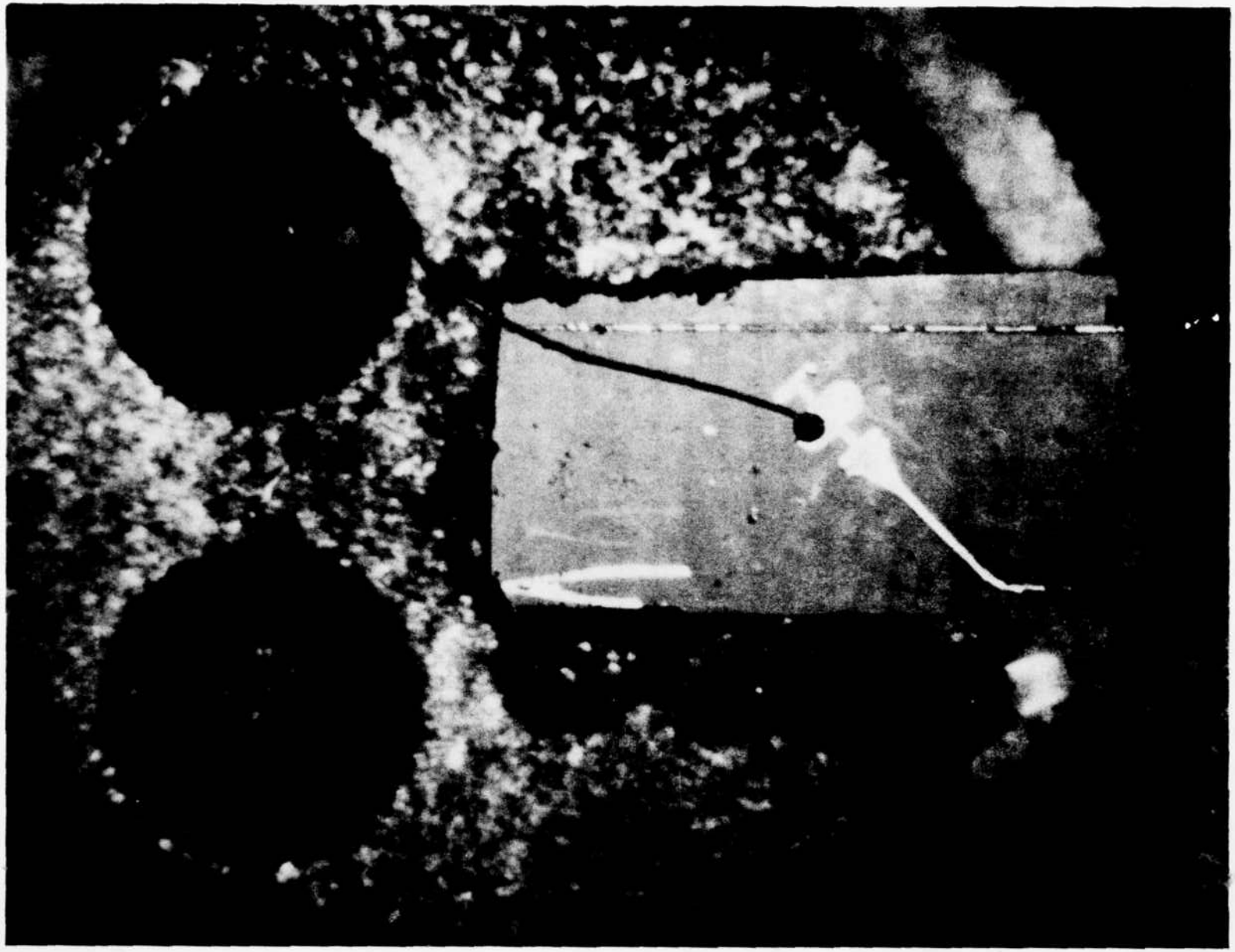

Figure 40 Photomicrograph (~ 10X) of the First Integrated Optical Circuit with an I-Bar Mesa and Channel Waveguide with Bend Mounted on a TO-46 Header

B. Device Performance

I-bar mesa laser-waveguides have been successfully fabricated and tested. The I-bars had been grown prior to the materials improvements previously mentioned. These devices had active regions of 1.5 μm and correspondingly high thresholds of 40 kA/cm^2. The as-grown waveguides are three-layer structures with nominal compositions of $Ga_{0.8}Al_{0.2}As$ - $Ga_{0.85}Al_{0.15}As$ - $Ga_{0.8}Al_{0.2}As$ with the central layer about 4.0 μm thick. Laser radiation from the I-bar was end-fired-coupled to the curved waveguide. Its radius of curvature was a severe 0.254 mm (10 mils). Measurements of the light transmitted through the waveguide and from the laser showed a transmission of about 35% of the laser output. The output was narrowband, suggesting that a selection of laser modes is taking place. The transmission figure was based on the power in the narrowband laser output, not on the total emission power spectrum of the laser. This unexpected selectivity is not understood at this time.

The successful testing of this device is a major accomplishment in this program. Although this structure has limitations which have become obvious in the growth, fabrication, and testing, it is a significant first step toward practical integration and supplies invaluable information in the design of the next-generation device.

C. Contacting

Work on reducing contact resistance on both I-bar and full-surface discrete lasers has continued. In order to achieve cw operation, series contact resistance (i.e., the diode series resistance) should be less than 1 Ω at the threshold current. Lower resistances, however, will increase the total power conversion efficiency. The major contribution to this series resistance arises from the metal-semiconductor-interface resistance. The lowest series resistance observed on our discrete lasers is 0.2 Ω; on the mesas, 7.0 Ω. These values correspond

to the same specific contact resistances of 2×10^{-4} Ω-cm^2 due to the differences in contact area. The improvement in discretes is due primarily to the introduction of a premetallization zinc diffusion into the surface p-type GaAs layer. Hole concentrations of 10^{20}/cc are achieved. In addition, Au-Zn or Ag-In-Zn followed by Ti-Au, Cr-Au, or Ni-Au metallization by evaporation or electroplating completes the contact. The higher resistance observed with mesa lasers is believed to be due to difficulties in cleaning the surface for the striped contact.

SECTION VI

ETCHED MESA DOUBLE HETEROJUNCTION LASERS AND WAVEGUIDES

One of the key problems in the development of integrated optical circuits is that of efficiently coupling light from a monolithic laser source to a waveguide circuit. Three coupling schemes have previously been reported: (1) end-fire coupling,[31,32] (2) taper coupling,[33,34] and (3) phase-matched coupling.[35,36] Devices using end-fire coupling have passive waveguides coplanar with the laser cavity. An alternate approach utilizes an intracavity taper to couple light from the laser to an underlying waveguide. A disadvantage of these coupling schemes is that they require the utmost control of the growth conditions[32,34] or a two-stage growth procedure.[31] A less complicated structure, from a fabrication point of view, has been reported by Suematsu, et al.[36,37] In these lasers the coupling between the laser cavity and an external passive waveguide is analogous to that of a directional coupler. To obtain efficient coupling, the propagation constants of the laser cavity and the passive waveguide must be closely matched. This imposes severe limitations on the dimensions and compositions of the layers. In this section we describe a device similar to the structure reported by Suematsu, et al.,[36,37] consisting of a monolithic laser on an underlying passive waveguide. The coupling mechanism differs, however, in that the modes of the waveguide are excited directly by the evanescent fields of radiation in the laser cavity without phase matching.

The following subsections discuss the device structure, the growth and fabrication, and test results for the etched mesa laser-waveguide structures.

A. Device Structure

The schematic in Figure 41 shows the structure for the laser-waveguide five-layer device with typical layer compositions and thicknesses. Starting from the substrate, the LPE layers are n-type $Ga_{0.7}Al_{0.3}As$ (3 μm), n-type $Ga_{0.85}Al_{0.15}As$ (5 μm), n-type GaAs active layer (0.5 μm), p-type $Ga_{0.7}Al_{0.3}As$ (1.5 μm), and p-type GaAs (1 μm) for contacting. The six-layer devices have

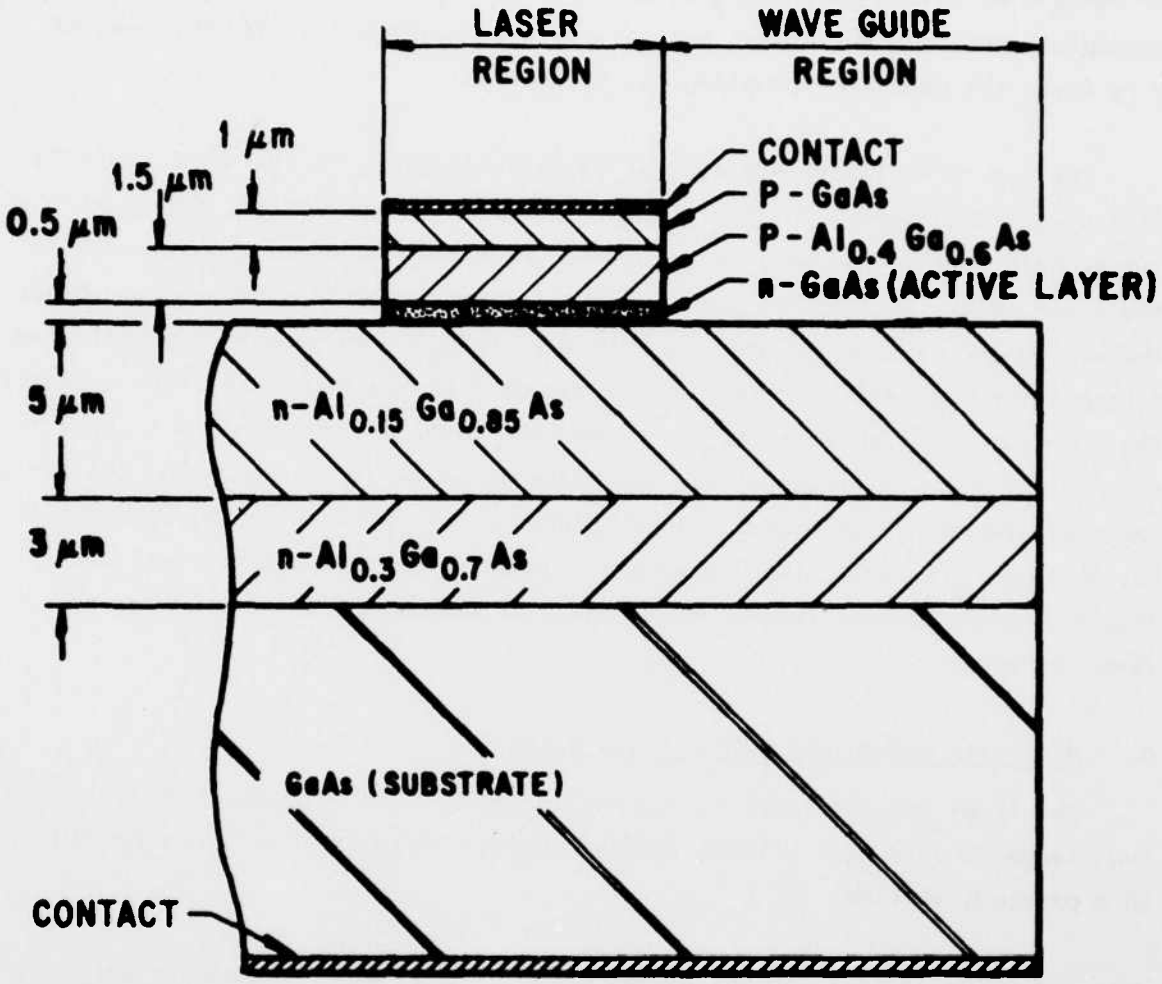

Figure 41 Schematic of the Etched Mesa Laser-Waveguide Five-Layer Structure

an additional thin n-type $Ga_{0.7}Al_{0.3}As$ (0.5 μm) layer between the n-$Ga_{0.85}Al_{0.15}As$ waveguide layer and the n-GaAs active layer. By increasing the thickness of this layer the amount of coupling can be reduced.

The top three layers are typical of those commonly found in (Al,Ga)As/GaAs heterojunction lasers. The fourth layer has a dual function; it serves as the n-type heterobarrier as well as being the "external" waveguide. Radiation in the laser region excites the modes of the surrounding waveguide region. Hence, the active and passive regions are strongly, rather than weakly, coupled. The bottom layer optically isolates the waveguide from the higher index GaAs substrate. The elimination of phase matching between the laser and the substrate permits more flexibility in tailoring the waveguide parameters. For example, the divergence of the waveguide output can be reduced by increasing the thickness of the fourth layer similar to the "leaky wave" lasers reported by Scifres et al.[38] This structure has the further advantage that the waveguide is transparent to the laser emission.

B. Materials Growth and Device Fabrication

The five- and six-layer structures are grown by liquid phase epitaxy using the standard horizontal sliding graphite boat. These systems have been described in a previous section.

Following crystal growth, standard photolithographic techniques are used to define a silicon nitride mask consisting of rectangles 300 μm x 200 μm. The crystal is then chemically etched in two steps. First, a calibrated $NaOH:H_2O_2$ etch[39] is used to remove the top three layers and etch into the fourth layer. This is followed by a 30 minute etch in the Superoxol solution described by Logan and Reinhart.[40] Since the Superoxol solution etches GaAs faster than (Al,Ga)As, this second etching step helps to "square up" the ends of the laser cavity as illustrated by the photograph in Figure 42. We find that the Superoxol etch is an important fabrication step that can in some instances be the difference

Figure 42 Cross Section of an Etched Mesa after the Second Preferential Etch to "Square Up" the Ends of the Laser Cavity

between a device that will lase and one that will not. The etching procedure can be used to control the degree of coupling. Etching partially into the waveguide results in increased reflectivity and a reduction in the amount of light coupled into the waveguide. Contact to the top of the etched mesa is made by selectively electroplating Au-Ni. An alloyed Au-Sn contact is made to the back of the substrate. For testing, the devices are soldered on the edge of TO-46 headers. The lasers are driven with 200 ns current pulses at a repetition rate of 100 Hz.

C. Device Testing and Results

Figure 43 is a photograph of the near field emission from an etched laser-waveguide device above threshold. The photograph was taken with an infrared microscope focused on the end of the waveguide and thus misrepresents the relative amount of light emerging from the waveguide compared to that from the laser. It does, however, clearly illustrate light coupling from the laser to the waveguide. The coupling efficiency of these devices is measured with a calibrated PIN photodiode in three steps. First, the total output from the laser and waveguide is measured for increasing drive current. Then the power in the waveguide is determined by blocking off light from the laser with a knife edge positioned between the laser and the end of the waveguide. Finally, the background light is measured with the knife edge in position and the end of the waveguide masked with a thick layer of black wax.

Figures 44 and 45 are representative of the data obtained by this procedure. These data were taken on five-layer and six-layer devices, respectively. The dashed curve and solid curve show the power in the laser and the waveguide, respectively. For the six-layer devices the average coupling efficiency (i.e., the percentage of the laser power coupled into the waveguide) was approximately 10%. The average laser threshold current density was 2.6 kA/cm^2. This is approximately 15% higher than cleaved discrete lasers fabricated from the same crystal. The increased laser threshold is due primarily to the additional loss of light into the waveguide and can be compensated by fabricating mirrors on the

Figure 43 Near Field Emission from an Etched Laser-Waveguide Device above Threshold. The mesa laser is shown as the bright area under the contact. The bright spot in the foreground is the output from the waveguide layer at the cleaved face.

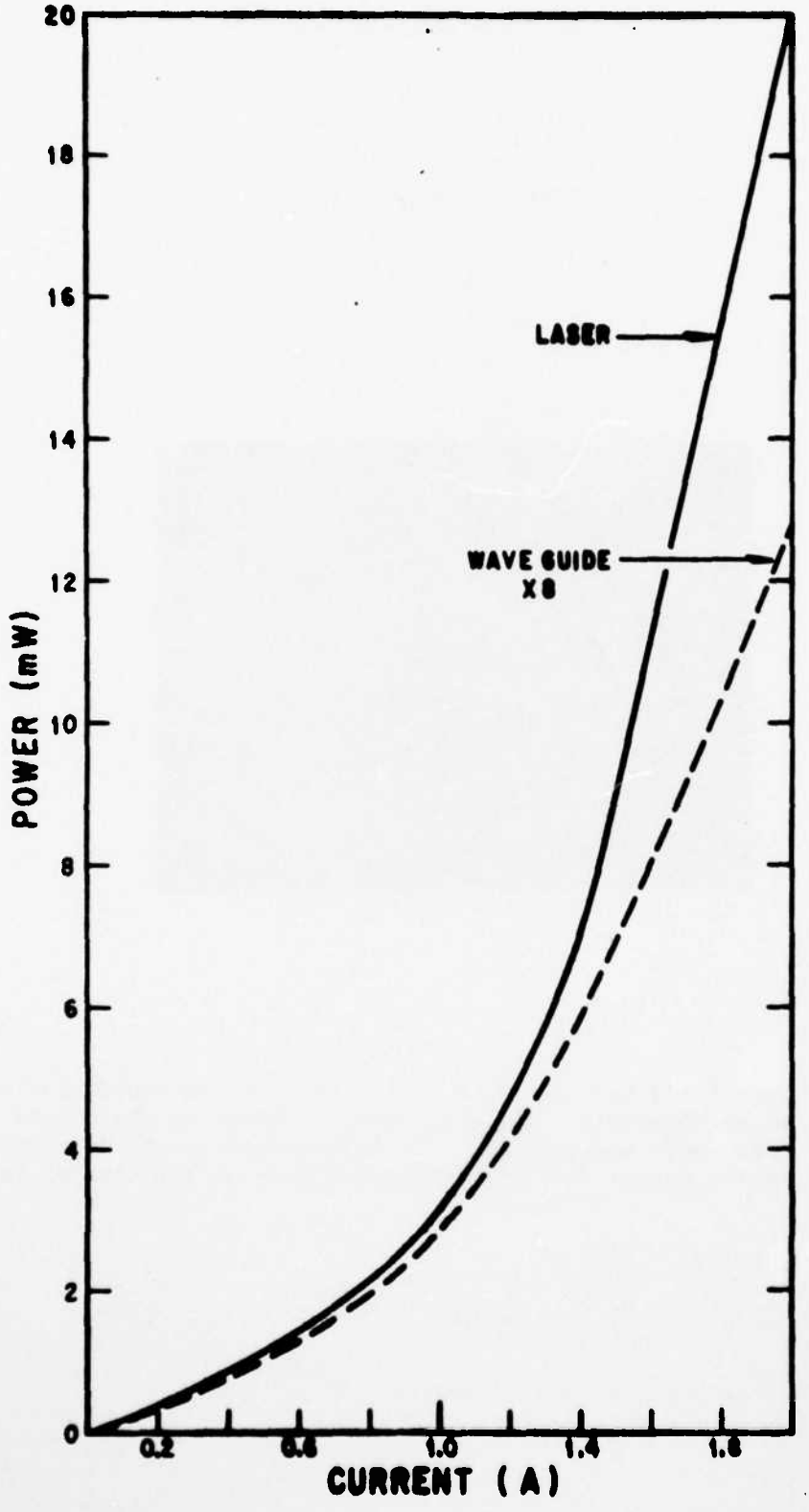

Figure 44 Power Output for the Laser and for the Waveguide in a Five-Layer Structure

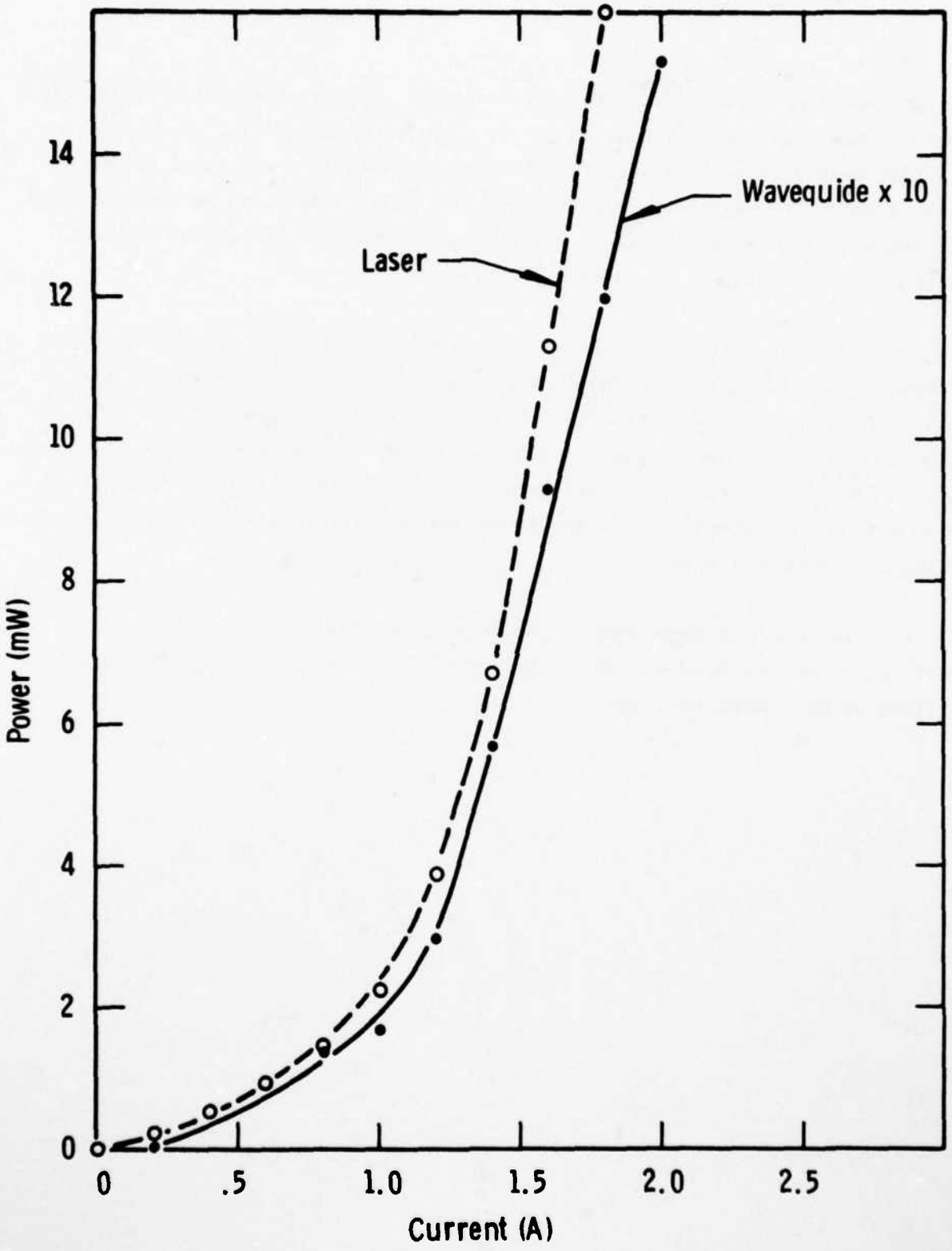

Figure 45 Power Output Measured for the Laser and for the Waveguide in a Six-Layer Structure

ends of the laser cavity.[36,37] In some instances the laser threshold is significantly higher than can be accounted for by light coupled into the waveguide. This discrepancy is probably attributable to unsatisfactory end faces on the etched lasers. In devices fabricated from five-layer structures we have observed coupling efficiencies as low as 3% and as high as 25% with corresponding laser thresholds in the range 3 to 10 kA/cm^2, respectively.

The far-field pattern of the emission from the waveguides has been measured by rotating a fiber optic bundle in an arc perpendicular to the plane of the waveguide. In a five-layer structure having a 5 μm-thick waveguide the full angle between half power points is approximately 5° and for a six-layer structure with a 4 μm-thick waveguide the divergence is 6°. By fabricating similar structures with stripe geometries, it should be possible to closely match the numerical aperture of optical fibers.

In this study, we have demonstrated evanescent field coupling between a monolithic laser and a waveguide. Coupling efficiencies as high as 25% have been obtained without phase matching.

SECTION VII

CHALCOGENIDE GLASS WAVEGUIDES

The initial concept for making an integrated optical circuit was to couple the output of optically pumped mesa lasers to glass waveguides. As the program progressed, the development of III-V waveguides appeared to be a better choice for integrated structures. Significant progress with chalcogenide waveguides, however, was made during the first phase of the program, but this work was not continued into the latter phases. This section describes the fabrication and performance of these glass waveguides.

Since chalcogenide glasses contain no light elements such as oxygen or fluorine, they are transparent at long wavelengths.[41] Many are also highly transmissive in the spectral region near 1 μm, where the propagation loss of optical fibers is low and sensitive detectors are available. Their high refractive indices make them compatible with GaAs optical circuit elements. The large acousto-optic figures of merit and relatively low acoustic absorption loss make them good materials for acousto-optic modulators.[42] The waveguiding properties of three such glasses, As_2S_3, $Ge_{28}Sb_{12}Se_{60}$ (TI #1173), and $Ge_{33}As_{12}Se_{55}$ (TI #20) have been investigated.

As_2S_3 is transparent well into the visible spectral region. However, the other two glasses have absorption edges near the spectral region of interest. Therefore, refractive indices and absorption coefficients were measured for these bulk glasses. These data are shown in Table III and Figure 46. Indices were measured by the method of minimum deviation.[44] Absorption coefficients were measured by a calorimetric method at 1.064 μm, 1.123 μm, and 1.358 μm with a YAlG:Nd laser as radiation source. Absorption spectra taken with a spectrophotometer were normalized to pass through the points measured calorimetrically.

Thin films were prepared by rf sputtering in an argon ambient. Sputtering targets of TI #1173 and TI #20 glasses were cast at Texas Instruments. The hot-pressed As_2S_3 target was purchased from Energy Conversion Devices of Troy, Michigan. Substrates were usually optical flats of borosilicate glass or quartz

Table III

Refractive Indices and Absorption Coefficients of Bulk Chalcogenide Glasses

$\lambda(\mu m)$	1.064	1.123	1.358
TI #1173			
n	2.707	2.688	2.662
α(dB/cm)	0.3	0.2	0.1
TI #20			
n	2.586	2.577	2.560
α(dB/cm)	0.4	0.4	0.3

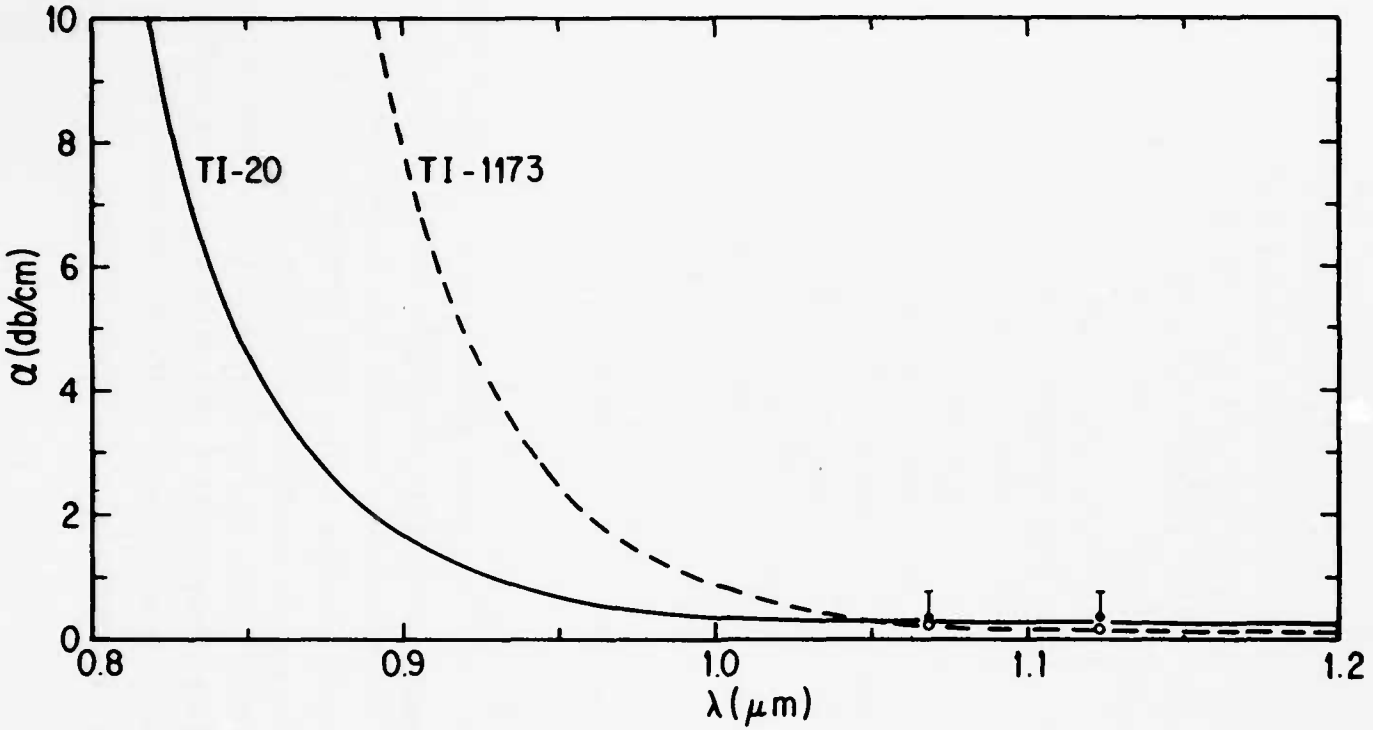

Figure 46 Absorption Loss vs Wavelength of TI #20 and TI #1173 Bulk Glasses in the Region Near the Fundamental Absorption Edge. The points were obtained by calorimetric measurements, as described in the text.

AD-A045 672 TEXAS INSTRUMENTS INC DALLAS CENTRAL RESEARCH LABS F/G 20/5
MONOLITHIC LASER.(U)
SEP 77 K L LAWLEY N00014-73-C-0288
UNCLASSIFIED TI-08-77-19 NL

2 OF 2
ADA
045672

END
DATE
FILMED
11-77
DDC

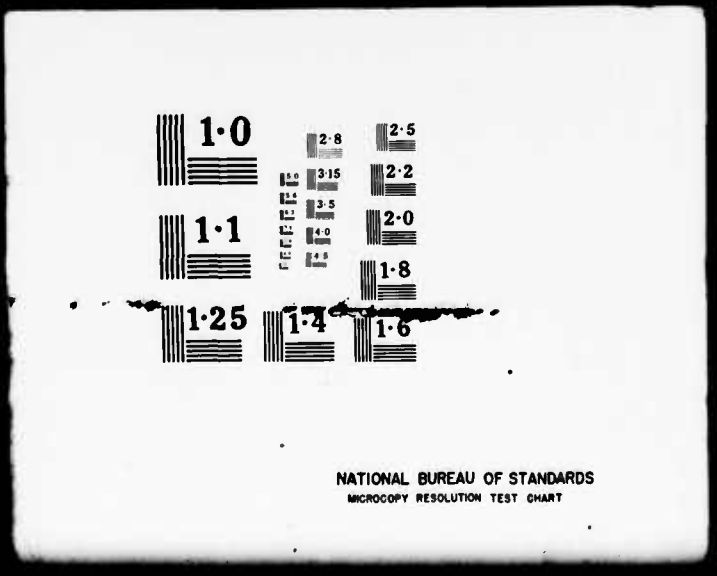

5.0 cm or 7.6 cm (2 to 3 inches) in diameter and 1.3 cm (0.5 inch) thick. Both targets and substrates were mounted on water-cooled plates, the substrate being mounted above the target so that sputtering was always upward. Substrates were cleaned in deionized water and detergent. Absence of dust particles and surface imperfections could be checked by dark-field microscopic examination. Composition of the films was determined by electron microprobe analysis. The TI #1173 and TI #20 films were found to be slightly richer in Ge than the bulk glasses. For most waveguiding experiments, a YAlG:Nd laser oscillating at 1.064 μm was used as the radiation source. The beam was coupled into the film with a prism coupler of GaAs. It was found convenient to use two different types of infrared-to-visible image converter: a small, hand-held type (Varo Corp., model 6929) and a larger type with camera attached (Wild, model M500). Thus, the converted image of the streak of light scattered from the guided wave could be photographed. The streak could also be photographed directly with 35 mm infrared-sensitive film. The angle of the input beam with respect to an axis perpendicular to the input surface of the prism could be measured. For lossy films the propagation loss could be measured from a plot of photographic film exposure density versus distance.

When the propagation loss of a film was less than about 5 dB/cm, it was necessary to measure the loss by another means. An output coupling prism, also of GaAs, was used. It could be translated along the path of the guided wave. The radiation coupled out was detected with a photomultiplier and a lock-in amplifier. Figure 47 shows typical data obtained for an As_2S_3 film 0.72 μm thick on a borosilicate glass substrate. Annealing at 265°C in a dry nitrogen atmosphere reduced losses in the TI #1173 films by about a factor of two. Annealing had no effect on the TI #20 films and led to surface degradation of the As_2S_3 films. Anneal point is different for each glass and is the value commonly used for commercial chalcogenide glasses.

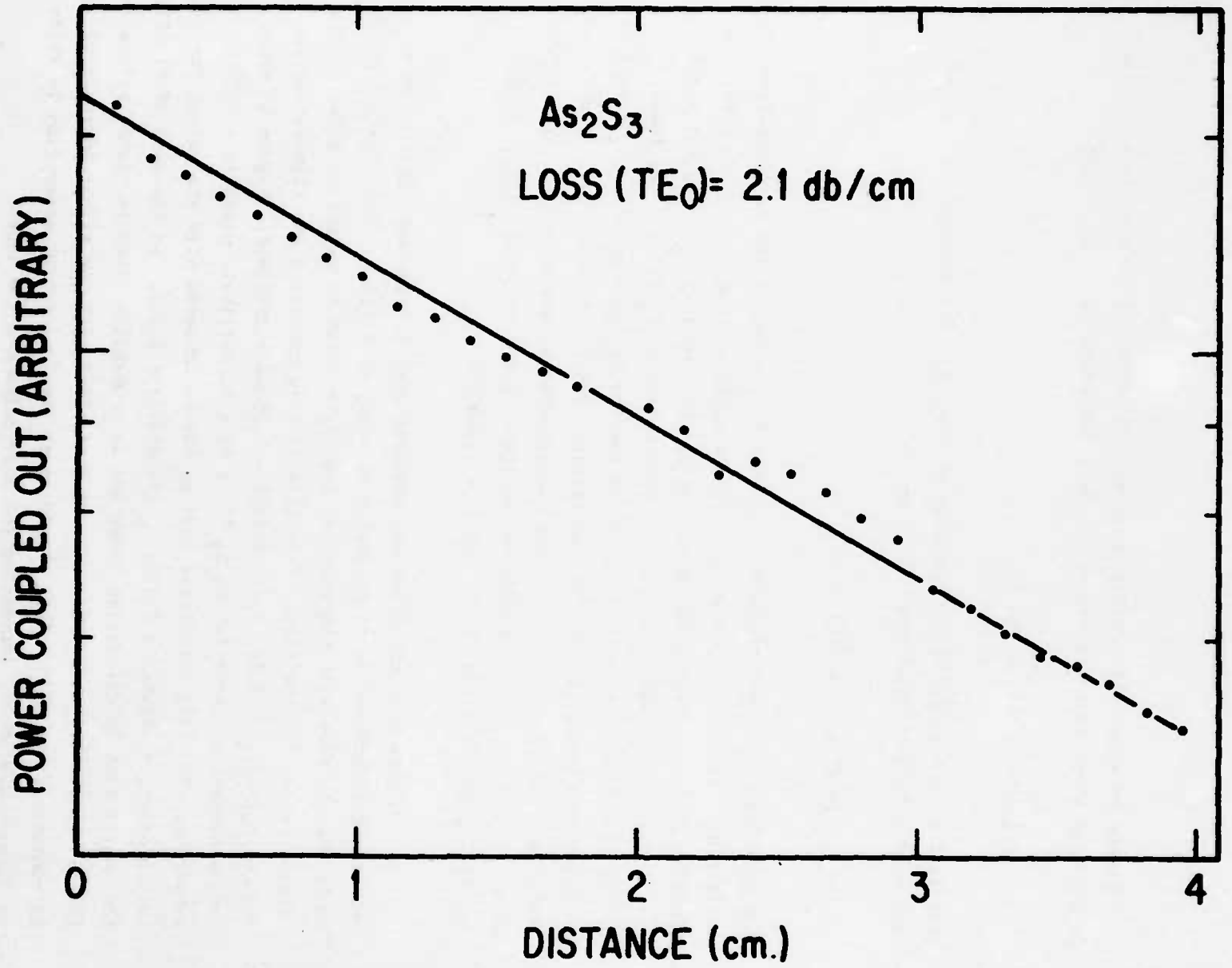

Figure 47 Power Coupled Out from the TE_0 Mode of an As_2S_3 Film 0.72 μm Thick vs Propagation Distance. The straight line is a least squares fit to the data. The slope is -2.1 dB/cm.

Figure 48 shows the typical dependence of propagation loss on mode index. In the case shown this dependence can be represented by the relation

$$L(m) = 3.7 + (0.70)\ (m + 1)^2 \quad .$$

L(m) is the loss in dB/cm for the mode of index m. The propagation loss of mode m of a film of thickness d is given by

$$L(m,d) = L_o + f(d)\ (m + 1)^2 \quad .$$

The parameter L_o is an irreducible minimum loss which is due to absorption and scattering. It is the loss which would be measured in a very thick film. The function f(d) decreases with increasing d. We find that L_o = 3.5 - 3.7 dB/cm for TI #1173 films and L_o = 0.35 - 0.4 dB/cm for As_2S_3 films. The lowest propagation loss measured was 0.4 dB/cm for the TE_o mode of an As_2S_3 film 2.08 μm thick on a borosilicate glass substrate. The TI #20 films exhibited the highest losses and for this reason were not investigated extensively. For the TE_o mode of a film 0.7 μm thick the propagation losses are 2 dB/cm for As_2S_3, 10 dB/cm for #1173, and 22 dB/cm for TI #20 (λ = 1.064 μm).

The thickness of the films was measured with a Michelson interferometer microscope attachment to an estimated accuracy of ± 150 Å. The coupling angles could then be used with the measured substrate index to establish a set of dispersion curves for the film. From this fitting procedure the film refractive indices $n_f(As_2S_3)$ = 2.36, n_f(TI #1173) = 2.75 were obtained. Figure 49 shows such a dispersion curve for As_2S_3 films on a borosilicate glass (n = 1.5066) substrate. The film refractive indices may be compared with the values for the bulk glasses, $n_b(As_2S_3)$ = 2.470, n_b (TI #1173) = 2.707. In the case of TI #1173 the shifts both in refractive index and in propagation loss to higher values in the film with respect to the bulk are consistent with the slight increase of Ge content of the film. This should cause the fundamental absorption to shift to longer wavelength, increasing the absorption and the index.

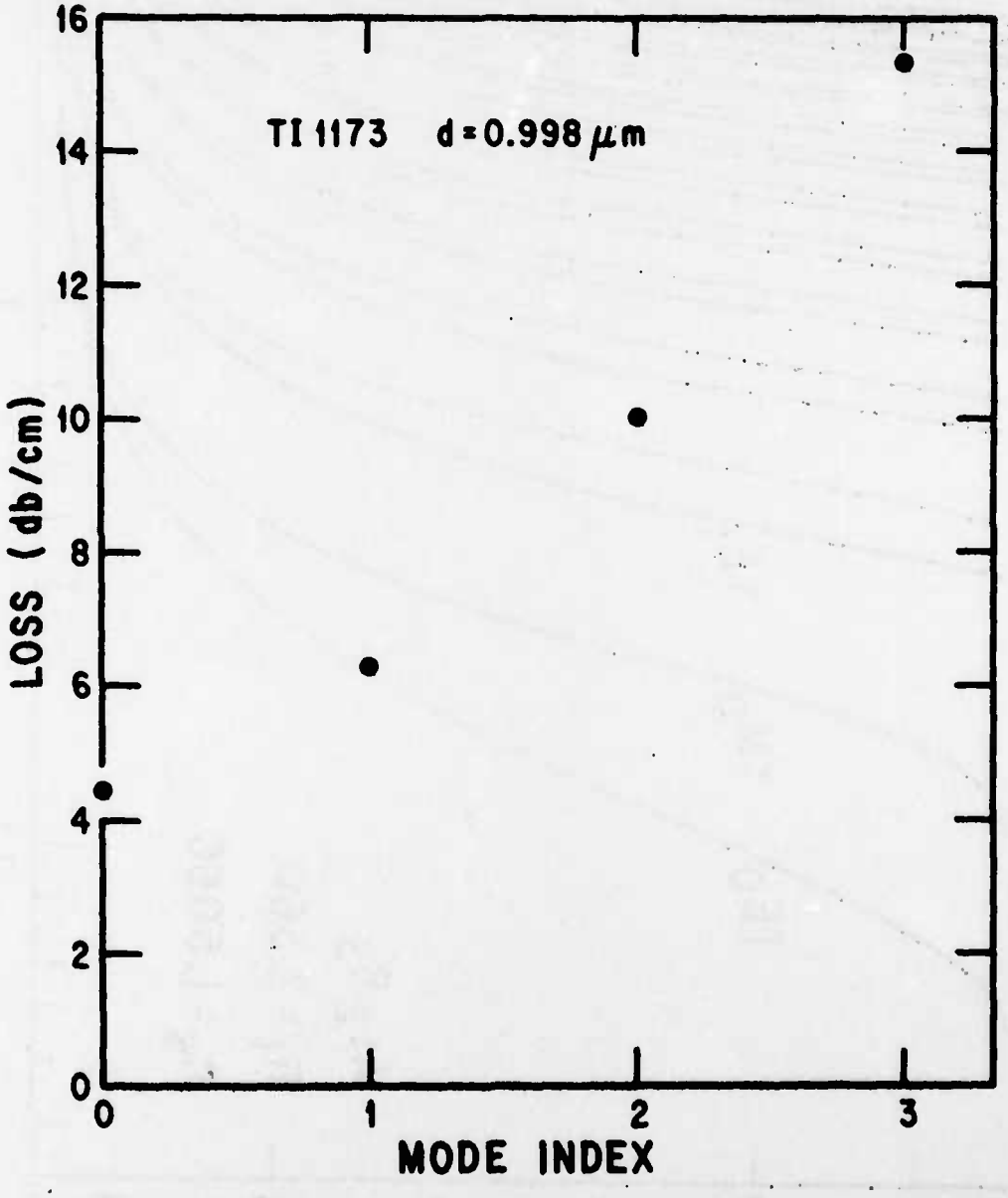

Figure 48 Propagation Loss vs Mode Index m for TE_m Modes of a TI #1173 Film 0.998 μm Thick. The substrate is borosilicate glass.

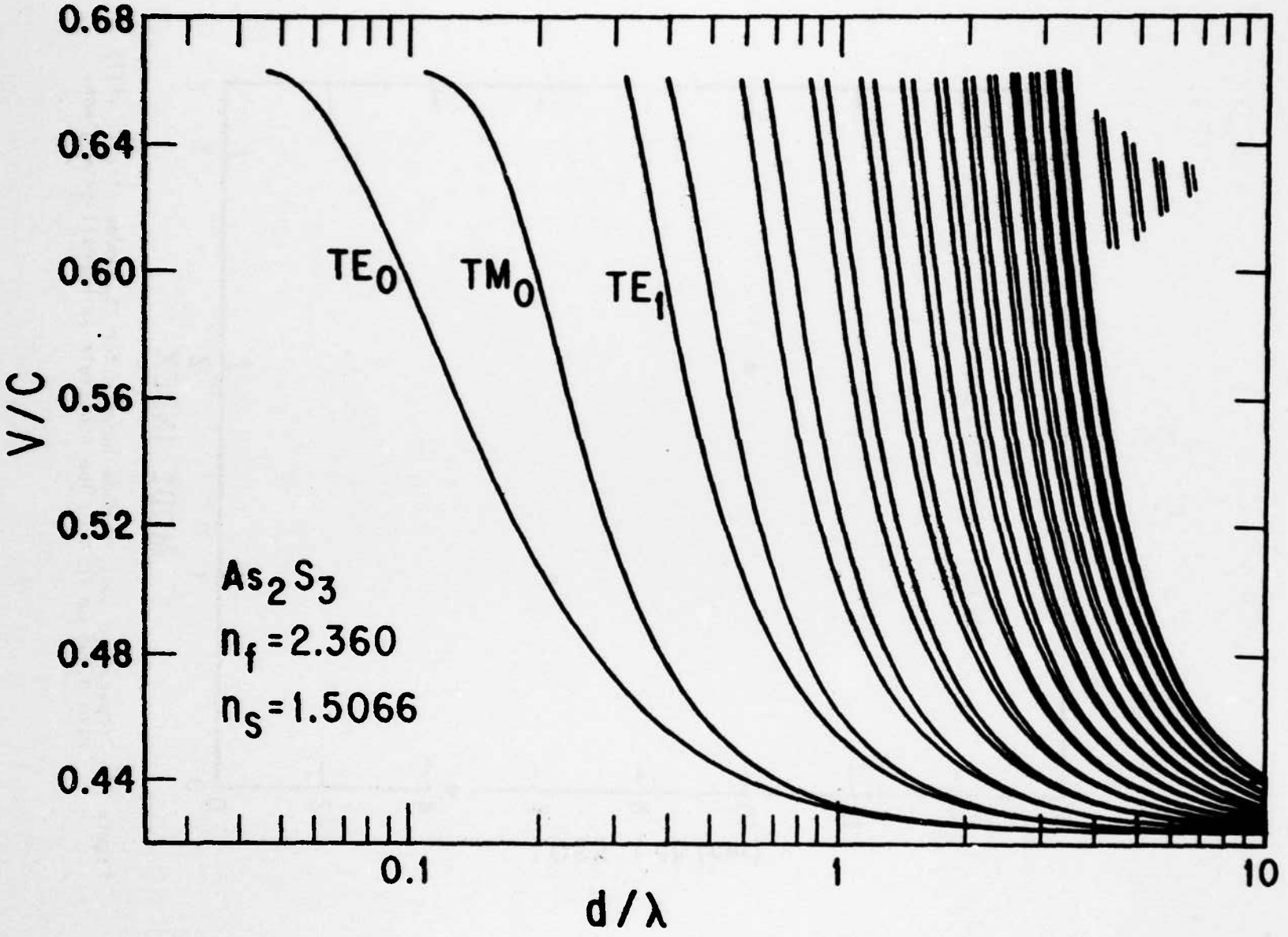

Figure 49 Dispersion Curves for As_2S_3 Films on Borosilicate Glass. V is the phase velocity of the guided wave, d is film thickness, and λ is the free space wavelength.

Delineated channel waveguides were also made. These were of the optical stripline type first studied by Furuta, et al.,[43] and consisted of a stripe of AZ1350 photoresist (n = 1.64) on a chalcogenide glass film on a borosilicate glass substrate. An image converter photograph of a 1.06 μm laser beam trapped in an optical stripline is shown in Figure 50. Thickness of the stripe was 0.3 μm, and widths of 5 μm, 10 μm, 20 μm, and 40 μm were used. The guided wave was launched into an uncovered portion of the film with a prism coupler and directed to the area covered by the stripe. Even when the angle between the initial direction of propagation and the direction of the stripe amounted to $\sim 20°$, the guided wave was "captured" by the stripe and propagated along it. Since the optical energy is largely confined to the film beneath the stripe, perfection of the sides of the stripe is not critical. The propagation loss of the wave guided beneath the stripe is the same as that of a guided wave in the uncovered film.

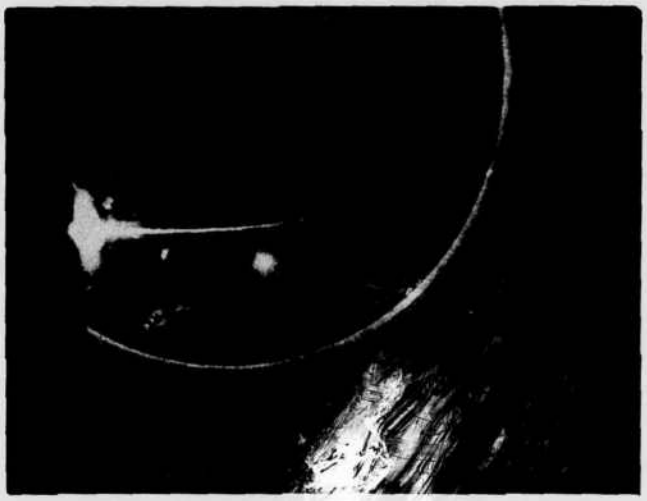

Figure 50 Photograph of a 1.06 μm Laser Beam Trapped in Two Dimensions While Propagating in a Two-Dimensional Film of TI #1173 Glass Sputtered on a Quartz Substrate and Overlaid by a Curved Strip of AZ1350 Photoresist

SECTION VIII

SUMMARY AND CONCLUSIONS

This report describes the accomplishment of a three-phased exploratory research program under Contract No. N00014-73-C-0288 to develop the first integrated optical transmitter.

The initial efforts involved the development of a unique (Ga,In)As surface laser and high index infrared glass waveguides. The surface laser is a vapor-grown mesa structure with vertical grown crystalline facets furnishing the optical feedback. The structure can be placed and grown at will on a GaAs substrate using conventional photolithographic techniques. This unique laser structure represents a radical departure from conventional semiconductor laser technology. Ternary alloy $Ga_{1-x}In_xAs$ mesas with $0 < x < 0.2$ were grown and the details of their morphology determined. Optically pumped laser emission from mesas with $0 < x < 0.1$ has been observed. Threshold pump powers, efficiencies, and emission characteristics have been determined. Also, a GaAs and $Ga_{1-x}In_xAs (x \leq 0.8)$ mesa diode laser was successfully fabricated. The p-n junction was formed by Zn diffusion and implantation into the top of the mesas. The $Ga_{1-x}In_xAs$ homojunction lasers are the first wavelength-tunable, monolithic electrical injection lasers and have been operated between liquid nitrogen and room temperatures. Monolithic arrays of up to six mesa lasers have been operated with all the lasers oscillating simultaneously. Because these devices are homojunctions, their threshold current densities at room temperature are very high (~ 170 kA/cm^2), and their efficiencies are low. These diode mesa lasers are the first monolithic, nondiscrete injection lasers ever made. They are the first diode lasers ever completely fabricated (including optical cavity formation) monolithically using conventional photolithographic fabrication technology. This development is a significant first in semiconductor laser technology with importance in both integrated optical source development and discrete laser technology.

A monolithic laser structure called an I-bar mesa laser was developed. This double heterojunction GaAs/GaAlAs laser was grown by selective liquid phase epitaxy. The best devices operated at 525 mA drive current with a pulsed,

300 K threshold current density of 7.5 kA/cm^2. Methods of fabricating these devices are discussed. Also, various types of grown waveguides including bends and Y's were demonstrated. For bends, a 3 dB signal attenuation is observed at a radius of curvature of $\sim$ 1.3 mm (50 mils). This radius appears to be a practical lower limit for integrated optical circuit waveguides. The I-bar mesas were combined on a chip with a grown three-layer waveguide. Measured intensity of light transmitted by end-firing from the laser through the curved waveguide was 35% of the laser emission with a narrowband output. Also, etched double heterojunction mesa laser structures were fabricated on underlying waveguides. The emission from these lasers was evanescently coupled to this guide. A coupling of 25% of the laser emission to the guide was observed.

Finally, high quality chalcogenide glass optical waveguides have been developed. Losses as low as 0.4 dB/cm were measured in sputtered As_2S_3 films. Channel optical stripline waveguides were fabricated by overlaying photoresist strips on the glass films. Low-loss channel waveguiding was observed in these structures.

At the end of this program, grown mesa lasers had been fabricated along with passive waveguides. The light generated by the injection lasers was coupled to the guide and transmitted around a 45° curve. This technology, coupled with light modulators and switches, will allow for the demonstration of such optical devices as transmitters for fiber optic communications. In addition to this application, such circuits could find future utility in spectrum analysis, optical logic, and signal processing in the infrared spectrum of the electromagnetic spectrum.

The major task remaining at the end of this program is the achievement of cw operation at room temperature (300 K). Devices were operated pulsed at 300 K; however, the lasing thresholds of the devices were high due to thick active layers in the DHJ and due to current spreading. A modified I-bar structure to reduce these effects was proposed. Work on this promising modification was in progress at the end of the contract.

ACKNOWLEDGMENTS

We particularly wish to thank H. Hendricks and his colleagues of NASA, Langley Field, for preparing the Zn ion-implanted samples. We are also gratful to D. W. Shaw for discussion of the mesa growth, K. C. Wiemer for advice on the Zn-doped SiO_2, A. R. Reinberg for oxide deposition, and G. P. Pollack for the spreading resistance probe measurements. We are also indebted to W. Abercrombie, D. W. Attaway, P. K. Bunch, M. Howell, S. H. Howison, W. L. Kriss, J. R. McIntire, F. D. Sinclair, and W. A. Dillon for their expert technical assistance.

REFERENCES

1. F. A. Blum, K. L. Lawley, R. K. Watts, F. H. Doerbeck, W. C. Scott, and W. C. Holton, "Monolithic Laser," Annual Interim Report, Contract No. N00014-73-C-0288, June 1974, AD785021.

2. F. A, Blum, D. W. Bellavance, J. C. Campbell, and K. L. Lawley, "Monolithic Laser," Annual Interim Report, Contract No. N00014-73-C-0288, July 1975.

3. K. L. Lawley, D. W. Bellavance, and J. C. Campbell, "Monolithic Laser," Annual Interim Report, Contract No. N00014-73-C-0288, March 1977.

4. D. W. Shaw, J. Electrochem. Soc. 113, 904 (1966).

5. D. W. Shaw, J. Electrochem. Soc. 115, 777 (1968).

6. H. F. Sterling and R. C. G. Swann, Sol. St. Electronics 8, 653 (1965).

7. M. H. Pilkuhn, Phys. Stat. Solidi 25, 9 (1968).

8. M. I. Nathan, A. B. Fowler, and G. Burns, Phys. Rev. Letters 11, 152 (1963).

9. H. M. Macksey, J. C. Campbell, G. W. Zack, and N. Holonyak, J. Appl. Phys. 43, 3534 (1974).

10. C. J. Nuese, M. Ettenberg, R. E. Enstrom, and H. Kressel, Appl. Phys. Letters 24, 224 (1974).

11. W. E. Ahearn and J. W. Crowe, IEEE J. Quantum Electron. QE-6, 377 (1970).

12. M. B. Panish, J. Appl. Phys. 44, 2667 (1973).

13. K. K. Shih and G. D. Pettit, J. Electron. Mat. 3, 391 (1974).

14. C. J. Hwang and J. C. Dyment, J. Appl. Phys. 44, 3240 (1973).

15. F. E. Rosztoczy and K. B. Wolfstirn, J. Appl. Phys. 42, 426 (1971).

16. A. J. Springthorpe, F. D. King, and A. Becke, J. Electron. Mat. 4, 101 (1975).

17. D. L. Rode, R. L. Brown, and M. A. Afromowitz, J. Cryst. Growth 30, 299 (1975).

18. J. P. Chane, L. Hollan, and C. Schiller, J. Cryst. Growth 13/14, 325 (1972).

19. S. Iida and K. Ito, J. Cryst. Growth 13/14, 336 (1972).

20. D. W. Shaw, R. W. Conrad, E. W. Mehal, and O. W. Wilson, Proceedings of the 1966 Symposium on GaAs, p. 10.

REFERENCES

(Continued)

21. T. Mikawa, O. Wada, and H. Takanashi, Jap. J. Appl. Phys. 11, 1756 (1972).

22. T. Kawakami and K. Sugiyama, Jap. J. Appl. Phys. 12, 1808 (1973).

23. I. Samid, C. P. Lee, A. Gover, and A. Yariv, Appl. Phys. Lett. 27, 405 (1975).

24. D. W. Bellavance, unpublished results.

25. F. A. Blum, K. L. Lawley, W. C. Scott, and W. C. Holton, Appl. Phys. Lett. 24, 430 (1974).

26. F. A. Blum, K. L. Lawley, F. H. Doerbeck, and W. C. Holton, Appl. Phys. Lett. 25, 620 (1974).

27. E. Pinkas, B. I. Miller, I. Hayashi, and P. W. Foy, J. Appl. Phys. 43, 2827 (1972).

28. J. K. Butler, C. S. Wang, and J. C. Campbell, J. Appl. Phys. 47, 4033 (1976).

29. K. L. Lawley and J. C. Campbell, "(Aℓ,Ga)As Devices for Waveguide Circuits," Technical Report No. 2, Contract No. N00014-75-C-0501, July 1976.

30. J. C. Campbell and D. W. Bellavance, "Bends and Curves in Optical Stripline Waveguides," Presented at the Device Research Conference, June 1976; Abstract IIA-3 (to be published).

31. C. E. Hurwitz, J. A. Rossi, J. J. Hsieh, and C. M. Wolfe, Appl. Phys. Lett. 27, 241 (1975).

32. F. K. Reinhart and R. A. Logan, Appl. Phys. Lett. 25, 622 (1974).

33. J. L. Merz, R. A. Logan, W. Wiegmann, and A. C. Gossard, Appl. Phys. Lett. 26, 337 (1975).

34. F. K. Reinhart and R. A. Logan, Appl. Phys. Lett. 26, 516 (1975).

35. R. K. Watts, J. Appl. Phys. 44, 5635 (1973).

36. Y. Suematsu, M. Yamada, and K. Hayashi, Proc. IEEE (Lett.) 63, 208 (1975).

37. Y. Suematsu, M. Yamada, and K. Hayashi, IEEE J. Quantum Electron. QE-11, 457 (1975).

38. D. R. Scifres, W. Streifer, and R. D. Burnham, Appl. Phys. Lett. 29, 23 (1976).

39. T. Kobayashi and K. Sugiyama, Jap. J. Appl. Phys. 12, 619 (1973).

REFERENCES

(Continued)

40. R. A. Logan and F. K. Reinhart, J. Appl. Phys. 44, 4172 (1973).

41. A. R. Hilton, Appl. Optics 5, 1877 (1966).

42. N. Uchida and N. Niizeki, Proc. IEEE 61, 1073 (1973).

43. H. Furuta, N. Noda, and A. Ihaya, Appl. Optics 13, 322 (1974).

44. F. A. Jenkins and H. E. White, Fundamentals of Optics (McGraw-Hill Book Co., New York, 1957), p. 21.

APPENDIX

JOURNAL ARTICLES AND CONFERENCE PRESENTATIONS

APPENDIX

JOURNAL ARTICLES AND CONFERENCE PRESENTATIONS

The following journal articles concerning work done under contract sponsorship were written.

1. F. A. Blum, K. L. Lawley, F. H. Doerbeck, and W. C. Holton, "Monolithic GaAs Injection Mesa Lasers with Grown Optical Facets," Appl. Phys. Lett. 25, 620 (1974).

2. F. A. Blum, K. L. Lawley, and W. C. Holton, "Monolithic Integrated Optical Circuits," Naval Res. Revs. 28, 1 (1975).

3. F. A. Blum, "Integrated Optics Mirrors Microwave Concepts" (Parts I and II), MicroWaves (April and May 1975); with cover photograph and feature editorial.

4. F. A. Blum, K. L. Lawley, and W. C. Holton, "Monolithic $Ga_{1-x}In_xAs$ Mesa Lasers with Grown Optical Facets," J. Appl. Phys. 46, 2605 (1975).

5. F. H. Doerbeck, K. L. Lawley, F. A. Blum, and J. C. Campbell, "Monolithic $Ga_{1-x}In_xAs$ Diode Lasers," IEEE J. Quantum Electron. QE-11, 464 (1975).

6. D. W. Bellavance and J. C. Campbell, "Room-Temperature Mesa Lasers Grown by Selective Liquid Phase Epitaxy," Appl. Phys. Lett. 29, 162 (1976).

7. D. W. Bellavance and J. C. Campbell, "Selective Liquid Phase Epitaxy for Integrated Optical Circuits," to be published in the Proceedings of the North American Conference on GaAs and Related Compounds.

8. J. C. Campbell and D. W. Bellavance, "Monolithic Laser/Waveguide Coupling by Evanescent Fields," to be published in the IEEE J. Quantum Electron.

The following presentations covering the work under this contract were given.

1. W. C. Scott, K. L. Lawley, and W. C. Holton, "Mesa Surface Laser," Topical Conference on Integrated Optics, New Orleans, Louisiana (January 1974).

2. R. K. Watts and J. R. McIntier, "Nonoxide Chalcogenide Glass Waveguides," Topical Conference on Integrated Optics, New Orleans, Louisiana (January 1974).

3. W. C. Holton, F. A. Blum, K. L. Lawley, F. H. Doerbeck, and D. W. Shaw, "Development of a $Ga_{1-x}In_xAs$ IOC Transmitter," Integrated Optics and Fiber Optics Communications Conference, San Diego, California (May 1974).

4. K. L. Lawley, F. A. Blum, W. C. Holton, and F. H. Doerbeck, "Mesa Growth of GaAs-(Ga,In)As for Integrated Optics Applications," Electrochemical Society Meeting, New York, New York (October 1974).

5. F. A. Blum, K. L. Lawley, F. H. Doerbeck, and W. C. Holton, "$Ga_{1-x}In_xAs$ Mesa Lasers with Grown Optical Facets," Optical Society of America Annual Meeting, Houston, Texas (October 1974).

6. F. A. Blum, K. L. Lawley, F. H. Doerbeck, and W. C. Holton, "Monolithic $Ga_{1-x}In_xAs$ Mesa Lasers with Grown Optical Facets," IEEE International Semiconductor Laser Conference, Atlanta, Georgia (November 1974).

7. D. W. Bellavance and J. C. Campbell, "Mesa Lasers with Room Temperature Operation Grown by Selective Liquid Phase Epitaxy," Topical Meeting on Integrated Optics, Salt Lake City, Utah (January 1976).

8. J. C. Campbell and D. W. Bellavance, "Bends and Curves in Optical Stripline Waveguides," 1976 Device Research Conference, Salt Lake City, Utah (June 1976).

9. D. W. Bellavance and J. C. Campbell, "Selective Liquid Phase Epitaxy for Integrated Optical Circuits," 6th International Symposium North American Conference on GaAs and Related Compounds, St. Louis, Missouri (September 1976).

10. D. W. Bellavance and J. C. Campbell, "$Ga_{1-x}Al_xAs$ Waveguides Grown by Selective Liquid Phase Epitaxy," 150th Meeting of the Electrochemical Society, Las Vegas, Nevada (October 1976).

DISTRIBUTION LIST

Office of Naval Research ATTN: Code 221 800 North Quincy Street Arlington, VA 22217	2
Office of Naval Research Branch Office 536 South Clark Street Chicago, IL 60605	1
Office of Naval Research Administrative Contracting Officer 800 North Quincy Street Arlington, VA 22217	1
Director Naval Research Laboratory ATTN: Code 2629 Code 2627 Washington, DC 20375	6 6
Defense Documentation Center Building 5 Cameron Station Alexandria, VA 22314	12


LME
7